LICENTIATE THESIS

Fluorine-Free Ionic Liquid Based Electrolytes

Synthesis and Structural Characterization

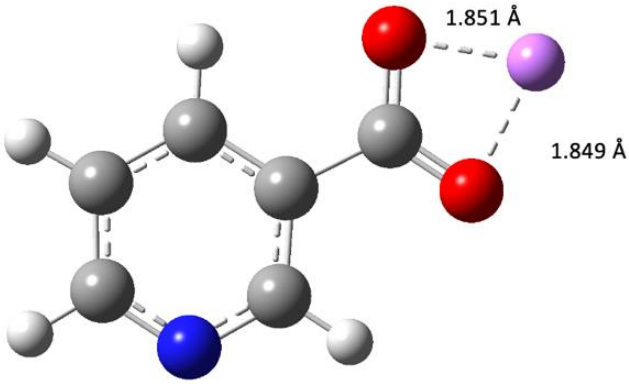

Mukhtiar Ahmed

Chemistry of Interfaces

LULEÅ UNIVERSITY OF TECHNOLOGY

Fluorine-Free Ionic Liquid Based Electrolytes

Synthesis and Structural Characterization

Mukhtiar Ahmed

Division of Chemical Engineering
Luleå University of Technology
SE- 971 87 Luleå
SWEDEN
September 2022

SUMMARY

Since their introduction by Sony in 1990, lithium-ion batteries (LIBs) have acquired a sizable market share. They have the best energy densities, a high open circuit voltage, a low self-discharge rate, no memory effect, and a slow loss of charge when not in use. These properties make them the most popular rechargeable batteries for portable gadgets, electric vehicles and aerospace applications. They do, however, pose major safety issues since the conventional electrolytes are made of fluorinated salts dissolved in volatile organic solvents, the former being meta-stable at ambient temperature and the latter being flammable with a high vapour pressure. Thus, there is an urge to develop thermally and electrochemically stable non-fluorinated electrolytes to improve the safety and performance of batteries. Electrolytes based on ionic liquids (ILs) in general offer a range of suitable advantages including low volatility and high thermal and electrochemical stabilities, and can additionally be made fluorine-free. In general, their physicochemical properties are determined by the interactions between the cations and anions, which are controlled by the chemical functionalities present, with vast freedom in structural design to reduce these interactions and enhance also the ion mobilities.

In this study, favouring from the "structural designability" of ILs, three different families of fluorine-free IL-based electrolytes are designed and created. These families of ILs comprising *n*- tetrabutylphosphonium-, imidazolium-, and pyridinium-based cations and pyridine, pyrazine and various oligoether functionalized anions. The structures and purity of these new ILs and their intermediate products are characterized by using multinuclear NMR, FTIR and mass spectrometry. Several features and properties of the novel ILs and electrolytes are investigated; thermogravimetric analysis, differential scanning calorimetry, ionic conductivity and electrochemical stability. These studies are further complemented by using PFG NMR diffusometry to understand the possible interaction mechanisms between the oppositely charged ions within the ILs and the electrolytes, and especially, the influence of Li^+ addition in the IL-based electrolytes. An overview of all the above mentioned synthesis and characterizations is presented.

Acknowledgements

First and foremost, I would like to thank my supervisors, Assoc. Prof. Faiz Ullah Shah and Prof. Patrik Johansson, for providing me with this opportunity, you brought me to the world of ionic liquids, electrochemistry and batteries, allowing me to pursue my own visions and restoring my faith in myself when times were tough, you are my inspiration. I enjoyed the time that we spent together. I am particularly grateful to the Swedish Energy Agency for supporting this research; without their assistance, this work would not have been feasible. I am thankful to Prof. Oleg Antzutkin for the valuable discussions and suggestions. I would like to thank Prof. Andrei Filippov for the NMR diffusion experiments and the useful discussions, as well as Dr. Soniya Rao for the computational analysis.

I am grateful to all COI members, past and present; I will never forget your company, fika, lunches, and endless conversations. Thank you, Dr. Sourav (DADA), and DIDI, for your unconditional love, support, and belief in me; you are always precious to me, and I cannot thank you enough for all of your love and support.

I appreciate your love and support, Sharma Jee. You are a great motivator, and I will never forget your wise counsels. Special thanks to Gillani Sahb and Tariq bhai; you are my go-to men; when I am stressed, you are the one I always contact; thank you for being there for me in both good and bad times. Thank you to all members "Fritid group" for making my days fly by; I had a great time with you guys, always appreciate your company. With you guys around, I never felt alone, you are always there when I need you, thank you buddies.

And last, but very certainly not least: I want to express my gratitude to my family, including my father, mother, brothers, and sisters, for their unwavering support and inspiration. I truly miss you guys, and I owe you all of my successes.

Mukhtiar Ahmed

List of papers

This thesis is based on the following three papers:

(I) Aromatic Heterocyclic Anion Based Ionic Liquids and Electrolytes
Mukhtiar Ahmed, Soniya Rao, Andrei Filippov, Patrik Johansson, and Faiz Ullah Shah
(*Manuscript*)

(II) Oligoether Substituted Aromatic Carboxylate Ionic Liquids and Electrolytes
Mukhtiar Ahmed, Andrei Filippov, Patrik Johansson, and Faiz Ullah Shah
(*Manuscript*)

(III) Fluorine-Free Ionic Liquids and Concentrated Electrolytes
Mukhtiar Ahmed, Andrei Filippov, Patrik Johansson, and Faiz Ullah Shah
(*Manuscript*)

My contribution to the papers:

(I) I designed the study together with my supervisors, performed all the synthesis and analyses except for computational study and PFG NMR, in which I partly participated during experiments. I authored the first draft and finalized it with comments from the co-authors.

(II) I planned all the work with the consents of my supervisors, synthesised all the compounds, performed all the analyses and experiments except for PFG NMR, in which I partly participated during experiments. I wrote the first draft and finalized it with comments from the co-authors.

(III) I designed the study together with my supervisors, carried out all the synthesis, performed all the analyses and experiments except for PFG NMR, in which I partly participated during experiments. I wrote the first draft of the manuscript and finalized it with comments from the co-authors.

To my Family (MSZGHRA)……..

Contents

1. Introduction

The continual rise in world's population, as well as societal economic and technical progress, has resulted in an increase in global energy demand, posing severe problems and environmental challenges. The vast extraction and consumption of fossil fuels, resulting in CO_2 emissions and pollution into the atmosphere, have hasten global climate change.[1] As a result, the use of renewable energy sources such as solar and wind energy is gaining emphasis to minimize greenhouse gas emissions. To compete with the most utilized fossil fuels, energy provided by fundamentally discontinuous and intermittent renewable sources requires effective storage for grid stability and global distribution.[2,3]

In this regard, the development of rechargeable batteries with high energy and power density, fast cycling rates, long service life, and made of economical materials could enable a gradual shift to ecologically friendly energy supply in the near future.[4,5] Furthermore, replacing internal combustion engines with zero-emission electrified systems *i.e.* electric vehicles (EVs) on a wide scale might reduce greenhouse gas emissions even further.[6] Preliminary efforts in this direction have already been made, with environmental regulations in place in numerous countries that encourage the use of EVs through consumer incentives.[7] However, in order to compete with the traditional vehicles, the real dissemination of EVs is dependent on the development of energy storage systems with high volumetric and gravimetric energy and power densities, safety and cost.[8]

Different types of batteries are being created and used based on different sorts of redox mechanisms and chemistries such as lithium-ion batteries (LIBs), lead acid batteries (Pb-A), nickel cadmium batteries (Ni–Cd), and Ni–MH (nickel metal hydride batteries) are just few examples of the most common batteries.[9] Among all, LIBs, are the most versatile and appealing energy storage systems and have triggered the global scale diffusion of a vast array of portable electronic devices, the demand of which is exponentially increased during the last 25 years, and will continue to be the most compelling choice not only for EVs but also other energy storage applications.[10] Significant efforts are being made by both academia and industry to produce new generations of batteries that are suitable for the upcoming challenging applications in terms of gravimetric and volumetric power density, energy density, durability, as well as sustainability and environmental compatibility.[11,12]

However, the safety issues are mainly related to flammability of the conventional electrolytes that are currently being used in LIBs. This drawback is progressively becoming even more serious, as the size of LIBs increases for their use in large energy storage devices such as hybrid electric vehicles (HEVs), and energy storage systems (ESSs) for smart grids.[13,14] Figure 1 depicts the increase in demand for LIBs from 19 gigawatt hours (GWh) in 2010 to 285 GWh in 2019, and expected to reach 2,000 GWh by 2030, accounting for around 8% of the global energy supply. In terms of installed capacity, passenger and commercial electric cars continue to be the most common applications for LIBs, followed by stationary (energy) storage.[15]

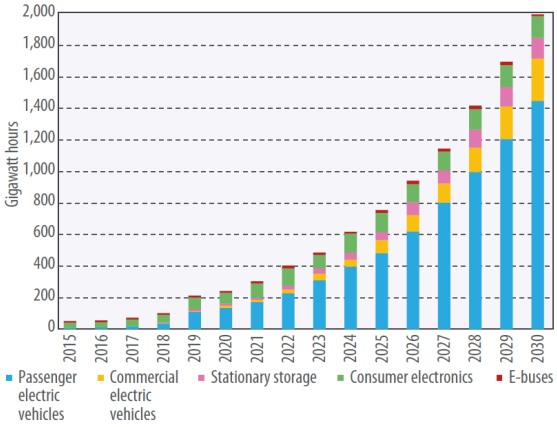

Figure 1. Global LIB materials demand forecast from electric vehicle sales, 2015–2030 (thousands of tonnes, GWh). Adapted from ref. 15.

2. An Electrolyte

An electrolyte acts as a medium between the two electrodes to transport ions and to compensate the charge of redox reactions occurring inside the anode and cathode.[16] Although an electrolyte is not directly engaged in a charge-storing redox process and neither directly influence the voltage or capacity of a battery, it is an important component with a significant impact on the overall performance and safety of any battery.[17] The separation of oxidation and reduction in electrochemical processes is intrinsically dependent on charge compensation *via* ionic currents. Because ion transport is often much slower than electron transport, the power output is directly tied to the electrolyte's ion transport capabilities.[18] Even more crucially, while the electrolyte is not engaged in charge-storing redox processes, it does take part in other redox events, and the harsh electrochemical environment of high-energy-density LIBs eventually leads to an electrolyte (side) reactions, which put extra responsibilities on the electrolyte and to perform, all of which must be executed flawlessly.[19.] Figure 2 shows schematic of a typical LIB comprising a cathode, an anode, a separator and an electrolyte.[20]

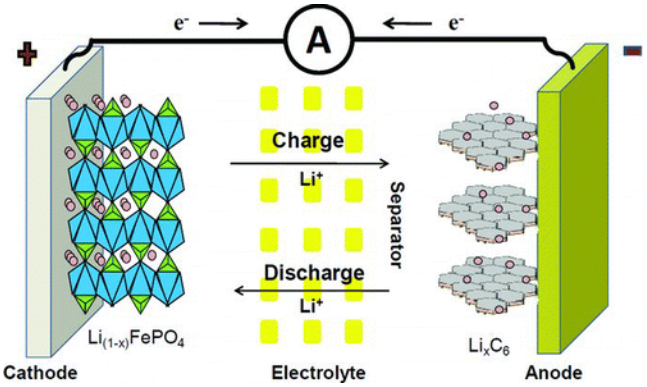

Figure 2. Schematic of a lithium-ion battery. Adapted from ref. 20.

Certain characteristics must be considered while developing an electrolyte system for an energy storage device in general, and LIBs in particular, which are enlisted below[21];

a. To prevent the side reactions such as breakdown of an electrolyte, the electrolyte should be chemically and electrochemically stable. The chemical and electrochemical instability of an electrolyte results in an irreversible charge loss due to the salt depletion and ion conduction obstruction, lowering the overall ionic conductivity.
b. To decrease cell polarization at high current densities, the electrolyte should provide high ionic conductivity (> 10^{-3} S cm^{-1}). The amount of charge carriers (salt concentration) and the mobility of ions, which is affected by viscosity of the electrolyte, affects ionic conductivity. With a significant concentration of the ionic salt and a low solvent viscosity, high ionic conductivity may be achieved.
c. The electrolyte salt should exhibit minimum ionic interactions to prevent ionic interactions and thus provide high ion mobility and ionic conductivity.
d. The electrolyte should remain liquid over a wide temperature range. The temperature range necessary to keep an electrolyte in a liquid state has a direct impact on the operational temperature range of the rechargeable batteries. Because ions mobility is restricted in the solid form, the ionic conductivity of a liquid electrolyte drops dramatically when solidified at lower temperatures.
e. The ions of an electrolyte should be small, which not only affect the volumetric and gravimetric energy densities, as well as the total cost of energy storage.
f. In last but not the least, an electrolyte should be nontoxic. Because the electrolyte may come in contact with the users in the event of a leakage, a non-toxic electrolyte is essential for mobile devices.

2.1 Problems with Conventional Electrolytes

Typically, an electrolyte is made by dissolving a lithium salt such as $LiPF_6$ in organic solvents such ethylene carbonate (EC) combined with linear aliphatic carbonates, primarily dimethyl and/or diethyl carbonates (DMC and DEC).[22,23] In this case, the electron-withdrawing effect of the fluoride's aids in the distribution of negative charges, decreasing the lattice energy of the salt, promoting ion dissociation, and facilitating salt dissolution in common organic solvents.[24] It is worth mentioning here that, the use of graphite as an anode material was made possible exclusively by the discovery that when EC reductively degraded at the graphite surface creating a stable, electrically insulating, but ionically conducting solid electrolyte interphase (SEI).[25] This electrolyte solution has undoubtedly contributed to the tremendous commercial success of LIBs over the last 25 years, and it is undoubtedly an excellent system for small-scale portable electronic devices. However, for large-scale applications such as EVs, raise valid issues about safety in various perspectives, which are detailed below one by one in more detail.[23]

2.1.1 Flammability

The organic solvent-based liquid electrolytes of LIBs are flammable by nature. The cascading thermal runaway event, which is regarded as the primary source of battery safety issues, is one of the most catastrophic failures of the LIB systems. Thermal runaway occurs when an exothermic process becomes uncontrollable. When the temperature of the battery rises over *ca.* 80°C, the rate of exothermic chemical reaction inside the battery increases, further heating the cell and thus resulting in a positive feedback cycle. The continuously rise in temperature, particularly in the case of large battery packs, may result in fire and explosion. Understanding the underlying causes and processes of thermal runaway can thus help in the design of new functional and safer electrolytes to improve the safety and durability of batteries.[26] The thermal runaway process may be separated into three stages, as shown in Figure 3.

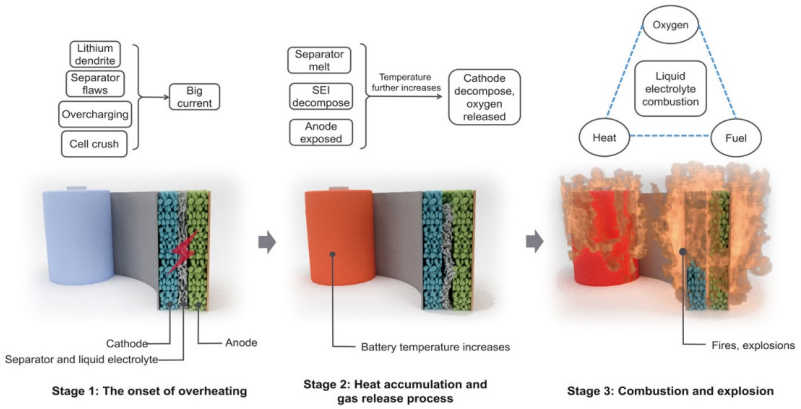

Figure 3. The three stages of the thermal runaway process of a battery cell. Adopted from ref. 26.

Stage 1: The onset of overheating. The battery changes from a normal to an abnormal state, and the internal temperature starts to increase. Stage 2: Heat accumulation and gas release process. The internal temperature quickly rises, and the battery undergoes exothermic reactions. Stage 3: Combustion and explosion. The flammable electrolyte combusts, leading to fire and even explosion.

2.1.2 The Fluorine Content

The conventional electrolyte salt, $LiPF_6$, contains about 75% fluorine content by weight, which is proven to decomposition at elevated temperature producing PF_5 and LiF, the former rapidly reacts with traces of water to release HF and PF_3O (Figure 4).[17] These decomposition products are extremely reactive towards both cathode and anode, adversely affecting the performance of a battery cell.[27] Fluorinated electrolyte components are also a source of worry during battery recycling, since they can pose major safety and environmental risks during handling and processing, including the release of poisonous HF and PF_5. Fluorine appears to be unavoidable in traditional battery systems, not only as a part of the electrolyte but also widely used as a component of binder in the form of polyvinylidene difluoride (PVdF).[28] With such a large level of fluorine contents in batteries, a slew of concerns arises, not only in terms of the battery cell performance, environmental and occupational safety but also at the recycling stages.[17]

$$Li^+ + PF_6^- \rightleftarrows LiPF_6 \rightleftarrows LiF + PF_5$$

$$PF_5 + H_2O \rightarrow POF_3 + 2HF$$

Figure 4. The decomposition pathway of $LiPF_6$.

2.1.3 The Possible Solution

Keeping in mind the problems associated with fluorine contents and flammability of the conventional electrolytes, creating non-fluorinated and non-flammable electrolytes is becoming an essential task to improve safety of electrolytes. Such fluorine-free electrolytes must meet a number of requirements including high thermal and electrochemical stabilities and high ionic conductivity. The emphasis has consequently been on developing fluorine-free electrolyte salts with weakly coordinating anions, in which the charge is delocalized over the anion and thus the dissociation energy is reduced.[29] Many of these non-fluorinated salts have been revealed higher thermal and electrochemical stabilities and proven to be competitive with "conventional" battery electrolytes in terms of ionic conductivity. Another important feature of the $LiPF_6$ electrolyte system is its ability to passivate aluminum cathode current collector, owing to its fluorine atoms.[17]

The fundamental issue with fluorine-free electrolyte salts is their poor performance at high potentials in passivating the aluminum, although corrosion tests using LiBOB-based electrolytes have demonstrated that the $[BOB]^-$ anion may passivate aluminum in the same way as $[BF_4]^-$ or $[PF_6]^-$ anions.[30] This passivation is hypothesized to be due to the formation of borate-containing species on aluminum, particularly $AlBO_3$, as revealed by Electrochemical Quartz Crystal Microbalance (EQCM). These findings suggest that fluorinated electrolytes are not always necessary for aluminum passivation and there is a clear possibility of developing fluorine-free electrolytes. In addition, developing fluorinated-free electrolytes would be a significant step towards developing more recyclable batteries with lower environmental concerns. Extensive research efforts are being made in recent years to identify and develop new electrolytes that might potentially address the problems associated with fluorinated electrolytes. Electrolytes based on ionic liquids (ILs) in general offer a range of suitable advantages including low volatility, high thermal and electrochemical stabilities, high ionic conductivity and can additionally be made fluorine-free and task-specific. The synthetic diversity allows for the design of appropriate functional groups with specific properties.[31,32]

2.2 Ionic Liquids

Ionic liquids (ILs) are salts having melting point at or below100 °C. Ethanolammonium nitrate with a melting point 52–55 °C was first IL discovered by S. Gabriel and J. Weiner in 1888.[33] The first room temperature IL with a melting point of 12 °C introduced in 1914 by P. Walden

was ethylammonium nitrate (EAN), which was created by neutralizing ethylamine with concentrated HNO_3.[34] EAN has physical properties comparable to water in that it is transparent, colorless and odorless but has a relatively higher viscosity. These early ILs were created to be utilized as solvent medium in high-temperature nuclear fuel reprocessing. However, due to their limited temperature range and chemical instability (as they rapidly interacted with air and moisture) and were not practicable.[35] Hurley and Wier have described the second generation of ILs made by combining alkylpyridinium chlorides with $AlCl_3$ in 1951.[36] Unfortunately, many of the second-generation ILs were not stable in the presence of moisture, highly corrosive, toxic, and regulating their acidity/basicity was a difficult task.[37]

Later, in 1992, Wilkes and Zaworotko have introduced moisture- and air-stable ILs from imidazolium cations and tetrafluoroborate anion, the combination revealed much better physical properties than the previously known ILs.[38] The extra π-electrons of the imidazolium cation greatly enhanced the positive charge delocalization *via* the creation of a resonance structure, lowering the melting point significantly below ambient temperature. The $[BF_4]^-$ anion is also chemically stable and relatively less reactive towards ambient moisture. Soon after this discovery, a research interest into ILs has been continuously growing and ILs have attracted the attention of academic and industrial researchers.

The common inorganic salts such as NaCl or KCl, have high melting points ranging from hundreds to thousands of °C, while on the other hand ILs typically remain liquids at ambient temperature. This is mainly because of the distinct chemical structures of ILs, which involves organic cations interacting with larger anions and positive charge of bulky organic cations is stabilized/delocalized by electronic or inductive interactions with adjacent chemical groups, resulting in a decrease in non-covalent attractions.[39,40] The strength of ionic binding is also reduced by the size of large ions, which lowers the potential of solid crystal formation. Furthermore, the nature of ionic species may be easily tuned to alter the physicochemical and electrochemical characteristics of ILs. Several ILs have been thoroughly explored based on this notion to improve their physicochemical and electrochemical capabilities.[41,42] Some of the most commonly studied ILs in various applications are shown in Figure 5.

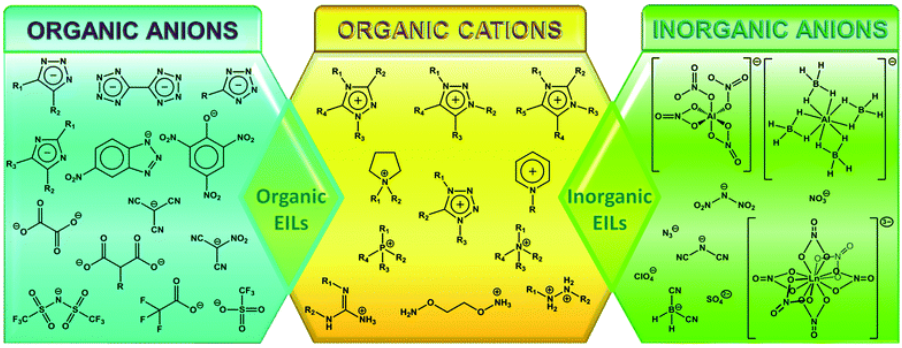

Figure 5. Structures of some commonly studied cations and anions of ILs. Adapted from ref. 43.

Because of their unusual ionic structure, ILs have tunable properties. First, since ILs possess stronger inter-ionic interactions rather than the inter molecular interactions as seen in organic solvents, they are more thermally stable than the traditional molecular solvents and have negligible vapor pressure, making ILs non-volatile and non-flammable.[44] In general, their physicochemical properties are determined by the interactions between the cations and anions, which are controlled by the chemical functionalities present. The vast freedom in structural design might help to reduce these interactions and enhance the ion mobilities.[45] They are also chemically and electrochemically robust; for example, ILs have high oxidative stability and can withstand voltages exceeding 4 V. These characteristics make ILs as an excellent choice for use as "task-specific" electrolytes in a variety of batteries.[46]

2.2.1 Ionic Liquid-Based Electrolytes

There are several advantages of IL-based electrolytes over conventional organic solvent-based electrolytes. First, as mentioned above, the concerns related to thermal instability, vapor pressure and flammability of the organic solvent-based electrolytes including afflict modern battery technology. Because of this thermal sensitivity, batteries must be cooled in many new applications using larger scale units.[47] Not only does this reduce the specific energy density obtainable (per weight or volume), but it also raises the cost owing to the additional engineering necessary to prevent thermal runaway (and possible fire or explosion). Currently, the prices of modern battery systems are mainly driven by the accompanying hardware rather than the cells (80% system costs vs. 20% for EVs and 60% system costs vs. 40% for stationary batteries). Batteries with IL-based electrolytes might not require sophisticated control systems for heat management due to their negligible vapour pressure and higher thermal stabilities. While ILs and their binary or ternary salt mixes have broad electrochemical windows and adequately high

ionic conductivity, the main drawback is their poor low-temperature charge-transport properties.[48] When compared to the supply of cooling systems, mild heating in conjunction with appropriate insulation is less expensive to construct.[49]

The second, and more significant, application of IL-based electrolytes is their use in next-generation batteries, particularly the ones that contain metal anodes. Among them are lithium-sulfur and lithium air (oxygen) batteries, as well as ongoing research on replacing the graphite anode in lithium-ion batteries with metallic lithium.[50] According to literature, several of the anions that give the finest liquid characteristics in IL-based electrolytes also have a significant impact on the efficiency with which lithium may be reversibly oxidized and reduced.[51] For example, in the case of Li-S batteries, this is the basis for the final negative electrode (in terms of energy density).[52] ILs and combinations of ILs with other solvents and additives have been examined as appropriate electrolytes since several of the cations and anions that are typical components of ILs share features of salts currently used in Li-S batteries.[53]

2.2.1.1 Fluorinated Ionic Liquid-Based Electrolytes

The most commonly studied IL-based electrolytes are based on fluorinated anions, *i.e.* bis(trifluoromethanesulfonyl)imide $(TFSI)^-$ and more recently bis(fluorosulfonyl)imide $(FSI)^-$ anions.[48] Typically, these electrolytes are made by dissolving LiTFSI/LiFSI salts in their parent ILs with well-known cations such as phosphonium, pyrrolidinium, imidazolium, morpholinium or piperidinium.[54-56] The H(TFSI) was first synthesised by Fotopoulos and DesMarteau as the highly acidic amine acid.[57] The same group investigated its chemistry further in subsequent publications and the favourable electrochemical properties of its Li-salt, such as wide ESW, reversible Li plating and stripping, and a relatively high conductivity were investigated initially in polymer matrixes[58] and later in liquid solution.[59,60] This was motivated in part by the desire to replace the unstable $Li[PF_6]$ salt with a chemically more stable lithium salt having comparable transport properties.[48] Some of the commonly studied fluorinated anions are shown in Figure 6.

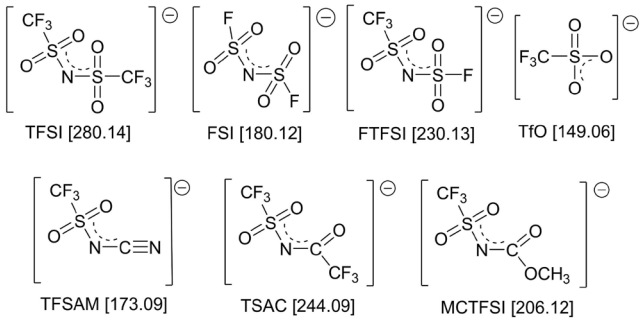

Figure 6. Imide type anions and their molar masses in []. Adapted from ref. 59.

Because of the low basicity, high degree of charge delocalization[61], and the presence of perfluorinated conferred by the two trifluoromethylsulfonyl groups in the [TFSI] anion, MacFarlane's group was able to create thermally and electrochemically stable ILs coupled with pyrrolidinium cations in 1999.[62] These anions have gained tremendous attentions in the ILs community, especially the ones working on energy storage devises. Katayama *et al.*[63] and Matsumoto *et al.*[64] have reported the first studies on the lithium electrochemistry of TFSI-based ILs. The creation of a protective (semi-passivating) SEI was hypothesized as the main cause of the reversible plating and stripping of lithium on numerous substrate materials. A number of spectroscopic methods were used to describe the SEI that occurs on lithium electrodes in subsequent studies.[65,66] As a result, numerous groups have demonstrated how a lithium metal electrode may function well in a device with an electrolyte based on a [TFSI] IL.[67-70]

These investigations have emphasized not only advancement in fundamental physicochemical features, but also the critical chemical role of sulfonyl- and fluoro-functionalities in the creation of a stable SEI on the electrode surfaces. Detailed combined XPS, SEM, and electrochemical investigations of SEI layers generated by chemical and electrochemical ion breakdown have revealed important information about their chemical composition, shape, and stability.

Despite the considerable efforts, a relatively small success with [TFSI]-based ILs have been realized. Overall, it appears that:[48] (i) the conductivity of mixtures of lithium salts and [TFSI]-based ILs is only just sufficient for low rates of charge-discharge duty; (ii) lithium-ion transport is sub-optimal at typical concentrations, limiting their higher rate performance; and (iii) the SEI formed in the presence of $[TFSI]^-$ anion does not provide long term stability to the lithium

electrode. Another disadvantage of thermally stable [TFSI]-based salts is that they cannot preserve the aluminum current collector in LIBs above 3.7 V vs. Li^+/Li.[71,72] This problem is worsened at high temperatures due to the breaking of passivation layer and increased solubility of surface species. It has been demonstrated that during the early stages of aluminium corrosion, $Al_x[TFSI]_y$ complexes were generated as a result of the interactions with the protective Al_2O_3 layer.[73] Although these complexes are moderately soluble in typical carbonate solvents and hence lack of passivation action, certain ILs may hinder their dissolution.

Furthermore, fluorinated ILs require laborious synthetic routes and hence relatively expensive, and the presence fluoride species pose risks to human health and the surrounding environment. From a safety and environmental standpoint, this has naturally sparked research towards the design of new fluorine-free IL-based electrolytes that can potentially replace fluorinated IL-based electrolytes.

2.2.1.2 Non-Fluorinated Ionic Liquid-Based Electrolytes

The transition from a traditional fossil-energy dominated world to a clean electrified world require a greener and sustainable energy storage technology. Therefore, there is an urge to replace the fluorinated electrolytes with non-fluorinated and greener electrolytes. One of the first attempt was undertaken in the mid-1990s to synthesize salts based on aromatic anions (following the Hückel rule) as prospective battery electrolytes, the idea was well supported by molecular modeling.[74-76] Among the various aromatic anions synthesized by cyclization, LiTDI salt (lithium 4,5-dicyano-2-(trifluoromethyl)imidazolate) was produced on a considerable scale.[77] LiPDI (lithium 4,5-dicyano-2-(pentafluoroethyl)imidazolate) and LiHDI (lithium 4,5-dicyano-2-(n-heptafluoropropyl)imidazolate) were also created.[78,79] The newly created unique salts were thermally stable, and unlike $LiPF_6$, they were also moisture stable. Furthermore, voltammetric tests indicated that the aromatic salts (LiTDI and LiPDI) based electrolytes were extremely stable on the surface of Pt electrode even in a broad potential window of 4.8 V *vs* Li^+/Li.[80]

In early 2012, Johansson *et al.*[81] presented the notion of pseudo-delocalized anions, which are anions having discrete positive and negative charge regions. Computer-aided calculations were used to evaluate these lithium salts as prospective electrolytes for lithium batteries, and fascinating synthetic targets for future study. Later in 2016, the hypothesis was validated, and the same group synthesized the first generation of pseudo-delocalized anions-based lithium and

sodium salts.[82] The salts have been thoroughly characterized using Raman and FT-IR spectroscopic techniques, thermogravimetry, X-ray crystallography, and ionic conductivity and electrochemical stability window measurements as aqueous electrolytes to reveal both basic properties in terms of thermal stability and solubility, as well as the ion-ion interactions and coordination. Together, they provided a picture of the salts potential as electrolyte components, especially for use in sodium-ion batteries and low voltage fluorine-free aqueous lithium-ion batteries.

Brennecke *et al.* proposed the synthesis of fluorine-free ILs based on aprotic heterocyclic anions (AHAs).[83] This study revealed that the ILs with both planar anions and cations have lower viscosities and higher ionic conductivities than those with more spherical geometries, while still retaining competitive EWs. Savateev *et al.*[84] presented the synthesis of three novel "completely organic" ILs, composed of heterocyclic cation and anion building blocks with high thermal and electrochemical properties. However, due to the presence of heteroatoms in both counter parts makes these systems heavy and resulted in a lower ionic conductivity as compared to the conventional fluorinated IL-based electrolytes.

Shah *et al.*[85] have reported on the ion dynamics in fluorine-free, hydrophobic, and hydrolytically stable phosphonium bis(salicylato)borate [$P_{4,4,4,8}$][BScB] IL-based electrolytes. However, these electrolytes have provided lower ionic conductivities than the conventional IL-based electrolytes due to the larger molecular masses of the cation and anion. More recently, Shah *et al.*[86] have introduced new classes of fluorine-free ILs composed of tetra(n-butyl)phosphonium $(P_{4444})^+$ and tetra(n-butyl)ammonium $(N_{4444})^+$ cations paired with 2-furoate $(FuA)^-$, tetrahydo-2-furoate $(HFuA)^-$, and thiophene-2-carboxylate $(TpA)^-$ anions. The effect of electron delocalization in anion and the mutual interactions between cations and anions on their physical and electrochemical properties was investigated in detail. Combined experimental and theoretical investigation revealed that the nature of the cation and anion, as well as electron delocalization in the anion, has a substantial influence on the physical and electrochemical characteristics of the ILs. Thermal investigation demonstrated that tetra(*n*-butyl)phosphonium-based ILs have lower glass transition temperatures and are thermally more stable than the tetra(*n*-butyl)ammonium-based ILs with common anions. The aromatic structure of 2-furoate and thiophene-2-carboxylate anions improved electrostatic interactions with cations, resulting in very stable ILs.

It was further demonstrated that the aromatic anions (FuA) and (TpA)-based ILs are more thermally stable and have larger ESWs than the analogous nonaromatic anion-based ILs (HFuA). Bearing in mind the superior physiochemical and electrochemical properties, (P_{4444})(FuA) IL was doped with Li(FuA) salt in different molar ratios to make LIB electrolytes.[87] It was revealed that the electrolytes have T_{onset} temperatures below 568 K and provide adequate ionic conductivities across a wide temperature range. The pulsed field gradient nuclear magnetic resonance (PFG-NMR) investigations indicated that the $(FuA)^-$ anion diffuses quicker than the $(P_{4444})^+$ cation in the pristine (P_{4444})(FuA) IL; however, doping of the neat IL with a Li salt slows down the anion diffusion. Over the entire temperature range investigated, the Li^+ ion interacts strongly with the carboxylate functionality in the $(FuA)^-$ anion and diffuses slower than other ions. ^{7}Li NMR and Fourier transform infrared (FTIR) spectroscopy indicated interactions of the Li^+ ion with the carboxylate group of the anion. With increasing Li^+ ion concentration, the transference number of the Li^+ ion has increased.

Passerini *et al*.[88] have synthesized *N*-methyl-*N*-butylpyrrolidinium (Pyr14)-based ILs with two different cyano-based anions, namely dicyanamide (DCA) and tricyanomethanide (TCM), and their mixtures with the respective Li salts (1:9 salt:IL molar ratio), as well as their mixtures (DCA–TCM), as potential electrolytes for lithium metal batteries (LMBs). The electrolytes exhibited high ionic conductivity (5 mS cm^{-1}) at ambient temperature, as well as an ESW up to 4 V, making them appropriate for low-voltage LMBs such as Li–sulfur batteries. The SEI formed by this class of IL-based electrolytes is studied for the first time, in addition to the detailed physicochemical (viscosity, ionic conductivity) and electrochemical (ESW, stripping/plating, and impedance spectroscopy in symmetrical Li cells) characterizations. X-ray photoelectron spectroscopy (XPS) revealed a SEI dominated by a polymer-rich layer including carbon–nitrogen single, double, and triple bonds, resulting in an excellent ionic conductivity and mechanical stability, as well as the cycle stability.

The field of fluorine-free IL-based electrolytes is still in its early phases, and much more research is needed to develop new electrolytes that can compete with the conventional fluorinated IL-based electrolytes. There is, however, little or no information available on the systematic battery performance of non-fluorinated IL-based electrolytes.

2.3 Scope of the Thesis

As it is obvious that electrolytes based on ILs offer a range of suitable advantages including low volatility, high thermal and electrochemical stabilities, high ionic conductivity and structural designability. The chemical structure and nature of the cation and anion components play an important role in governing the key physicochemical and electrochemical properties of IL-based electrolytes. Therefore, this thesis is focussed on the design, synthesis, physicochemical and electrochemical characterizations of new fluorine-free ILs and electrolytes to establish a systematic correlation between the chemical structure and the key properties.

Paper 1 is dedicated to the synthesis, thermal and electrochemical characterizations, and DFT calculations of five new ionic materials derived from nitrogen containing heterocyclic aromatic anions. The established structure-reactivity relationship significantly contributes to the understanding of how minor structural tuning of one counter part of ionic materials can have a significant impact on the overall physiochemical properties, and simply altering the position of nitrogen atom around the aromatic ring can produce ionic materials ranging from supercooled liquids to room temperature liquid ILs and ionic plastic crystals.

Paper 2 is focussed on the synthesis of five new ILs with anions based on oligoether substituted aromatic carboxylates coupled to a common *n*- tetrabutylphosphonium $(P_{4444})^+$ cation. The electrolytes created by doping two selected ILs with 10 mol % of lithium salts containing common anions are studied in detail. The nature and position of the attached oligoether chain to the phenyl ring influenced the physicochemical and electrochemical properties, in particular thermal stability, phase behavior, ion transport, and inter-ionic interactions.

Paper 3 discusses the synthesis, physicochemical and electrochemical properties of four new fluorine-free ILs with imidazolium and pyrrolidinium cations, coupled to two different oligoether-based anions such as 2-(2-methoxyethoxy)acetic acid, $(MEA)^-$ and 2-[2-(2-methoxyethoxy)ethoxy]acetate anion $(MEEA)^-$. The physicochemical and electrochemical properties including thermal stability, phase behavior, ionic conductivity, and ion diffusion are studied.

3. Experimental

3.1 Materials

Unless otherwise noted, all commercial reagents were utilized without any additional purification. 2-picolic acid (2-PyrA), nicotinic acid (3-PyrA), *iso*nicotinic acid (4-PyrA), pyrazinoic acid (2,5-PyrA), 2,6-pyridinedicarboxylic acid (Pyr-2,6-diA), salicylic acid (ACS reagents, >95 % purity), 4-toluenesulfonyl chloride (ACS reagents, >97 % purity), 2-ethoxyethanol (>99 % purity), *iso*-propoxy ethanol (>99 % purity), diethylene glycol monoethyl ether (>99 % purity) 1,2-dimethylimidazole (ACS reagents, >97 % purity), *n*-methylpyrrolidine (ACS reagents, >97 % purity), 1-bromobutane (>99 % purity), silver(I) oxide (>99.9 % purity), 2-[2-(2-methoxyethoxy)ethoxy]acetic acid (>97 % purity), 2-(2-methoxyethoxy)acetic acid (>97 % purity), aqueous solution of tetrabutylphosphonium hydroxide (40 wt % in water), lithium hydroxide monohydrate (ACS reagents, >98 % purity) were received from Sigma-Aldrich. Sodium sulphate, methanol, dichloromethane (DCM) and diethylether were purchased from VWR (BDH) chemicals.

3.2 Synthesis

The detailed synthesis and characterization of each intermediate and final product is discussed in the corresponding paper. Here, a brief summary of few compounds is presented.

3.2.1 Synthesis of Aromatic Acids

The oligoether functionalized aromatic acids were synthesized using a multistep synthesis protocol. In a typical experiment, the synthetic procedure of 2-(2-isopropoxyethoxy)benzoic acid (2-IEBA) is regarded as an example, which is detailed below. All the other oligoether functionalized aromatic acids are synthesized using the same procedure.

A solution of 2-isopropoxyethyl 4-methylbenzenesulfonate (38.7 g, 0.15 moles, 1.5 equiv. in 100 ml of dry acetonitrile), methyl salicylate (15.2g, 0.1 moles, 1 equiv.) and potassium carbonate (69 g, 0.5 moles, 5 equiv.) in dry acetonitrile (250 mL) was heated at 70 °C under N_2 and continuous stringing for 48 hrs. The yellow suspension was filtered off and the solid was washed with acetonitrile (60 mL). The extract and washes were concentrated *via* rotary evaporation. The residue was extracted with DCM (3 x 50 mL). The organic phase was washed with water (6 x 150 mL). The organic layer was dried over $MgSO_4$, gravity filtered, and the solvent was removed by rotary evaporation to afford the product **B2** as a yellow oil. **B2** was dissolved in THF:MeOH (1:1, 50 mL) and dropped into the aqueous solution of $LiOH.H_2O$ (3

equiv.), stirred at room temperature for 12 hrs, neutralized with 0.1 M HCl and extracted with DCM (3 x 25 mL). The organic phase was washed with water (6 x 150 mL), dried over MgSO4, gravity filtered, and the solvent was removed by rotary evaporation to afford the product 2-(2-isopropoxyethoxy)benzoic acid (2-IEBA) as a dark yellow liquid. All the acids were separated in good yields *ca.* 60%.

2-(2-isopropoxyethoxy)benzoic acid (2-IEBA): Dark yellow liquid. ^{1}H NMR (400.21 MHz, $CDCl_3$), $^{\delta}$(ppm): 10.34 (*b*, 1H), 8.16-8.14 (*d*, $^{3}J_{HH}$ = 8.2 Hz 1H), 7.56-7.52 (*d*, $^{3}J_{HH}$ = 8.1 Hz, 1H), 7.11-7.03 (*t*, $^{3}J_{HH}$ = 8.3 Hz 1H), 4.37-4.34 (*t*, $^{3}J_{HH}$ = 4.3 Hz, 2H, O-CH_2-), 3.84-3.82 (*t*, $^{3}J_{HH}$ = 4.5 Hz, 2H, -CH_2-O), 3.72-3.66 (*sept*, $^{3}J_{HH}$ = 6.1 Hz, 1H, -CH), 1.21-1.20 (*d*, $^{3}J_{HH}$ = 6.1 Hz, 6H, -CH_3) ppm. ^{13}C NMR (100.64 MHz, $CDCl_3$): 171.20, 163.58, 132.43, 121.78, 114.56, 72.47, 68.12, 66.45, 22.19.

3-(2-isopropoxyethoxy)benzoic acid (3-IEBA):: Dark yellow liquid. ^{1}H NMR (400.21 MHz, $CDCl_3$), $^{\delta}$(ppm): 11.66 (*b*, 1H), 7.73-7.71 (*d*, $^{3}J_{HH}$ = 7.6 Hz 1H), 7.66 (*s*, 1H),7.40-7.36 (*t*, $^{3}J_{HH}$ = 8.0 Hz 1H), 7.19-7.18 (*t*, $^{3}J_{HH}$ = 8.0 Hz 1H), 4.20-4.17 (*t*, $^{3}J_{HH}$ = 4.8 Hz, 2H, O-CH_2-), 3.85-3.82 (*t*, $^{3}J_{HH}$ = 4.7 Hz, 2H, -CH_2-O), 3.76-3.69 (*sept*, $^{3}J_{HH}$ = 6.7 Hz, 1H, -CH), 1.24-1.23 (*d*, $^{3}J_{HH}$ = 6.2 Hz, 6H, -CH_3) ppm. ^{13}C NMR (100.64 MHz, $CDCl_3$): 171.20, 163.58, 132.43, 121.78, 114.56, 72.47, 68.12, 66.45, 22.19.

4-(2-isopropoxyethoxy)benzoic acid (4-IEBA): Dark yellow liquid. ^{1}H NMR (400.21 MHz, $CDCl_3$), $^{\delta}$(ppm): 8.07-8.05 (*d*, $^{3}J_{HH}$ = 8.6 Hz, 2H), 7.99-7.97 (*d*, $^{3}J_{HH}$ = 8.6 Hz, 2H), 4.21-4.18 (*t*, $^{3}J_{HH}$ = 4.6 Hz, 2H, O-CH_2-), 3.83-3.81 (*t*, $^{3}J_{HH}$ = 5.2 Hz, 2H, -CH_2-O), 3.81-3.68 (*sept*, 3J_{HH} = 6.0 Hz, 1H, -CH), 1.24-1.22 (*d*, $^{3}J_{HH}$ = 6.1 Hz, 6H, -CH_3) ppm. ^{13}C NMR (100.64 MHz, $CDCl_3$): 171.20, 163.58, 132.43, 121.78, 114.56, 72.47, 68.12, 66.45, 22.19.

2-(2-ethoxyethoxy)benzoic acid (2-EEBA): Dark yellow liquid. ^{1}H NMR (400.21 MHz, $CDCl_3$), $^{\delta}$(ppm): 10.81 (*b*, 1H), 8.14-8.12 (*d*, $^{3}J_{HH}$ = 7.9 Hz 1H), 7.55-7.51 (*t*, $^{3}J_{HH}$ = 7.6 Hz, 1H), 7.13-7.11 (*d*, $^{3}J_{HH}$ = 7.5 Hz 1H), 7.10-7.03 (*t*, $^{3}J_{HH}$ = 8.3 Hz, 1H), 4.37-4.34 (*t*, $^{3}J_{HH}$ = 4.3 Hz, 2H, O-CH_2-), 3.84-3.82 (*t*, $^{3}J_{HH}$ = 4.2 Hz, 2H, -CH_2-O), 3.62-3.56 (*t*, $^{3}J_{HH}$ = 6.9 Hz, 2H, -CH_2-O), 1.25-1.21 (*d*, $^{3}J_{HH}$ = 6.9 Hz, 3H, -CH_3) ppm. ^{13}C NMR (100.64 MHz, $CDCl_3$): 165.85, 157.64, 134.93, 133.71, 122.62, 118.74, 113.75, 69.48, 67.86, 67.09, 15.03.

2-(2-(2-methoxyethoxy)ethoxy)benzoic acid (2-MEMBA): Dark yellow liquid. ^{1}H NMR (400.21 MHz, $CDCl_3$), $^{\delta}$(ppm): 10.91 (*b*, 1H), 8.18-8.16 (*d*, $^{3}J_{HH}$ = 8.0 Hz 1H), 7.55-7.52 (*d*, $^{3}J_{HH}$ = 8.1 Hz, 1H),7.14-7.06 (*t*, $^{3}J_{HH}$ = 8.1 Hz 1H), 4.40-4.37 (*t*, $^{3}J_{HH}$ = 4.6 Hz, 2H, O-CH_2-), 3.95-3.92 (*t*, $^{3}J_{HH}$ = 4.9 Hz, 2H, -CH_2-O), 3.64-3.62 (*t*, $^{3}J_{HH}$ = 4.3 Hz, 2H, -CH_2-O), 3.54-3.53 (*t*, $^{3}J_{HH}$ = 5.2 Hz, 2H, -CH_2-O), 1.20 (*t*, $^{3}J_{HH}$ = 5.1 Hz, 3H, -CH_3) ppm. ^{13}C NMR (100.64 MHz, $CDCl_3$): 165.71, 157.57, 134.92, 133.81, 122.65, 118.70, 113.57, 71.05, 69.93, 69.33, 68.83, 66.87, 15.23.

3.2.2 Synthesis of Ionic Materials

An aqueous solution of the tetrabutylphosphonium hydroxide (13.82 g, 50 mmol) was added dropwise into the stirred aqueous solution of the acid (50 mmol in 50 ml of water). The reaction mixture was stirred at room temperature for 4 hours and progress of the reaction was monitored *via* thin layer chromatography (TLC) and upon completion of the reaction water was removed under reduced pressure using a rotary evaporator. The products were washed three times with 50 ml of diethyl ether before being dissolved in dichloromethane and dried over anhydrous Na_2SO_4. Finally, the solution was filtered, residual solvent was removed under reduced pressure, and the final products were dried in a vacuum oven at 80 °C for more than 4 days. All the products were separated in quantitative yields.

(P_{4444})(2-IEBA): Pale yellow liquid. MS (ESI). $[C_{16}H_{36}P]^{+}$: Calcd m/z 259.2556. Found m/z 259.2565, $[C_{12}H_{15}O_4]^{-}$: Calcd m/z 223.0975, Found m/z 223.1071. ^{1}H NMR (400.21 MHz, $CDCl_3$), $^{\delta}$(ppm): 7.45-7.44 (*d*, $^{3}J_{HH}$ = 6 Hz 1H), 7.09-7.07 (*d*, $^{3}J_{HH}$ = 7.5 Hz, 1H), 6.85-6.82 (*m*, 2H), 4.18-4.16 (*t*, $^{3}J_{HH}$ = 5.6 Hz, 2H, O-CH_2-), 3.76-3.73 (*t*, $^{3}J_{HH}$ = 5.1 Hz, 2H, -CH_2-O), 3.61-3.58 (*sept*, $^{3}J_{HH}$ = 5.1 Hz, 1H, -CH), 2.41-2.34 (*m*, 8H, P-CH_2-), 1.48-1.46 (*m*, 16H, -CH_2-), 1.21-1.20, (*d*, $^{3}J_{HH}$ = 6.1 Hz, 6H, -CH_3) ppm. 0.84-0.87 (t, $3J_{HH}$ = 7.1 Hz, 12H, -CH_3) ppm. ^{13}C NMR (100.64 MHz, $CDCl_3$): 171.20, 163.58, 132.43, 121.78, 114.56, 72.47, 68.12, 66.45, 22.19. ^{31}P NMR (162.01 MHz, $CDCl_3$): 33.00 ppm.

(P_{4444})(3-IEBA): Pale yellow liquid. MS (ESI). $[C_{16}H_{36}P]^{+}$: Calcd m/z 259.2556. Found m/z 259.2569, , $[C_{12}H_{15}O_4]^{-}$: Calcd m/z 223.0975, Found m/z 223.0934. ^{1}H NMR (400.21 MHz, $CDCl_3$), $^{\delta}$(ppm): 7.67-7.65 (*m*, 2H), 7.20-7.16 (*m*,1H), 6.90-6.88 (*m*, 1H), 4.17-4.13 (*t*, $^{3}J_{HH}$ = 5.0 Hz, 2H, O-CH_2-), 3.78-3.75 (*t*, $^{3}J_{HH}$ = 6.11 Hz, 2H, -CH_2-O), 3.72-3.67 (*sept*, $^{3}J_{HH}$ = 6.6 Hz, 1H, -CH), 2.45-2.38 (*m*, 8H, P-CH_2-), 1.52-1.47 (*m*, 16H, -CH_2-), 1.20-1.18, (*t*, $^{3}J_{HH}$ = 5.2 Hz, 6H, -CH_3) ppm. 0.98-0.92 (t, $3J_{HH}$ = 3.5 Hz, 12H, -CH_3) ppm. ^{13}C NMR (100.64 MHz,

$CDCl_3$): 171.48, 158.57, 142.61, 128.08, 122.25, 116.48, 114.71, 72.06, 67.86, 66.83, 24.21, 24.07, 24.06, 24.03, 22.27, 19.18, 18.17, 13.60. ^{31}P NMR (162.01 MHz, $CDCl_3$): 33.03 ppm.

(P_{4444})(4-IEBA): Pale yellow liquid. MS (ESI). $[C_{16}H_{36}P]^+$: Calcd m/z 259.2556. Found m/z 259.2565, $[C_{12}H_{15}O_4]^-$: Calcd m/z 223.0975, Found m/z 223.0934. ^1H NMR (400.21 MHz, $CDCl_3$), $^{\delta}$(ppm): 7.99-7.97 (*d*, $^3J_{HH}$ = 8.4 Hz, 2H), 6.82-6.80 (*d*, $^3J_{HH}$ = 8.4 Hz, 2H), 4.10-4.08 (*t*, $^3J_{HH}$ = 4.9 Hz, 2H, O-CH_2-), 3.77-3.64 (*m*, 2H), 1.42-1.40 (*m*, 16H, -CH_2-), 1.20-1.18, (*t*, $^3J_{HH}$ = 5.2 Hz, 6H, -CH_3) ppm. 0.98-0.92 (t, $3J_{HH}$ = 3.5 Hz, 12H, -CH_3) ppm. ^{13}C NMR (100.64 MHz, $CDCl_3$): 171.82, 160.00, 132.72, 131.14, 113.37, 116.48, 72.25, 67.77, 66.67, 24.10, 23.95, 23.89, 23.85, 22.19, 19.00, 18.53, 13.54. ^{31}P NMR (162.01 MHz, $CDCl_3$): 32.96 ppm.

(P_{4444})(2-EEBA): Pale yellow liquid. MS (ESI). $[C_{16}H_{36}P]^+$: Calcd m/z 259.2556. Found m/z 259.2565, , $[C_{12}H_{15}O_4]^-$: Calcd m/z 223.0975, Found m/z 223.1074.^1H NMR (400.21 MHz, $CDCl_3$), $^{\delta}$(ppm): 7.45-7.43 (*d*, $^3J_{HH}$ = 7.2 Hz 1H), 7.09-7.05 (*d*, $^3J_{HH}$ = 7.9 Hz, 1H), 6.85-6.81 (*m*, 2H), 4.19-4.16 (*t*, $^3J_{HH}$ = 5.4 Hz, 2H, O-CH_2-), 3.76-3.73 (*t*, $^3J_{HH}$ = 5.3 Hz, 2H, -CH_2-O), 3.57-3.51 (*t*, $^3J_{HH}$ = 6.9 Hz, 2H), 2.39-2.36 (*m*, 8H, P-CH_2-), 1.46-1.44 (*m*, 16H, -CH_2-), 1.19-1.17, (*d*, $^3J_{HH}$ = 7 Hz, 3H, -CH_3) ppm. 0.84-0.87 (t, $3J_{HH}$ = 7.1 Hz, 12H, -CH_3) ppm. ^{13}C NMR (100.64 MHz, $CDCl_3$): 172.67, 155.29, 134.71, 129.02, 127.54, 120.93, 114.18, 69.32, 68.93, 66.88, 24.18, 24.03, 23.98, 19.01, 18.54, 15.41, 13.66. ^{31}P NMR (162.01 MHz, $CDCl_3$): 33.03 ppm.

(P_{4444})(2-MEMBA): Pale yellow liquid. MS (ESI). $[C_{16}H_{36}P]^+$: Calcd m/z 259.2556. Found m/z 259.2552, $[C_{13}H_{17}O_5]^-$: Calcd m/z 253.1081, Found m/z 253.1321. ^1H NMR (400.21 MHz, $CDCl_3$), $^{\delta}$(ppm): 7.43-7.41 (*m,* 1H), 7.08-7.04 (*m*, 1H), 6.83-6.79 (*m*, 2H), 4.17-4.15 (*t*, $^3J_{HH}$ = 5.2 Hz, 2H, O-CH_2-), 3.82-3.79 (*t*, $^3J_{HH}$ = 5.3 Hz, 2H, -CH_2-O), 3.68-3.66 (*t*, $^3J_{HH}$ = 4.3 Hz, 2H), 3.56-3.45 (*m*, 8H) 2.33-2.30 (*m*, 8H, P-CH_2-), 1.46-1.44 (*m*, 16H, -CH_2-), 1.19-1.17, (*d*, $^3J_{HH}$ = 7 Hz, 6H, -CH_3) ppm. 0.84-0.87 (t, $3J_{HH}$ = 7.1 Hz, 12H, -CH_3) ppm. ^{13}C NMR (100.64 MHz, $CDCl_3$): 172.78, 155.29, 134.42, 128.93, 127.67, 120.84, 114.51, 77.59, 77.28, 76.96, 70.77, 69.97, 68.88, 66.68, 24.13, 23.98, 23.95, 23.90 18.96, 18.49, 15.27, 13.61. ^{31}P NMR (162.01 MHz, $CDCl_3$): 33.04 ppm.

3.2.3 Synthesis of Lithium Salts

All the lithium salts were prepared by direct neutralization of acids with Lithium bicarbonate ($LiHCO_3$). Under continuous stirring, aqueous solutions of the acids were treated with solid

$LiHCO_3$ in small portions, until the generation of gas bubbles stopped. All the salts were obtained in quantitative yields after lyophilization and subsequent drying in vacuo.

3.4 Physiochemical Characterizations

3.4.1 Nuclear Magnetic Resonance Spectroscopy

The structures and purity of all the synthesized ILs were confirmed by using a Bruker Ascend Aeon WB 400 (Bruker BioSpin AG, Fallanden, Switzerland) NMR spectrometer. $CDCl_3$ was used as a solvent. The working frequencies were 400.21 MHz for ^{1}H, 100.64 MHz for ^{13}C, and 162.01 MHz for ^{31}P. Data were processed using Bruker Topspin 3.5 software.

3.4.2 FTIR Spectroscopy

The attenuated total reflection Fourier transform infrared (ATR-FTIR) spectra of samples were recorded using a Bruker IFS 80v spectrometer equipped with a deuterated triglycine sulfate (DTGS) detector and diamond ATR accessory, employing the double-side forward–backward acquisition mode. The total number of scans was 256, co-added and signal-averaged at an optical resolution of 4 cm^{-1}.

3.4.3 Thermal Analysis

Thermogravimetric analysis (TGA) was performed using a PerkinElmer TGA 8000 under N_2 gas at a heating rate of 10 °C per min using ca. 2-4 mg samples. The onset of decomposition temperature, T_{onset}, was calculated from the intersection of the baseline weight and the tangent of the weight versus temperature curve using Pyris software. Differential scanning calorimetry (DSC) was performed using a PerkinElmer DSC 6000 on 2-5 mg of sample placed in an aluminum pan. DSC data were collected at a scanning rate of 5 °C min^{-1} for both cooling and heating traces ranging from -75 to 200 °C. To maintain an inert environment inside the sample chamber, dry N_2 gas was delivered at a constant flow rate of 20 mL min^{-1}. The T_g was determined by using the inflection mid-point of the initial *S*-shaped transition slope and determined from the onset with the aid of Pyris software.

3.4.4 Pulsed Field Gradient Diffusometry

NMR self-diffusion measurements were performed using a Bruker Ascend/Aeon WB 400 (Bruker BioSpin AG) NMR spectrometer with a resonance frequency of 400.27 MHz for ^{1}H and 155.56 MHz for ^{7}Li. Pulsed-Field Gradient (PFG) NMR self-diffusion measurements were performed on ^{1}H with a PFG NMR probe Diff50 (Bruker) with a maximum amplitude of the

magnetic field gradient pulse of 29.73 T m^{-1}. The samples were placed in a standard 5 mm NMR glass tube and closed with a plastic stopper to avoid contact with air. Prior to measurements, each sample was equilibrated at a specific temperature for 30 min. The details of the PFG NMR technique for measuring molecular diffusion coefficients are available elsewhere.[89] The diffusivity of a molecule is the diffusion decay (DD) of amplitude A of NMR spectral line, obtained by Fourier transformation of a descending half of stimulated-echo (StE), as a function of the amplitude of applied pulsed field gradient. For the stimulated echo pulse sequence used, diffusion decay of A in the case of simple non-associating molecular liquid can be described by the Eq.(1):[90]

$$A(g,\delta,t_d) = A(0)\exp(-\gamma^2 g^2 \delta^2 D t_d) \quad (1)$$

where $A(0)$ is the factor proportional to the proton content in the system, and to spin-lattice and spin-spin relaxation times, γ is the gyromagnetic ratio for a used nucleus; g and δ are the amplitude and duration of the gradient pulse; t_d is the diffusion time; and D is the self-diffusion coefficient. t_d was in the range 4-100 ms for ^{1}H diffusion and 5-15 ms for ^{7}Li diffusion.

3.3 Electrochemical Characterization

All the electrochemical characterizations were performed by using a Metrohm Autolab PGSTAT302N electrochemical workstation with a FRA32M module for impedance measurements, all of which were controlled by Nova 2.02 software. Prior to each measurement, the electrodes were polished with a 0.25 m of Kemet diamond paste.

3.3.1 Linear Sweep Voltammetry

A sealed Microcell HC from RHD instruments was used to hold about 70 µL of sample. Linear sweep voltammetry (LSV) was performed with a three-electrode setup: a Pt wire with a diameter of 0.25 mm and/or GC with a diameter of 2 mm as working electrodes (WE), a Pt crucible as counter electrode (CE), as well as sample container, and an Ag wire coated with AgCl as a pseudo-reference electrode (RE). Both cathodic and anodic scans were recorded at a rate of 1 mV s^{-1}. The electrochemical potentials were calibrated using ferrocene (Fc) as internal reference and shifted using $E_{Li/Li^+} \approx E_{Fc/Fc^+} + 3.2$ V.[91] The ESWs limits were defined by a 0.1 mA cm^{-2} cut-off current density.

3.3.2 Ionic conductivity

The ionic conductivity was obtained from the impedance measurements performed in a frequency range from 1 Hz to 1 MHz with an AC voltage amplitude of 10 mV_{rms}. All the impedance spectra were measured during heating and cooling over a temperature range from -20 to 100 ± 0.1 °C. A two-electrode configuration was employed for ionic conductivity measurements, with a wire Pt as WE and a 70 µL Pt crucible as a sample container, as well as CE. The cell constant was calculated using a Metrohm 100 S cm^{-1} KCl standard solution (K_{cell} = 18.5396 cm^{-1}). The cell was thermally equilibrated for 10 minutes before recording the impedance spectra.

4. Results and Discussion

A brief summary of synthesis is presented, followed by assessing the phase and thermal behaviour of the synthesized ionic materials, before moving on to more LIB-relevant performance parameters such as ionic conductivity, ESW, and self-diffusion of electrolytes made and finally some examples of FTIR spectroscopic data for addressing the local interactions, coordination, and ion–ion interactions are discussed.

4.1 Synthesis of Ionic Liquids

A multistep synthetic protocol is used to create the ether functionalized acids and their ILs. A brief description of synthesis and characterization is provided below, and the details are given in the manuscript. We begin by tosylation of the alcohols to replace –OH by a better leaving group and make it acceptable for its use as an alkylating agent (Scheme 1a).

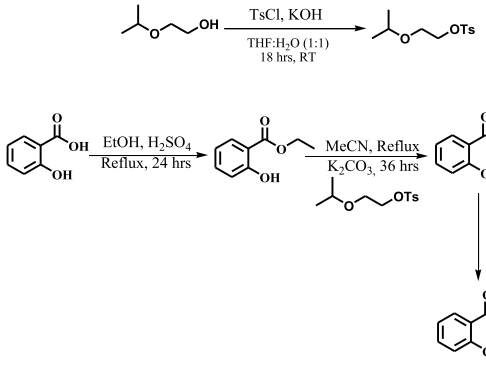

Scheme 1. (a) Tosylation of *iso*-propoxy ethanol (2-IE), (b) Synthetic rout for 2-(2-isopropoxyethoxy)benzoic acid (2-IEBA).

In second step, the tosylated alcohols are reacted with methyl esters in the presence of a mild base *i.e*; K_2CO_3 and acetonitrile as a reaction medium to obtain ether functionalized methylsalicylates. The esters are further converted into their corresponding acids *via* basic ester hydrolysis (Scheme 1b). Finally, the heterocyclic (**Paper I**), aromatic oligoether (**Paper II**) and oligoether acids (**Paper III**) are converted into ionic materilas *via* a simple neutralization reaction with *n*-tetrabutylphosphonium, imidazolium and pyrrolidinium hydroxides in aqueous medium. The structures and abbreviation of the ionic component of the synthesized ILs are shown in Scheme 2.

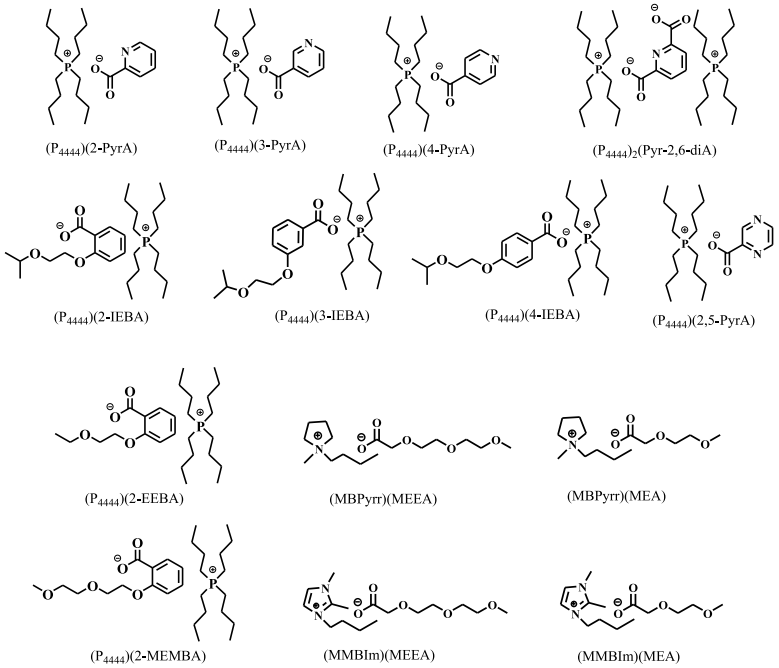

Scheme 2. Chemical structures and abbreviations of the ionic components of all the synthesized ILs.

The chemical structures of all the ILs agree well with the NMR spectroscopic analysis and the mass spectrometric data. First, the ^{1}H NMR spectra of the ILs show characteristic resonance lines for the methylene protons of the ether chains in the anions in the range from 3.5 to 4.3 ppm (**Paper II** and **Paper III**), and the presence of aromatic resonance lines, 6.5-8.5 ppm (Paper I). Second, the absence of the broad resonance line for the acidic proton and the appearance of distinct resonance lines in the aliphatic region; 0.90–1.0 ppm for the terminal methyl groups, the multiplet 1.46–1.54 ppm for the methylene protons, and another multiplet 2.39–2.46 ppm for the aliphatic alkyl chains attached to the $(P_{4444})^{+}$ cation (**Paper I** and **Paper II**) and presence of characteristic resonance lines for the butyl chain, methylene protons alpha to the charged nitrogen atom appear in the range of 4.1 to 4.5 ppm for imidazolium and 3.5 to 3.7 ppm for pyrrolidinium based ILs, and methyl protons with distinct triplet appear at 0.9 to 1 ppm for both systems (**Paper III**), corroborated the successful deprotonation of the corresponding acids and formation of the ionic materials. Third, the ^{13}C NMR spectra revealed resonance lines in the region 65–80 ppm attributed to the aliphatic carbon directly attached to the oxygen atoms in ether chains of the anions (**Paper II** and **Paper III**). In addition, the ^{13}C

resonance lines for the carboxylate groups in the anions are found in the range 165–180 ppm. Finally, the ^{31}P NMR spectra indicate single resonance lines at *ca.* 33 ppm for each IL (**Paper I** and **Paper II**).

4.2 Thermal Properties

One of the fundamental qualities that distinguishes IL-based electrolytes from typical organic solvent-based electrolytes is their higher thermal stability.[92] Generally, thermal stability measurements are carried out by thermogravimetric analysis (TGA), more specifically ramped temperature analysis (also called step-tangent or dynamic TGA analysis) with most common heating rates of 10 °C min^{-1} and 20 °C min^{-1}. Here, it is important to mention that the thermal decomposition temperature greatly depends on the heating rate. In these experiments, the decomposition temperature obtained are considered as the short-term thermal stability and indicated with $T_{onset,}$ which is a number computed by thermal analysis software, and defined as the intersection of the zero-weight-loss baseline and the tangent of the weight-temperature curve as decomposition proceeds. The actual degradation already starts at a lower temperature (T_{start}) than the T_{onset}. T_z (decomposition degree z) is another measure used to describe short-term thermal stability, as it indicates the temperatures at various decomposition degrees (Figure 7).[93]

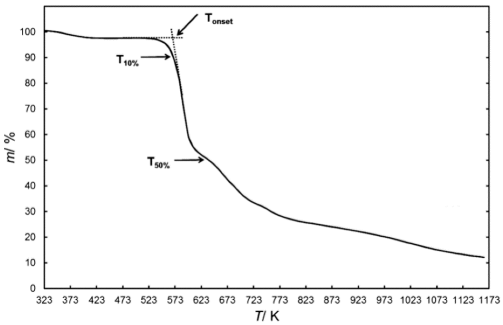

Figure 7. Thermal parameters of ILs obtained from dynamic TGA curves. Adapted from ref. 93.

Thermal stability of ILs depends upon the chemistries of cation and anions and their ionic interactions. Figure 8 shows the TGA curves of some neat ILs and their electrolytes. All the systems show excellent short-term thermal stability up to 280 °C at a scan rate of 10 °C min^{-1}, showing considerably improved thermal stability compared to any traditional organic-solvent-based electrolytes. However, the thermal stability measured by dynamic TGA is overestimated

and must be complimented with the isothermal TGA to determine the precise thermal stability of IL-based electrolytes. Neat ILs with heterocyclic anions showed better thermal stability than carbocyclic anions, and ILs with donating groups at meta-position with respect to the carboxyl group improve thermal stability significantly, which suggest that the thermal stability of neat ILs is heavily dependent on the anion chemistry, including the delocalization of electrons around aromatic rings and ion polarity. In general, doping the neat ILs with lithium salts brings an additional polarity and electrostatic interactions to the systems and lead to further improvement in thermal stability (Figures 8a and 8c). The increase in thermal stability is attributed to the rigid, planar, aromatically stabilized structures of anions and hence efficient electron delocalization (Figures 8b and 8d).

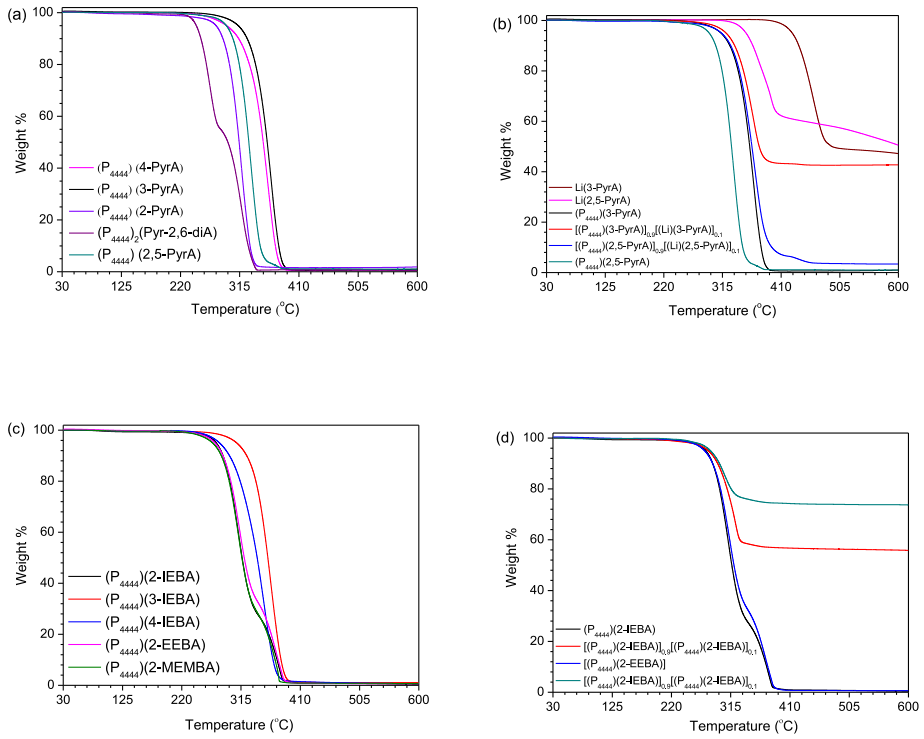

Figure 8. TGA thermograms of the neat ILs (a), (c) and the electrolytes made (b) and (d).

Differential scanning calorimetry (DSC) traces of the neat ILs and the electrolytes are shown in Figure 9. Multiple solid–solid phase transitions are observed for (P_{4444})(4-PyrA) and $(P_{4444})_2$(Pyr-2,6-diA), indicating ionic plastic crystal behavior.[94-96] (P_{4444})(4-PyrA) displays a low temperature glass transition at –35 °C, multiple solid–solid phase transitions at –9, 2 and

36 °C and, finally, a sharp melting transition with an onset at 42 °C. The DSC trace of $(P_{4444})_2$(Pyr-2,6-diA) shows a T_g at −16 °C, a relatively broader peak indicating multiple exothermic cold crystallizations at 31°C, followed by a sharp T_m with onset at *ca.* 118 °C (Figure 9b). A similar thermal behavior is observed for the neat (P_{4444})(3-PyrA) but in a much lower temperature range and behaved as a supercooled liquid upon heating, revealing T_g, T_c and T_m at −53, −15, and 31 °C, respectively. The neat (P_{4444})(2-PyrA), (P_{4444})(2,5-PyrA), (P_{4444})(2-IEBA), (P_{4444})(3-IEBA), (P_{4444})(4-IEBA), (P_{4444})(2-EEBA) and (P_{4444})(2-MEMBA) exhibit only glass transitions (Figure 9a and c).

The addition of 10 mol % of Li(3-PyrA) salt to (P_{4444})(3-PyrA) lead to a slight shift in the glass transition to −55 °C, however, both the crystallization and melting peaks are completely disappeared, and the resulting electrolyte behaves as a pure glass-forming liquid. This dramatic change in the thermal behavior is associated with the smaller radius of Li^+, causing an increase in the ionic strength and/or ion-ion interactions leading to the disruption of crystallization and melting peaks.[87] A similar change in the glass transition is observed for (P_{4444})(2,5-PyrA), (P_{4444})(2-IEBA), (P_{4444})(2-EEBA) when doped with 10 mol % Li-salt.

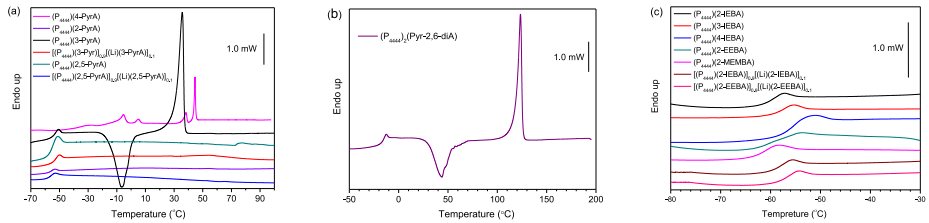

Figure 9. DSC traces for some neat ionic materials and their electrolytes.

4.3 Ionic Conductivity

When creating electrolytes for LIBs, conductivity is an important feature to be considered.[97,98] The ionic conductivities of some ILs and their electrolytes are shown in Figure 10. In the case of the ILs with aromatic heterocyclic anion (**Paper I**), the neat (P_{4444})(3-PyrA) IL and its electrolyte shows higher ionic conductivity over the whole temperature range as compared with the neat (P_{4444})(2,5-PyrA) IL and the corresponding electrolyte. The difference in ionic conductivity of these systems is linked to the simultaneous influence of electronic structures and flexibility of the ions generated by variations in the geometrical forms or steric hindrance.[99] In the case of (P_{4444})(3-PyrA), the negative inductive and resonance effects in the anion reduces the ionic interactions and thus provide higher ionic conductivity than the (P_{4444})(2,5-PyrA) IL.

For the aromatic carbocyclic ILs, we found that changing the position of the ether functionality can influence the ionic conductivity to a larger extent than changing length of the ether functional group. The (P_{4444})(2-IEBA) IL with ortho substitution shows the highest conductivity among its structural analogues, which is attributed to the reduced ionic interactions as a result of the repulsion between the terminal isopropyl group of the $(2\text{-IEBA})^-$ anion and alkyl chains of the $(P_{4444})^+$ cation. The para substituted (P_{4444})(4-IEBA) IL reveals the lowest ionic conductivity because the ether group is far from carboxylate group and there is no hindrance for the $(P_{4444})^+$ cation to approach the $(4\text{-IEBA})^-$ anion. The (P_{4444})(2-EEBA) IL with a shorter ether chain provide comparable ionic conductivity to the (P_{4444})(2-MEMBA) IL with a slightly longer ether chain, which is in accordance with the previous findings for ether functionalized cation-based ILs[100] (Figure 10b, **Paper II**).

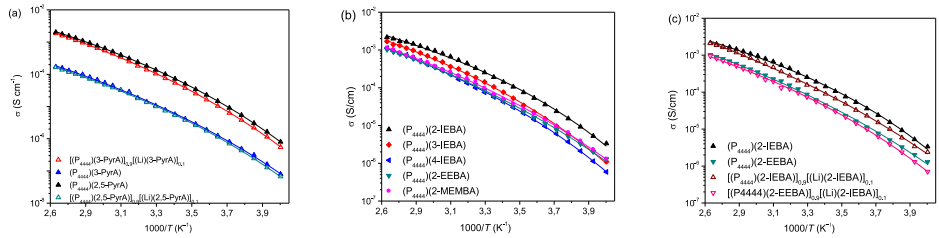

Figure 10. Ionic conductivity as a function of temperature for the neat ILs and the electrolytes (a) **Paper I**, for the neat ILs (b) and the electrolytes (c) **Paper II.**

The addition of Li^+ ions to the ILs lead to a slight decrease in the ionic conductivity of the electrolytes, which is primarily due the reduction of free volume as a result of stronger electrostatic interactions (Figures 10a and 10c). It is quite expected because the incorporation of Li^+ ions into ILs is known to create clusters by simultaneous coordination with multiple anions, leading to dynamic cross-linking and thus reduce the overall ionic mobility. The ionic conductivities are further analyzed by fitting the data to the Vogel-Fulcher-Tammann (VFT) equation.[101,102]

$$\sigma = \sigma_0 \exp\left(\frac{-B}{(T - T_0)}\right) \qquad (2)$$

Where σ_0 is a pre-exponential factor, B and T_0 are adjustable parameters of Equation (2), where the former is an empirical material-dependent fitting parameter related to the dynamic T_g and activation/pseudo activation energy (E_σ) of the system, and later referred to the ideal vitreous

transition temperature, at which configurational entropy vanishes, which can be determined by fitting the temperature-dependent conductivity data to the VFT equation for the best linearity relationship. The E_σ value of (P_{4444})(2,5-PyrA) is slightly greater than the E_σ of (P_{4444})(3-PyrA) (Table 1), suggesting a relatively larger thermal energy is required to achieve the same ion mobility. The resulting VFT parameters for IEBA-based neat ILs show that the E_σ decreases in the order (P_{4444})(4-IEBA) > (P_{4444})(3-IEBA) > (P_{4444})(2-IEBA) (Table 1), which agrees well with the DSC data and again indicates that a higher thermal energy is required to reach the same ion mobility.

On the other hand, an increase in the E_σ values is observed for the electrolytes, which is yet another indication of relatively stronger interactions between the Li^+ ion and the organic ions within the electrolytes. As expected, the T_0 values in all these systems are about 50-60 K smaller than the glass transition temperatures T_g and agree well to the empirical approximation of ionic liquids-based electrolytes: $T_0/T_g \approx 0.75$.[103]

Table 1. VFT equation parameters and apparent activation energies for ionic conductivity of the neat aromatic heterocyclic anions based ILs and the electrolytes.

System	σ_0 (mS/cm)	B (K)	T_0 (K)	E_σ, (kJ/mol)
(P_{4444}) (3-PyrA)	1.218	1381	156	11.4
(P_{4444}) (2,5-PyrA)	0.135	1496	150	12.4
[(P_{4444})(3-PyrA)]$_{0.9}$ [(Li)(3-PyrA)]$_{0.1}$	2.352	1600	148	13.3
[(P_{4444}) (2,5-PyrA)]$_{0.9}$ [(Li)(2,5-PyrA)]$_{0.1}$	0.216	1626	143	13.5
(P_{4444})(2-IEBA)	0.293	993	167	8.3
(P_{4444})(3-IEBA)	0.616	1254	159	10.4
(P_{4444})(4-IEBA)	2.45	1690	132	14.1
(P_{4444})(2-EEBA)	0.933	1609	135	13.4
(P_{4444})(2-MEMBA)	0.556	1416	144	11.8
[(P_{4444})(2-IEBA)]$_{0.9}$ [(Li)(2-IEBA)]$_{0.1}$	0.678	1422	151	11.8
[(P_{4444})(2-EEBA)]$_{0.9}$ [(Li)(2-EEBA)]$_{0.1}$	0.376	1331	152	11.1

4.4 Electrochemical stability

Applicability of IL-based electrolytes in LIBs is profoundly governed by their ability to withstand the working potential range. A relatively reliable means to measure the potential range of stability is by performing either linear sweep or cyclic voltammetry.[104] In this thesis, the electrochemical stability of all the ILs and the electrolytes is determined by using linear sweep voltammetry (LSV). Both cathodic and anodic LSV experiments were performed at 20

°C using a scan rate of 1 mV s^{-1}. The ESWs limits were defined by a 0.1 mA cm^{-2} cut-off current density.

Figure 11a shows the cathodic and anodic scans of the neat aromatic heterocyclic anions based ILs and the electrolytes. During cathodic scans, all the ILs and electrolytes reveal continuous reduction below 1 V (*vs* Li/Li^+), which is consistent with the previous reports on phosphonium-based ILs.[86,105,106] The low cathodic stability of phosphonium-based ILs is attributed to the presence of acidic alpha methylene protons of the phosphonium cations.[107] (P_{4444})(3-PyrA) shows improved cathodic potential among other neat ILs which again would be related to the electronic donating effect of the nitrogen atom towards carboxylate group *via* resonance effect, resulted in shielding of alpha protons of cations through strong ionic interaction (**Paper I**). For the same reason among the oligoether functionalized ILs, (P_{4444})(3-IEBA) shows improved cathodic potential as compared with the other neat ILs, which again might be related to the electron donating effect of the oxygen atom towards carboxylate group *via* resonance effect. On the anodic side, anions of the neat ILs are oxidizing between 3.50-4.00 V (*vs* Li/Li^+). An increase in the number of ethoxy units in the anions increases the anodic limit (**Paper II**).

The $[(P_{4444})(2\text{-EEBA})]_{0.9}[(Li)(2\text{-EEBA})]_{0.1}$ electrolyte shows an oxidation peak at 3.79 V (*vs* Li/Li^+), which might be due to the oxidation of the ethoxy groups present in the anion.[108] In addition, two pronounced peaks C_1 and C_2 observed on the cathodic scan side at 1.30, and 0.75 *vs* Li/Li^+ V. The C_1 and C_2 peaks can be associated with the underpotential deposition (UPD) of lithium and partial decomposition of the $(P_{4444})^+$ cation on GC electrode.[56,57] The UPD layer formation can modify the nature of the GC working electrode surface, which is beneficial for the extended cathodic limits of the electrolytes, where the Li^+ ions can pass and prevent further reduction of the $(P_{4444})^+$ cation.

Overall, the ESWs (*ca.* 2.29–3.74 V) (Table 2) of these novel ILs are comparable with the commonly studied imidazolium-[109] and phosphonium[110]-based ILs containing TFSI and other fluorinated anions. However, all of these ESWs should be regarded as the upper limits because we are utilizing a sweep approach and the ILs and the electrolytes are viscous at room temperature.

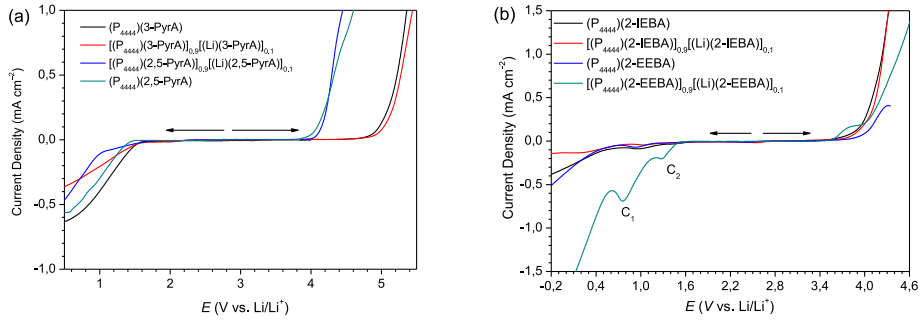

Figure 11. LSV curves of the neat aromatic heterocyclic anions based ILs and electrolytes (a) and the aromatic carbocyclic ILs and electrolytes (b).

Table 2. Cathodic limit and anodic limit and ESWs of the neat ILs and the electrolytes at 20 °C using GC as a WE. The ESWs limits were defined by a 0.1 mA cm^{-2} cut-off current density.

System	E_C (V vs Li/Li^+)	E_A (V vs Li/Li^+)	ESW
(P_{4444})(2-IEBA)	0.53	3.85	3.32
(P_{4444})(3-IEBA)	0.40	3.89	3.49
(P_{4444})(4-IEBA)	0.88	4.01	3.13
(P_{4444})(2-EEBA)	0.43	4.02	3.59
(P_{4444})(2-MEMBA)	1.12	4.20	3.08
$[(P_{4444})$(2-IEBA)$]_{0.9}$ $[$(Li)(2-IEBA)$]_{0.1}$	0.42	3.89	3.47
$[(P_{4444})$(2-EEBA)$]_{0.9}$ $[$(Li)(2-EEBA)$]_{0.1}$	1.39	3.68	2.29
(P_{4444}) (3-PyrA)	4.97	1.39	3.57
$[(P_{4444})$(3-PyrA)$]_{0.9}$ [Li(3-PyrA)$]_{0.1}$	5.03	1.29	3.74
(P_{4444}) (2,5-PyrA)	4.09	1.27	2.82
$[(P_{4444})$ (2,5-PyrA)$]_{0.9}$ [Li(2,5-PyrA)$]_{0.1}$	4.15	1.02	3.13

4.5 NMR Diffusometry

Following the establishment of overall mobilities at a more macroscopic level using DSC and impedance spectroscopy, PFG NMR diffusometry was used to better understand the ionic mobility and, in particular, the effect of Li^+ ion addition on the overall diffusivity of the IL-based electrolytes. It is observed that the diffusional decays (DDs) for the neat ILs and the IL-based electrolytes has a single exponential form (Equation 1) and are not affected by the diffusion time t_d. Experimental DDs are then fitted to Equation 1 to obtain the diffusion coefficients.

For the all system, as expected, the PFG NMR diffusion coefficients of all species show monotonous increases as a function of temperature and follows the VFT behavior, temperature

dependency of self-diffusion coefficients of these systems is shown in Figure 12. For neat system containing heterocyclic moieties (**Paper I**) the diffusion of ions are accordance to ionic sizes, and the anions diffuse faster than the cation across the whole temperature range. A comparison between two neat systems show that the $(2,5\text{-PyrA})^-$ diffuse slower than (3-PyrA), which is again due presence of an extra nitrogen atom in the aromatic rings which not only increase the ionic size but also can increase ionic interactions.

Interestingly, for oligoether substituted carbocyclic ILs (**Paper II**) self-diffusion coefficients of cation (D_{cation}) and anion (D_{anion}) in all the neat ILs measured by ^{1}H NMR is approximately same and cannot be separated, which is primarily due that their comparable molar masses (Figures 12b). For heterocyclic systems, doping Li salts, reduces the diffusion of both cation and anion to the same extent, indicating the formation of aggregates, facilitated by interaction of anion with Li ions through the present nitrogen atom. The addition of lithium salts to the ILs lead to a decrease in diffusivity of both cations and anions due to additional electrostatic interactions in the systems leading ion clustering and thus reduced diffusivity (Figures 12a).

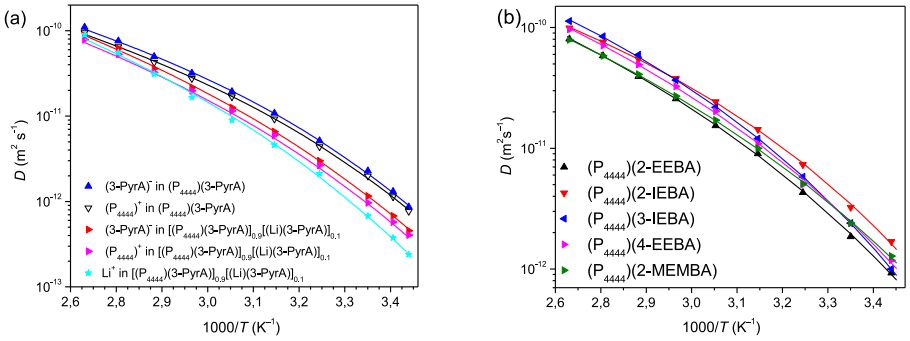

Figure 12. Diffusion coefficients of ions in the (a) neat (P_{4444})(3-PyrA) IL and its electrolyte and (b) the neat aromatic carbocyclic IL. Symbols indicate experimental data and the solid lines represent the VFT fittings.

4.6 Infrared Spectroscopy

FTIR spectroscopy is employed to better understand the ionic interactions in the neat ILs and the electrolytes, mainly focusing on the symmetric and asymmetric stretching of the carboxylate group, C–O stretching and CH_2 rocking bands of the anions (Figure 13). In the case of (P_{4444})(3-PyrA) and (P_{4444})(2,5-PyrA) ILs, the prominent single bands centered at 1603 cm^{-1} and 1615

cm^{-1} with shoulders on the right side, suggesting single mode of interaction, which is more similar to a carbonyl group interaction.[111] The symmetric stretching band of the carboxylate group appears as a single and symmetrical peak at *ca.* 1350 cm^{-1} for (P_{4444})(3-PyrA) and (P_{4444})(2,5-PyrA) ILs again indicates one kind of ionic interactions and justifying the low melting of these materials. For the other systems, (P_{4444})(2-PyrA), (P_{4444})(4-PyrA) and (P_{4444})$_2$(Pyr-2,6-diA) the asymmetric stretching bands appeared in the frequency range (1570–1650 cm^{-1}) and the symmetric stretching bands at (1320–1370 cm^{-1}), suggesting the presence of long range strong ionic interactions justifying their room temperature solid/semi-solid nature. A similar sort of absorption peaks for the carbonyl group was observed for the oligoether substituted ILs, which are detailed in **Paper II.**

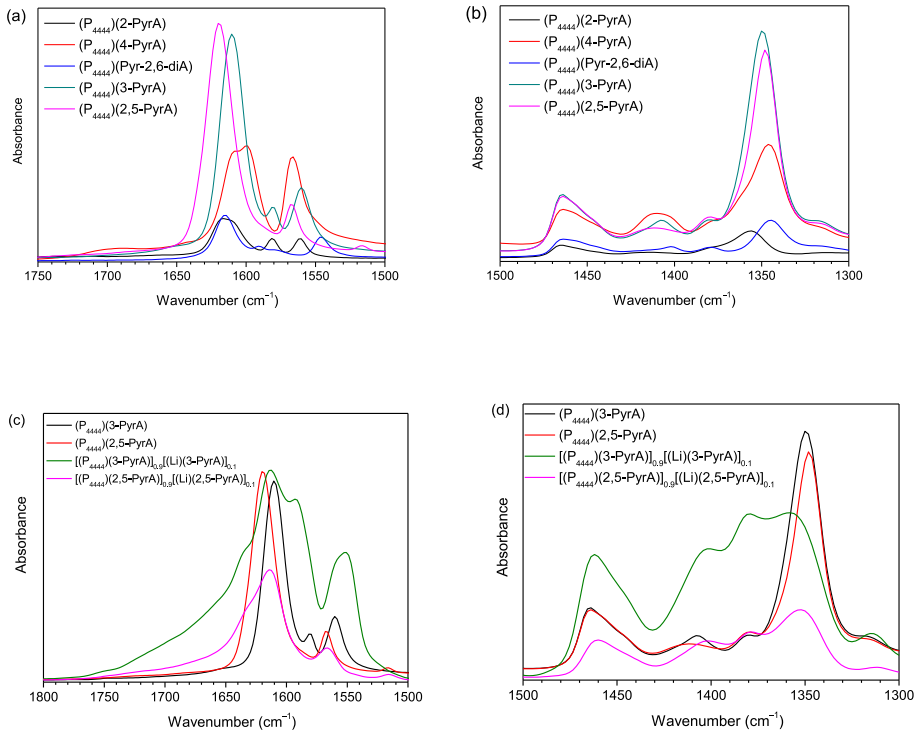

Figure 13. FTIR spectra of (a and b) the neat ILs and (c and d) the electrolytes.

The modes of cation–anion interactions change upon doping of the neat ILs with the corresponding lithium salts. In the case of [(P_{4444})(2,5-PyrA)]$_{0.9}$[(Li)(2,5-PyrA)]$_{0.1}$ electrolyte, two new asymmetric stretching bands at 1380 and 1400 cm^{-1} appeared in addition to original peak at 1350 cm^{-1} (Figure 7d), while a significant broadening of the asymmetric band at 1615

cm^{-1} with distinct shoulders at both sides occurred. Similar spectral features are observed in the case of $[(P_{4444})(3\text{-PyrA})]_{0.9}[(Li)(3\text{-PyrA})]_{0.1}$ electrolyte. These drastic changes in the infrared absorption behavior clearly suggests the interaction of Li^+ ion with carboxylate groups of the anions.

5. Conclusions

In this work, new classes of fluorine-free ILs comprising different anions and the most popular cations such as phosphonium, pyrrolidinium and imidazolium. The established structure-reactivity relationship significantly contributes to the understanding of how minor structural tuning of one counterpart can have a significant impact on the overall physiochemical properties of the ionic materials. The ILs and electrolytes comprising aromatic heterocyclic analogous anions based on pyridine and pyrazine coupled to a common $(P_{4444})^+$ cation revealed promising physicochemical and electrochemical performance. The neat (P_{4444})(3-PyrA) IL and its electrolyte exhibit much superior thermal and electrochemical stabilities, higher ionic conductivity and ion diffusivity. Among all the ions, Li^+ ions revealed slowest diffusivity in the electrolytes suggesting stronger electrostatic interactions leading to ion association. It is found that altering the position of nitrogen atom in the aromatic ring of the anion can dramatically affect the cation-anion interactions and influence the overall physiochemical properties of the ionic materials, ranging from RTILs and organic ionic plastic crystals.

In the case of ILs and the electrolytes with anions based on oligoether substituted aromatic carboxylates coupled to a common *n*- tetrabutylphosphonium $(P_{4444})^+$ cation, the nature and position of the attached oligoether chain to the phenyl ring dramatically influenced the physicochemical and electrochemical properties. Despite the structural similarities, (P_{4444})(2-IEBA) IL offered key beneficial properties including lower T_g, higher ionic conductivity and higher ion diffusivity. This IL, however, revealed lower dynamic thermal stability than its structural isomers (P_{4444})(3-IEBA) and (P_{4444})(4-IEBA) ILs. As expected, the addition of Li^+ ions to the ILs decrease ionic mobility and leading to reduced ionic conductivity and ion diffusivity, although a monotonous increase in both the ionic conductivity and ion diffusivity is observed as a function of temperature. The anions diffused faster within the electrolytes than the $(P_{4444})^+$ cation and Li^+ ion, in spite of the fact that FTIR revealed interactions between the Li^+ ions and the carboxylate group of the anions.

The other new classes of fluorine-free oligoether functionalized ILs and their concentrated electrolytes with two different cations such as imidazolium and pyrrolidinium coupled to two oligoether anions, $(MEA)^-$ and $(MEEA)^-$, revealed quite different thermal properties but comparable ion transport behaviors. The pyrrolidinium-based ILs exhibited lower thermal stability but at the same time revealed lower glass transition temperatures than the corresponding imidazolium-based ILs. It was found that the solubility of the lithium salts is quite high in these ILs, up to 80 mol % of the lithium salts are dissolved in the parent ILs.

Altogether, the newly created ILs and the electrolytes have promising properties to be used as electrolytes in next-generations batteries operating at elevated temperatures and over a wide potential range.

6. References

(1) Höök, M.; Tang, X. Depletion of fossil fuels and anthropogenic climate change—A review. *Energy policy* **2013,** *52*, 797.

(2) Etacheri, V.; Marom, R.; Elazari, R.; Salitra, G.; Aurbach, D. Challenges in the development of advanced Li-ion batteries: a review. *Energy & Environmental Science* **2011,** *4* (9), 3243.

(3) Zeng, X.; Li, M.; Abd El-Hady, D.; Alshitari, W.; Al-Bogami, A. S.; Lu, J.; Amine, K. Commercialization of lithium battery technologies for electric vehicles. *Advanced Energy Materials* **2019,** *9* (27), 1900161.

(4) Kim, H.; Park, Y.-U.; Park, K.-Y.; Lim, H.-D.; Hong, J.; Kang, K. Novel transition-metal-free cathode for high energy and power sodium rechargeable batteries. *Nano Energy* **2014,** *4*, 97.

(5) Wang, G.; Wang, F.; Zhang, P.; Zhang, J.; Zhang, T.; Müllen, K.; Feng, X. Polarity-switchable symmetric graphite batteries with high energy and high power densities. *Advanced Materials* **2018,** *30* (39), 1802949.

(6) Nealer, R.; Hendrickson, T. Review of recent lifecycle assessments of energy and greenhouse gas emissions for electric vehicles. *Current Sustainable/Renewable Energy Reports* **2015,** *2* (3), 66.

(7) Sierzchula, W.; Bakker, S.; Maat, K.; Van Wee, B. The influence of financial incentives and other socio-economic factors on electric vehicle adoption. *Energy policy* **2014,** *68*, 183.

(8) Balali, Y.; Stegen, S. Review of energy storage systems for vehicles based on technology, environmental impacts, and costs. *Renewable and Sustainable Energy Reviews* **2021,** *135*, 110185.

(9) Dehghani-Sanij, A.; Tharumalingam, E.; Dusseault, M.; Fraser, R. Study of energy storage systems and environmental challenges of batteries. *Renewable and Sustainable Energy Reviews* **2019,** *104*, 192.

(10) Choi, D.; Shamim, N.; Crawford, A.; Huang, Q.; Vartanian, C. K.; Viswanathan, V. V.; Paiss, M. D.; Alam, M. J. E.; Reed, D. M.; Sprenkle, V. L. Li-ion battery technology for grid application. *Journal of Power Sources* **2021,** *511*, 230419.

(11) Yu, X.; Manthiram, A. Sustainable battery materials for next-generation electrical energy storage. *Advanced Energy and Sustainability Research* **2021,** *2* (5), 2000102.

(12) Lin, Z.; Liu, T.; Ai, X.; Liang, C. Aligning academia and industry for unified battery performance metrics. *Nature communications* **2018,** *9* (1), 1.

(13) Park, G.; Nakamura, H.; Lee, Y.; Yoshio, M. The important role of additives for improved lithium ion battery safety. *Journal of Power Sources* **2009,** *189* (1), 602.

(14) Doi, T.; Zhao, L.; Zhou, M.; Okada, S.; Yamaki, J.-i. Quantitative studies on the thermal stability of the interface between graphite electrode and electrolyte. *Journal of Power Sources* **2008,** *185* (2), 1380.

(15) https://www.iea.org/reports/global-ev-outlook-2020

(16) Jow, T. R.; Xu, K.; Borodin, O.; Ue, M. *Electrolytes for lithium and lithium-ion batteries*; Springer, 2014.

(17) Hernández, G.; Mogensen, R.; Younesi, R.; Mindemark, J. Fluorine-Free Electrolytes for Lithium and Sodium Batteries. *Batteries & Supercaps* **2022**, e202100373.

(18) Xu, K. Electrolytes and interphases in Li-ion batteries and beyond. *Chemical reviews* **2014,** *114* (23), 11503.

(19) Zhang, S. S. A review on electrolyte additives for lithium-ion batteries. *Journal of Power Sources* **2006,** *162* (2), 1379.

(20) Zhang, X.; Ji, L.; Toprakci, O.; Liang, Y.; Alcoutlabi, M. Electrospun nanofiber-based anodes, cathodes, and separators for advanced lithium-ion batteries. *Polymer Reviews* **2011,** *51* (3), 239.

(21) Yim, T.; Kwon, M. S.; Mun, J.; Lee, K. T. Room temperature ionic liquid-based electrolytes as an alternative to carbonate-based electrolytes. *Israel Journal of Chemistry* **2015,** *55* (5), 586.

(22) Smart, M.; Ratnakumar, B.; Surampudi, S. Electrolytes for low-temperature lithium batteries based on ternary mixtures of aliphatic carbonates. *Journal of the Electrochemical Society* **1999,** *146* (2), 486.

(23) Kalhoff, J.; Eshetu, G. G.; Bresser, D.; Passerini, S. Safer electrolytes for lithium-ion batteries: state of the art and perspectives. *ChemSusChem* **2015,** *8* (13), 2154.

(24) Von Aspern, N.; Röschenthaler, G. V.; Winter, M.; Cekic-Laskovic, I. Fluorine and lithium: ideal partners for high-performance rechargeable battery electrolytes. *Angewandte Chemie International Edition* **2019,** *58* (45), 15978.

(25) Asenbauer, J.; Eisenmann, T.; Kuenzel, M.; Kazzazi, A.; Chen, Z.; Bresser, D. The success story of graphite as a lithium-ion anode material–fundamentals, remaining challenges, and recent developments including silicon (oxide) composites. *Sustainable Energy & Fuels* **2020,** *4* (11), 5387.

(26) Liu, K.; Liu, Y.; Lin, D.; Pei, A.; Cui, Y. Materials for lithium-ion battery safety. *Science advances* **2018,** *4* (6), eaas9820.

(27) Han, J. G.; Kim, K.; Lee, Y.; Choi, N. S. Scavenging materials to stabilize LiPF6-containing carbonate-based electrolytes for Li-ion batteries. *Advanced Materials* **2019,** *31* (20), 1804822.

(28) Chou, S.-L.; Pan, Y.; Wang, J.-Z.; Liu, H.-K.; Dou, S.-X. Small things make a big difference: binder effects on the performance of Li and Na batteries. *Physical Chemistry Chemical Physics* **2014,** *16* (38), 20347.

(29) Krossing, I.; Raabe, I. Noncoordinating anions—fact or fiction? A survey of likely candidates. *Angewandte Chemie International Edition* **2004,** *43* (16), 2066.

(30) Xu, K.; Zhang, S.; Jow, T. R.; Xu, W.; Angell, C. A. LiBOB as salt for lithium-ion batteries: a possible solution for high temperature operation. *Electrochemical and Solid-State Letters* **2001,** *5* (1), A26.

(31) Ilyas, F.; Ishaq, M.; Jabeen, M.; Saeed, M.; Ihsan, A.; Ahmed, M. Recent trends in the benign-by-design electrolytes for zinc batteries. *Journal of Molecular Liquids* **2021,** *343*, 117606.

(32) Tang, S.; Baker, G. A.; Zhao, H. Ether-and alcohol-functionalized task-specific ionic liquids: attractive properties and applications. *Chemical Society Reviews* **2012,** *41* (10), 4030.

(33) Gabriel, S.; Weiner, J. Ueber einige abkömmlinge des propylamins. *Berichte der deutschen chemischen Gesellschaft* **1888,** *21* (2), 2669.

(34) Walden, P. Ueber die Molekulargrosse und elektrische Leitfahigkeit einiger geschmolzenen Salze. *Известия Российской академии наук. Серия математическая* **1914,** *8* (6), 405.

(35) Sun, X.; Luo, H.; Dai, S. Ionic liquids-based extraction: a promising strategy for the advanced nuclear fuel cycle. *Chemical reviews* **2012,** *112* (4), 2100.

(36) Zhang, Q.; Shreeve, J. n. M. Energetic ionic liquids as explosives and propellant fuels: a new journey of ionic liquid chemistry. *Chemical reviews* **2014,** *114* (20), 10527.

(37) de María, P. D. *Ionic liquids in biotransformations and organocatalysis: solvents and beyond*; John Wiley & Sons, 2012.

(38) Wilkes, J. S.; Zaworotko, M. J. Air and water stable 1-ethyl-3-methylimidazolium based ionic liquids. *Journal of the Chemical Society, Chemical Communications* **1992,** (13), 965.

(39) Ohno, H.; Fukumoto, K. Electrochemistry 2008, 76, 16–23; c) M. Armand, F. Endres, DR MacFarlane, H. Ohno, B. Scrosati. *Nat. Mater* **2009,** *8*, 621.

(40) Abu-Lebdeh, Y.; Abouimrane, A.; Alarco, P.-J.; Armand, M. Ionic liquid and plastic crystalline phases of pyrazolium imide salts as electrolytes for rechargeable lithium-ion batteries. *Journal of power sources* **2006,** *154* (1), 255.

(41) Ui, K.; Minami, T.; Ishikawa, K.; Idemoto, Y.; Koura, N. Development of non-flammable lithium secondary battery with ambient-temperature molten salt electrolyte: Performance of binder-free carbon-negative electrode. *Journal of power sources* **2005,** *146* (1-2), 698.

(42) MacFarlane, D.; Tachikawa, N.; Forsyth, M.; Pringle, J.; Howlett, P.; Eliott, G.; Davis, J. James H., M. Watanabe, P. Simon and CA Angell. *Energy Environ. Sci* **2014,** *7*, 232.

(43) Sebastiao, E.; Cook, C.; Hu, A.; Murugesu, M. Recent developments in the field of energetic ionic liquids. *Journal of Materials Chemistry A* **2014,** *2* (22), 8153.

(44) Ye, Y.-S.; Rick, J.; Hwang, B.-J. Ionic liquid polymer electrolytes. *Journal of Materials Chemistry A* **2013,** *1* (8), 2719.

(45) Marr, P. C.; Marr, A. C. Ionic liquid gel materials: applications in green and sustainable chemistry. *Green Chemistry* **2016,** *18* (1), 105.

(46) MacFarlane, D. R.; Forsyth, M.; Howlett, P. C.; Kar, M.; Passerini, S.; Pringle, J. M.; Ohno, H.; Watanabe, M.; Yan, F.; Zheng, W. Ionic liquids and their solid-state analogues as materials for energy generation and storage. *Nature Reviews Materials* **2016,** *1* (2), 1.

(47) Roe, C.; Feng, X.; White, G.; Li, R.; Wang, H.; Rui, X.; Li, C.; Zhang, F.; Null, V.; Parkes, M. Immersion cooling for lithium-ion batteries–A review. *Journal of Power Sources* **2022,** *525*, 231094.

(48) Rüther, T.; Bhatt, A. I.; Best, A. S.; Harris, K. R.; Hollenkamp, A. F. Electrolytes for lithium (sodium) batteries based on ionic liquids: Highlighting the key role played by the anion. *Batteries & Supercaps* **2020,** *3* (9), 793.

(49) Li, J.; Zhu, Z., 2014.

(50) Forsyth, M.; Porcarelli, L.; Wang, X.; Goujon, N.; Mecerreyes, D. Innovative electrolytes based on ionic liquids and polymers for next-generation solid-state batteries. *Accounts of chemical research* **2019,** *52* (3), 686.

(51) Piper, D. M.; Evans, T.; Leung, K.; Watkins, T.; Olson, J.; Kim, S. C.; Han, S. S.; Bhat, V.; Oh, K. H.; Buttry, D. A. Stable silicon-ionic liquid interface for next-generation lithium-ion batteries. *Nature communications* **2015,** *6* (1), 1.

(52) Barghamadi, M.; Best, A. S.; Bhatt, A. I.; Hollenkamp, A. F.; Musameh, M.; Rees, R. J.; Rüther, T. Lithium–sulfur batteries—the solution is in the electrolyte, but is the electrolyte a solution? *Energy & Environmental Science* **2014,** *7* (12), 3902.

(53) Barghamadi, M.; Best, A. S.; Bhatt, A. I.; Hollenkamp, A. F.; Mahon, P. J.; Musameh, M.; Rüther, T. Effect of LiNO3 additive and pyrrolidinium ionic liquid on the solid electrolyte interphase in the lithium–sulfur battery. *Journal of Power Sources* **2015,** *295*, 212.

(54) Haskins, J. B.; Bennett, W. R.; Wu, J. J.; Hernández, D. M.; Borodin, O.; Monk, J. D.; Bauschlicher Jr, C. W.; Lawson, J. W. Computational and experimental investigation of Li-doped ionic liquid electrolytes:[pyr14][TFSI],[pyr13][FSI], and [EMIM][BF4]. *The Journal of Physical Chemistry B* **2014,** *118* (38), 11295.

(55) Brutti, S.; Simonetti, E.; De Francesco, M.; Sarra, A.; Paolone, A.; Palumbo, O.; Fantini, S.; Lin, R.; Falgayrat, A.; Choi, H. Ionic liquid electrolytes for high-voltage, lithium-ion batteries. *Journal of Power Sources* **2020,** *479*, 228791.

(56) Nirmale, T. C.; Khupse, N. D.; Kalubarme, R. S.; Kulkarni, M. V.; Varma, A. J.; Kale, B. B. Imidazolium-Based Dicationic Ionic Liquid Electrolyte: Strategy toward Safer Lithium-Ion Batteries. *ACS Sustainable Chemistry & Engineering* **2022**.

(57) Foropoulos Jr, J.; DesMarteau, D. D. Synthesis, properties, and reactions of bis ((trifluoromethyl) sulfonyl) imide,(CF3SO2) 2NH. *Inorganic Chemistry* **1984,** *23* (23), 3720.

(58) Benrabah, D.; Baril, D.; Sanchez, J.-Y.; Armand, M.; Gard, G. G. Comparative electrochemical study of new poly (oxyethylene)–Li salt complexes. *Journal of the Chemical Society, Faraday Transactions* **1993,** *89* (2), 355.

(59) Choquette, Y.; Brisard, G.; Parent, M.; Brouillette, D.; Perron, G.; Desnoyers, J. E.; Armand, M.; Gravel, D.; Slougui, N. Sulfamides and glymes as aprotic solvents for lithium batteries. *Journal of the Electrochemical Society* **1998,** *145* (10), 3500.

(60) Zhang, H.; Han, H.; Cheng, X.; Zheng, L.; Cheng, P.; Feng, W.; Nie, J.; Armand, M.; Huang, X.; Zhou, Z. Lithium salt with a super-delocalized perfluorinated sulfonimide anion as conducting salt for lithium-ion cells: Physicochemical and electrochemical properties. *Journal of Power Sources* **2015,** *296*, 142.

(61) Izgorodina, E. I.; Forsyth, M.; MacFarlane, D. R. Towards a better understanding of 'delocalized charge'in ionic liquid anions. *Australian journal of chemistry* **2007,** *60* (1), 15.

(62) Macfarlane, D. R.; Meakin, P.; Sun, J.; Amini, N.; Forsyth, M. Pyrrolidinium imides: a new family of molten salts and conductive plastic crystal phases. *The Journal of Physical Chemistry B* **1999,** *103* (20), 4164.

(63) Katayama, Y.; Morita, T.; Yamagata, M.; Miura, T. Electrodeposition of metallic lithium on a tungsten electrode in 1-butyl-1-methylpyrrolidinium bis (trifluoromethanesulfone) imide room-temperature molten salt. *Electrochemistry* **2003,** *71* (12), 1033.

(64) MATSUMOTO, H.; KAGEYAMA, H.; MIYAZAKI, Y. Effect of ionic additives on the limiting cathodic potential of EMI-based room temperature ionic liquids. *Electrochemistry* **2003,** *71* (12), 1058.

(65) Howlett, P. C.; Brack, N.; Hollenkamp, A. F.; Forsyth, M.; Macfarlane, D. R. Characterization of the lithium surface in N-methyl-N-alkylpyrrolidinium bis (trifluoromethanesulfonyl) amide room-temperature ionic liquid electrolytes. *Journal of the electrochemical society* **2006,** *153* (3), A595.

(66) Zhao, L.; Yamaki, J.-i.; Egashira, M. Analysis of SEI formed with cyano-containing imidazolium-based ionic liquid electrolyte in lithium secondary batteries. *Journal of power sources* **2007,** *174* (2), 352.

(67) Sakaebe, H.; Matsumoto, H.; Tatsumi, K. Application of room temperature ionic liquids to Li batteries. *Electrochimica Acta* **2007,** *53* (3), 1048.

(68) Seki, S.; Mita, Y.; Tokuda, H.; Ohno, Y.; Kobayashi, Y.; Usami, A.; Watanabe, M.; Terada, N.; Miyashiro, H. Effects of alkyl chain in imidazolium-type room-temperature ionic liquids as lithium secondary battery electrolytes. *Electrochemical and Solid-State Letters* **2007,** *10* (10), A237.

(69) Shin, J.-H.; Henderson, W. A.; Passerini, S. An elegant fix for polymer electrolytes. *Electrochemical and solid-state letters* **2005,** *8* (2), A125.

(70) Shin, J.-H.; Henderson, W.; Appetecchi, G.; Alessandrini, F.; Passerini, S. Recent developments in the ENEA lithium metal battery project. *Electrochimica acta* **2005,** *50* (19), 3859.

(71) Sayed, F. N.; Rodrigues, M.-T. F.; Kalaga, K.; Gullapalli, H.; Ajayan, P. Curious case of positive current collectors: Corrosion and passivation at high temperature. *ACS applied materials & interfaces* **2017,** *9* (50), 43623.

(72) Matsumoto, K.; Inoue, K.; Nakahara, K.; Yuge, R.; Noguchi, T.; Utsugi, K. Suppression of aluminum corrosion by using high concentration LiTFSI electrolyte. *Journal of power sources* **2013,** *231*, 234.

(73) Garcia, B.; Armand, M. Aluminium corrosion in room temperature molten salt. *Journal of power sources* **2004,** *132* (1-2), 206.

(74) Armand, M.; Johansson, P. Novel weakly coordinating heterocyclic anions for use in lithium batteries. *Journal of power sources* **2008,** *178* (2), 821.

(75) Jankowski, P.; Dranka, M.; Wieczorek, W.; Johansson, P. TFSI and TDI anions: Probes for solvate ionic liquid and disproportionation-based lithium battery electrolytes. *The Journal of Physical Chemistry Letters* **2017,** *8* (15), 3678.

(76) Johansson, P.; Nilsson, H.; Jacobsson, P.; Armand, M. Novel Hückel stabilised azole ring-based lithium salts studied by ab initio Gaussian-3 theory. *Physical Chemistry Chemical Physics* **2004,** *6* (5), 895.

(77) Niedzicki, L.; Żukowska, G.; Bukowska, M.; Szczeciński, P.; Grugeon, S.; Laruelle, S.; Armand, M.; Panero, S.; Scrosati, B.; Marcinek, M. New type of imidazole based salts designed specifically for lithium ion batteries. *Electrochimica acta* **2010,** *55* (4), 1450.

(78) Niedzicki, L.; Kasprzyk, M.; Kuziak, K.; Żukowska, G.; Armand, M.; Bukowska, M.; Marcinek, M.; Szczeciński, P.; Wieczorek, W. Modern generation of polymer electrolytes based on lithium conductive imidazole salts. *Journal of Power Sources* **2009,** *192* (2), 612.

(79) Niedzicki, L.; Kasprzyk, M.; Kuziak, K.; Żukowska, G.; Marcinek, M.; Wieczorek, W.; Armand, M. Liquid electrolytes based on new lithium conductive imidazole salts. *Journal of Power Sources* **2011,** *196* (3), 1386.

(80) Niedzicki, L.; Grugeon, S.; Laruelle, S.; Judeinstein, P.; Bukowska, M.; Prejzner, J.; Szczecinski, P.; Wieczorek, W.; Armand, M. New covalent salts of the 4+ V class for Li batteries. *Journal of Power Sources* **2011,** *196* (20), 8696.

(81) Jónsson, E.; Armand, M.; Johansson, P. Novel pseudo-delocalized anions for lithium battery electrolytes. *Physical Chemistry Chemical Physics* **2012,** *14* (17), 6021.

(82) Hosseini-Bab-Anari, E.; Boschin, A.; Mandai, T.; Masu, H.; Moth-Poulsen, K.; Johansson, P. Fluorine-free salts for aqueous lithium-ion and sodium-ion battery electrolytes. *RSC advances* **2016,** *6* (88), 85194.

(83) Shi, C.; Quiroz-Guzman, M.; DeSilva, A.; Brennecke, J. F. Physicochemical and electrochemical properties of ionic liquids containing aprotic heterocyclic anions doped with lithium salts. *Journal of The Electrochemical Society* **2013,** *160* (9), A1604.

(84) Savateev, A.; Liedel, C.; Tröger-Müller, S.; de León, A. S.; Antonietti, M.; Dontsova, D. Halogen free 1, 2, 3-and 1, 2, 4-triazolide based ionic liquids: synthesis and properties. *Chemical Communications* **2017,** *53* (73), 10192.

(85) Shah, F. U.; Gnezdilov, O. I.; Gusain, R.; Filippov, A. Transport and association of ions in lithium battery electrolytes based on glycol ether mixed with halogen-free orthoborate ionic liquid. *Scientific reports* **2017,** *7* (1), 1.

(86) Khan, I. A.; Gnezdilov, O. I.; Wang, Y.-L.; Filippov, A.; Shah, F. U. Effect of Aromaticity in Anion on the Cation–Anion Interactions and Ionic Mobility in Fluorine-Free Ionic Liquids. *The Journal of Physical Chemistry B* **2020,** *124* (52), 11962.

(87) Khan, I. A.; Gnezdilov, O. I.; Filippov, A.; Shah, F. U. Ion Transport and Electrochemical Properties of Fluorine-Free Lithium-Ion Battery Electrolytes Derived from Biomass. *ACS Sustainable Chemistry & Engineering* **2021,** *9* (23), 7769.

(88) Karimi, N.; Zarrabeitia, M.; Mariani, A.; Gatti, D.; Varzi, A.; Passerini, S. Nonfluorinated ionic liquid electrolytes for lithium metal batteries: ionic conduction, electrochemistry, and interphase formation. *Advanced Energy Materials* **2021,** *11* (4), 2003521.

(89) Blümich, B.; Wiley Online Library, 1995.

(90) Tanner, J. E. Use of the stimulated echo in NMR diffusion studies. *The Journal of Chemical Physics* **1970,** *52* (5), 2523.

(91) Marinković, A.; Drmanić, S.; Jovanović, B. Ž.; Misić-Vuković, M. Investigations of the reactivity of pyridine carboxylic acids with diazodiphenylmethane in protic and aprotic solvents, Part I: Pyridine mono-carboxylic acids. *Journal of the Serbian Chemical Society* **2005,** *70* (4), 557.

(92) Shah, F. U.; Khan, I. A.; Johansson, P. Comparing the thermal and electrochemical stabilities of two structurally similar ionic liquids. *Molecules* **2020,** *25* (10), 2388.

(93) Efimova, A.; Pfützner, L.; Schmidt, P. Thermal stability and decomposition mechanism of 1-ethyl-3-methylimidazolium halides. *Thermochimica Acta* **2015,** *604*, 129.

(94) Pringle, J. M.; Howlett, P. C.; MacFarlane, D. R.; Forsyth, M. Organic ionic plastic crystals: recent advances. *Journal of Materials Chemistry* **2010,** *20* (11), 2056.

(95) Jin, L.; Howlett, P.; Efthimiadis, J.; Kar, M.; Macfarlane, D.; Forsyth, M. Lithium doped N, N-dimethyl pyrrolidinium tetrafluoroborate organic ionic plastic crystal electrolytes for solid state lithium batteries. *Journal of materials chemistry* **2011,** *21* (27), 10171.

(96) Shah, F. U.; Glavatskih, S.; Dean, P. M.; MacFarlane, D. R.; Forsyth, M.; Antzutkin, O. N. Halogen-free chelated orthoborate ionic liquids and organic ionic plastic crystals. *Journal of Materials Chemistry* **2012,** *22* (14), 6928.

(97) Ghandi, K. A review of ionic liquids, their limits and applications. *Green and sustainable chemistry* **2014,** *2014*.

(98) Ueno, K.; Tokuda, H.; Watanabe, M. Ionicity in ionic liquids: correlation with ionic structure and physicochemical properties. *Physical Chemistry Chemical Physics* **2010,** *12* (8), 1649.

(99) Nordness, O.; Brennecke, J. F. Ion dissociation in ionic liquids and ionic liquid solutions. *Chemical Reviews* **2020,** *120* (23), 12873.

(100) Fang, S.; Zhang, Z.; Jin, Y.; Yang, L.; Hirano, S.-i.; Tachibana, K.; Katayama, S. New functionalized ionic liquids based on pyrrolidinium and piperidinium cations with two ether groups as electrolytes for lithium battery. *Journal of Power Sources* **2011,** *196* (13), 5637.

(101) Garca-Coln, L.; Del Castillo, L.; Goldstein, P. Theoretical basis for the Vogel-Fulcher-Tammann equation. *Physical Review B* **1989,** *40* (10), 7040.

(102) Bandrés, I.; Montaño, D. F.; Gascón, I.; Cea, P.; Lafuente, C. Study of the conductivity behavior of pyridinium-based ionic liquids. *Electrochimica acta* **2010,** *55* (7), 2252.

(103) Silvester, D. S. Recent advances in the use of ionic liquids for electrochemical sensing. *Analyst* **2011,** *136* (23), 4871.

(104) Chavan, S. N.; Tiwari, A.; Nagaiah, T. C.; Mandal, D. Ether and siloxane functionalized ionic liquids and their mixtures as electrolyte for lithium-ion batteries. *Physical Chemistry Chemical Physics* **2016,** *18* (24), 16116.

(105) Wibowo, R.; Jones, S. E. W.; Compton, R. G. Investigating the electrode kinetics of the Li/Li+ couple in a wide range of room temperature ionic liquids at 298 K. *Journal of Chemical & Engineering Data* **2010,** *55* (3), 1374.

(106) Fraser, K. J.; MacFarlane, D. R. Phosphonium-based ionic liquids: an overview. *Australian journal of chemistry* **2009,** *62* (4), 309.

(107) Tsunashima, K.; Sugiya, M. Physical and electrochemical properties of low-viscosity phosphonium ionic liquids as potential electrolytes. *Electrochemistry Communications* **2007,** *9* (9), 2353.

(108) Shah, F. U.; Gnezdilov, O. I.; Khan, I. A.; Filippov, A.; Slad, N. A.; Johansson, P. Structural and ion dynamics in fluorine-free oligoether carboxylate ionic liquid-based electrolytes. *The Journal of Physical Chemistry B* **2020,** *124* (43), 9690.

(109) Kazemiabnavi, S.; Zhang, Z.; Thornton, K.; Banerjee, S. Electrochemical stability window of imidazolium-based ionic liquids as electrolytes for lithium batteries. *The Journal of Physical Chemistry B* **2016,** *120* (25), 5691.

(110) De Vos, N.; Maton, C.; Stevens, C. V. Electrochemical stability of ionic liquids: general influences and degradation mechanisms. *ChemElectroChem* **2014,** *1* (8), 1258.

(111) Shah, F. U.; Holmgren, A.; Rutland, M. W.; Glavatskih, S.; Antzutkin, O. N. Interfacial behavior of orthoborate ionic liquids at inorganic oxide surfaces probed by NMR, IR, and raman spectroscopy. *The Journal of Physical Chemistry C* **2018,** *122* (34), 19687.

Paper I

Aromatic Heterocyclic Anion Based Ionic Liquids and Electrolytes

Mukhtiar Ahmed, Soniya Rao, Andrei Filippov, Patrik Johansson, and Faiz Ullah Shah

(*Manuscript*)

Aromatic Heterocyclic Anion Based Ionic Liquids and Electrolytes

Mukhtiar Ahmed[1], Soniya Rao[2], Andrei Filippov[1], Patrik Johansson[2*], and Faiz Ullah Shah[1*]

[1]Chemistry of Interfaces, Luleå University of Technology, SE-971 87 Luleå, Sweden

[2]Department of Physics, Chalmers University of Technology, SE-412 96 Gothenburg, Sweden

[*]Corresponding authors:

patrik.johansson@chalmers.se

faiz.ullah@ltu.se

Abstract

This study is focused on five new ionic materials comprising distinct aromatic heterocyclic anions based on pyridine and pyrazine combined with a common *n*-tetrabutylphosphonium cation, $(P_{4444})^+$. Two of the ionic materials are room temperature ionic liquids (RTILs), one semi-solid and two organic ionic plastic crystals with melting points > 20 °C. For both the neat RTILs and the Li^+ conducting electrolytes, created by 10 mol % doping with the corresponding Li-salts, the interactions mainly depend on the position of the nitrogen atom with respect to the carboxylate group in the anions. Furthermore, for the RTILs the anions diffuse faster than the $(P_{4444})^+$ cation, but are slowed down by doping the neat RTILs with lithium salts due to increased ionic interactions. The carboxylate group of the anions interacts strongly with the Li^+ cation, as suggested by both experimental and computational studies.

Introduction

Since their introduction by Sony in 1990, lithium-ion batteries (LIBs) have acquired a sizable market share.[1,2] They have the best energy densities, a high open circuit voltage, a low self-discharge rate, no memory effect, and a slow loss of charge when not in use. These properties make them the most popular rechargeable batteries for portable gadgets, electric vehicles and aerospace applications.[3,4] They do, however, have serious safety issues due to the electrolytes made up of fluorinated salts dissolved in flammable organic solvents.[5,6] Several attempts have been made to use nonflammable solvents, thermally and electrochemically stable (non-fluorinated) Li-salts, as well as additives to improve the safety.[7-12]

Electrolytes based on ionic liquids (ILs) in general offer a range of suitable advantages[13-15] including low volatility and high thermal and electrochemical stabilities, and can additionally be made task-specific and fluorine-free.[16,17] In general, their physicochemical properties are determined by the interactions between the cations and anions, which are controlled by the chemical functionalities present, with vast freedom in structural design to reduce these interactions and enhance also the ion mobilities.[18] The selection of cation and anion in an IL also play a crucial role in determining the thermal and electrochemical stabilities as well as ionic mobility.

In this work, we investigate the effect of structural variations in novel ionic materials derived from nicotinic acid more commonly known as niacin, a form of vitamin B_3.[19,20] Nicotinic acid is chosen due to its sustainable nature, and the small and compact structure of the anion. In addition, structural analogues of nicotinic acid are selected for a systematic comparison, all the anions are based on six-membered aromatic nitrogen heterocycles and coupled with a common tetra(*n*-butylphosphonium) cation $(P_{4444})^+$. Doping of the ILs with the analogous lithium salts renders Li^+ conducting electrolytes. Both the neat ILs and the electrolytes are studied through

experimental and computational studies with respect to basic physicochemical including ionic interactions and mobilities of all the ions and electrochemical properties.

Experimental

Materials

2-picolic acid (2-PyrA), nicotinic acid (3-PyrA), *iso*nicotinic acid (4-PyrA), pyrazinoic acid (2,5-PyrA), 2,6-pyridinedicarboxylic acid (Pyr-2,6-diA), an aqueous solution of tetrabutylphosphonium hydroxide (40 wt % in water), lithium hydroxide monohydrate (ACS reagents, >98 % purity) were received from Sigma-Aldrich and used without further purification. Sodium sulphate and diethyl ether were purchased from VWR (BDH) chemicals. The electrolytes were prepared by mixing 10 mol % of Li(3-PyrA) and Li(2,5-PyrA) in corresponding RTILs. For concentration higher than 10 mol %, phase separation was detected and, therefore, higher concentrations were not prepared.

Synthesis

Ionic Materials: An aqueous solution of the tetrabutylphosphonium hydroxide (50 mmol), was added drop wise into the stirred aqueous solution of the acid (50 mmol in 50 ml of water) – thus in stoichiometric amounts. The reaction mixture was stirred at room temperature for 4 hours and the progress of the reaction was monitored *via* thin layer chromatography (TLC) and upon completion water was removed under reduced pressure using a rotary evaporator. The products were washed three times with 50 ml diethyl ether before being dissolved in dichloromethane and dried with anhydrous sodium sulphate. Finally, the solution was filtered, residual solvent was removed under reduced pressure, and the final products were dried in a vacuum oven at 80 °C for more than 4 days. All the products were separated in quantitative yields. After purification and drying; (P_{4444})(3-PyrA) and (P_{4444})(2,5-PyrA) were obtained as RTILs, (P_{4444})(4-PyrA) and (P_{4444})(Pyr-2,6-diA) solids, and (P_{4444})(2-PyrA) as a semi-solid. The water content was measured by Karl Fischer titration (using Metrohm 917 Coulometer, Switzerland)

and was determined to be less than 60 ppm for all the synthesized ionic materials. The formation and purity of the synthesized ionic materials were assessed by mass spectrometry and multinuclear (^{1}H, ^{13}C, and ^{31}P) NMR spectroscopy.

Lithium Salts: Lithium (Li) salts of nicotinic acid (3-PyrA) and pyrazinoic acid (2,5-PyrA) were prepared by direct neutralization of the acids with lithium bicarbonate ($LiHCO_3$). Under continuous stirring, aqueous solutions of the acids were treated with solid $LiHCO_3$ in small portions, until the generation of gas bubbles stopped. The salts were obtained in quantitative yields after lyophilization and subsequent drying in vacuum oven.

Nuclear Magnetic Resonance Spectroscopy

The structures and purity of all the synthesized compounds were confirmed by using a Bruker Ascend Aeon WB 400 (Bruker BioSpin AG, Fallanden, Switzerland) NMR spectrometer. $CDCl_3$ and D_2O were used as solvents for the ionic materials and the lithium salt, respectively. The working frequencies were 400.21 MHz for ^{1}H, 100.64 MHz for ^{13}C, 155.53 MHz for ^{7}Li and 162.01 MHz for ^{31}P. Data were processed using Bruker Topspin 3.5 software.

Thermal Analysis

Thermogravimetric analysis (TGA) was performed using a PerkinElmer TGA 8000 under N_2 gas at a heating rate of 10 °C per min using *ca.* 2-4 mg samples. The onset of decomposition temperature, T_{onset}, was calculated from the intersection of the baseline weight and the tangent of the weight versus temperature curve using Pyris software. Differential scanning calorimetry (DSC) was performed using a PerkinElmer DSC 6000 on *ca.* 2-5 mg of sample placed in an aluminum pan. DSC data were collected at a scanning rate of 5 °C min^{-1} for both cooling and heating traces ranging from -75 to 200 °C. To maintain an inert environment inside the sample chamber, dry N_2 gas was delivered at a constant flow rate of 20 mL min^{-1}. The T_g was determined by using the inflection mid-point of the initial *S*-shaped transition slope and determined from the onset with the aid of Pyris software.

Electrochemical Characterization

The electrochemical stability and ionic conductivity were determined using a Metrohm Autolab PGSTAT302N electrochemical workstation with a FRA32M module for impedance measurements, all of which were controlled by Nova 2.02 software. A sealed Microcell HC from RHD instruments was used to hold about 70 µL of sample. To determine the electrochemical stability window (ESW), linear sweep voltammetry (LSV) was performed with a three-electrode setup: a Pt wire with a diameter of 0.25 mm as working electrode (WE), a Pt crucible as counter electrode (CE), as well as sample container, and an Ag wire coated with AgCl as a pseudo-reference electrode (RE). Both cathodic and anodic scans were recorded at a rate of 1 mV s^{-1}. The electrochemical potentials were calibrated using ferrocene (Fc) as internal reference and shifted using $E_{Li/Li^+} \approx E_{Fc/Fc^+} + 3.2$ V.[21] The ESWs limits were defined by a 0.1 mA cm^{-2} cut-off current density.

The ionic conductivity was obtained from the impedance measurements performed in a frequency range from 1 Hz to 1 MHz with an AC voltage amplitude of 10 mV_{rms}. All the impedance spectra were measured during heating and cooling over a temperature range from -20 to 100 ± 0.1 °C and the obtained ionic conductivities during heating and cooling match very well (Figure S17), thus only heating cycle data are presented. A two-electrode configuration was employed for ionic conductivity measurements, with a wire Pt as WE and a 70 µL Pt crucible as a sample container, as well as CE. Prior to each measurement, both the electrodes were polished with a 0.25 m of Kemet diamond paste. The cell constant was calculated using a Metrohm 100 S cm^{-1} KCl standard solution (K_{cell} = 18.5396 cm^{-1}). The cell was thermally equilibrated for 10 minutes before recording the impedance spectra.

Pulsed Field Gradient Diffusometry

NMR self-diffusion measurements were performed using a Bruker Ascend/Aeon WB 400 (Bruker BioSpin AG) NMR spectrometer with a resonance frequency of 400.27 MHz for ^{1}H and 155.56 MHz for ^{7}Li. Pulsed-Field Gradient (PFG) NMR self-diffusion measurements were performed on ^{1}H with a PFG NMR probe Diff50 (Bruker) with a maximum amplitude of the magnetic field gradient pulse of 29.73 T m^{-1}. The samples were placed in a standard 5 mm NMR glass tube and closed with a plastic stopper to avoid contact with air. Prior to measurements, each sample was equilibrated at a specific temperature for 30 min. The details of the PFG NMR technique for measuring molecular diffusion coefficients are available elsewhere.[22] The diffusivity of a molecule is the diffusion decay (DD) of amplitude A of NMR spectral line, obtained by Fourier transformation of a descending half of stimulated-echo (StE), as a function of the amplitude of applied pulsed field gradient. For the stimulated echo pulse sequence used, diffusion decay of A in the case of simple non-associating molecular liquid can be described by the Eq.(1):[23]

$$A(g,\delta,t_d) = A(0)\exp(-\gamma^2 g^2 \delta^2 D t_d) \quad (1)$$

where $A(0)$ is the factor proportional to the proton content in the system, and to spin-lattice and spin-spin relaxation times, γ is the gyromagnetic ratio for a used nucleus; g and δ are the amplitude and duration of the gradient pulse; t_d is the diffusion time; and D is the self-diffusion coefficient. t_d was in the range 4-100 ms for ^{1}H diffusion and 5-15 ms for ^{7}Li diffusion. No diffusion time dependence was observed in these measurements.

FTIR Spectroscopy

The attenuated total reflection Fourier transform infrared (ATR-FTIR) spectra of samples were recorded using a Bruker IFS 80v spectrometer equipped with a deuterated triglycine sulfate (DTGS) detector and diamond ATR accessory, employing the double-side forward–backward

acquisition mode. The total number of scans was 256, co-added and signal-averaged at an optical resolution of 4 cm^{-1}.

Computational Studies

The computational studies focus on the properties of Li^+-anion ion-pairs. First, geometry optimized structures of the 2-PyrA, 3-PyrA, 4-PyrA, and 2,5-PyrA Li^+ ion-pairs, interactions by the carboxyl group (Fig. S1), were obtained by density functional theory (DFT) employing the M06-2X functional[24,25] and the 6-311+ (d, p) basis set using Gaussian-16.[26-28] The structures were verified to be minima by calculating the second derivatives of the energy with respect to nuclear displacements. The ultrafine grid option was used in all cases.

Second, to gain further insight into how the charge distribution affects the ion-pair formation we evaluate the donor-acceptor interactions using Natural Bonding Orbitals (NBOs)[29] and the second-order Fock matrix (Tables S4-S8). The stabilization energy E[25] associated with donor NBO(i) and acceptor NBO(j) was computed by:

$$E^{(2)} = \Delta E_{ij} = q_i \left(\frac{(F(i,j))^2}{\varepsilon_j - \varepsilon_i}\right. \qquad (2)$$

where q_i is the orbital occupancy, ε_i and ε_j are diagonal elements (orbital energies) and $F_{(i,j)}$ is the off-diagonal NBO Fock matrix element.

Results and Discussions

We start with a brief description of the five ionic materials, followed by thermal properties assessment and the effect anion chemistry on the thermal stability of the synthesized ionic materials. The ionic materials and the IL electrolytes were further accessed by more LIB-relevant performance parameters such as ionic conductivity, ion diffusion, variable-temperature line width and chemical shift analysis and electrochemical stability before progressing to FTIR and computational calculations to further describe the local interactions, coordination, and ion–ion interactions.

Basics of synthesized ionic materials

The chemical structures of the ionic materials (Scheme 1) agree well with the NMR analysis (as well as the mass spectra SI). First, the aliphatic alkyl chains attached to the P_{4444} cation show distinct resonance lines in the ^{1}H NMR spectrum a triplet at 0.93 ppm for the terminal methyl groups, a multiplet 1.46-1.54 ppm for the methylene protons, and another multiplet 2.39-2.46 ppm for the eight protons of the carbon atoms directly attached to the phosphorous atom. Second, the presence of aromatic resonance lines, 6.5-8.5 ppm, and the lack of the broad resonance line for any acidic proton corroborated the deprotonation of the acids (Figures S1-5). Third, the aliphatic carbon atoms display characteristic resonance lines in the region 13-24 ppm in the ^{13}C NMR spectra (Figure S5-10), while those of the carboxylate groups in the anions are found in the range 168-171 ppm. Finally, the ^{31}P NMR spectra indicate a single resonance line at *ca.* 33 ppm (Figures S10-15).

Turning to the aggregation states of the five systems (P_{4444})(3-PyrA) and (P_{4444})(2,5-PyrA) are RTILs, (P_{4444})(2-PyrA) is a semi-solid, while $(P_{4444})_2$(Pyr-2,6-diA) and (P_{4444})(4-PyrA) are solids. The latter can arguably be due to stronger interionic interactions as well as the comparatively more symmetric $(4\text{-PyrA})^-$ and $(\text{Pyr-2,6-diA})^-$ anions, as symmetry is known to facilitate crystallinity.[30-32]

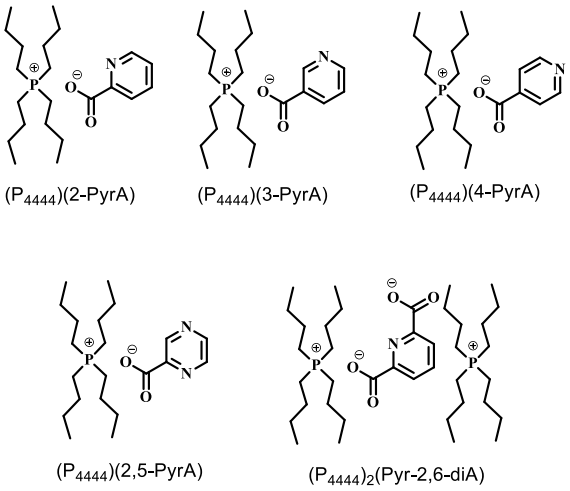

Scheme 1. Chemical structures and abbreviations of the five ionic materials.

Thermal Properties

The thermal stability of the neat ILs having a common *n*-butylphosphonium cation is ranging from 245 ºC to 330 ºC, mainly depending on nature of the coupled anion (Figure 1a and Table 1). The order of thermal stability is found in the following decreasing order: (P_{4444})(3-PyrA) > (P_{4444})(4-PyrA) > (P_{4444})(2,5-PyrA) > (P_{4444})(2-PyrA) > $(P_{4444})_2$(Pyr-2,6-diA). The general trend here is that thermal stability of the neat ILs increases as delocalization of the negative charge on anion increases. The fact that (P_{4444})(3-PyrA) IL exhibits the highest thermal stability, while (P_{4444})(4-PyrA) and (P_{4444})(2-PyrA) ILs have rather lower T_d values. This might be explained by the negative inductive and resonance effects (electron-donating effect) of the pyridine nitrogen, which can cause an extended delocalization of electrons and leading to a more polarizable structure resulting in better stabilized and thermally stable anion (Scheme 2).[33-35] In the case of (P_{4444})(2,5-PyrA), the presence of an extra nitrogen atom at 5-potision neutralizes the electron withdrawing effect generated by the nitrogen at 2-position and stabilize the anion to a greater extent as compared with the anion in (P_{4444})(2-PyrA), as evident from the T_d value of (P_{4444})(2,5-PyrA) IL.

The thermal stabilities of these new ILs are comparable to the previously phosphonium-based halogen-free ILs.[36,37] It is noteworthy that thermal stability of the Li-salts of these anions is substantially higher (by almost 100 ºC) than the corresponding neat ILs, which is attributed to the rigid, planner and aromatically stabilized structures of these anions that can facilitate efficient delocalization of electrons. The thermal stability of ILs is slightly improved by the addition of the 10 mol % Li salts by enhancing the rigidity of the resulting electrolytes (Figure 1b and Table 1).

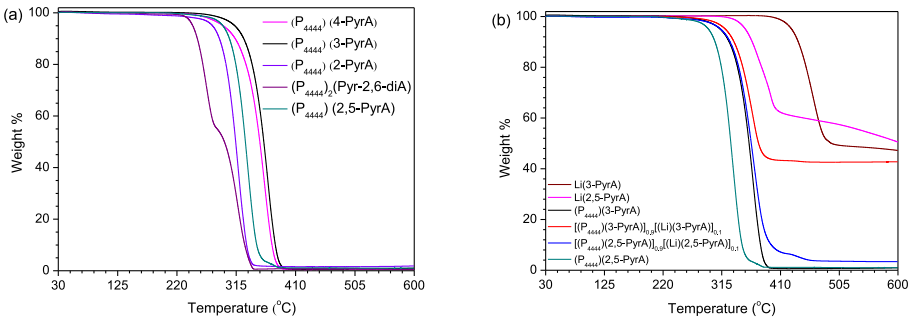

Figure 1. TGA thermograms of the neat ILs (a) and the Li(3-PyrA), Li(2,5-PyrA) $[(Li)^{+}(3\text{-}PyrA)]_{0.1}[(P_{4444})(\ (3\text{-}PyrA))]_{0.9}$ and $[(Li)^{+}(2,5\text{-}PyrA)]_{0.1}[(P_{4444})(2,5\text{-}PyrA)\ ]_{0.9}$ (b).

Differential scanning calorimetry (DSC) traces of the neat ILs and the electrolytes are shown in Figure 2 and their glass transition temperatures (T_g), exothermic cold crystallization (T_c), and melting points (T_m) are tabulated in Table 1. Multiple solid–solid phase transitions are observed for $(P_{4444})(4\text{-}PyrA)$ and $(P_{4444})_2(Pyr\text{-}2,6\text{-}diA)$, indicating ionic plastic crystal behavior.[38,39] $(P_{4444})(4\text{-}PyrA)$ displays a low temperature glass transition at –35 °C, multiple solid–solid phase transitions at –9, 2 and 36 °C and, finally, a sharp melting transition with an onset at 42 °C. The DSC trace of $(P_{4444})_2(Pyr\text{-}2,6\text{-}diA)$ shows a T_g at –16 °C, a relatively broader peak indicating multiple exothermic cold crystallizations at 31°C, followed by a sharp T_m with onset at ca. 118

°C (Figure 2b). A similar thermal behavior is exhibited by the neat (P_{4444})(3-PyrA) but in a much lower temperature range and behaved as a supercooled liquid upon heating, revealing T_g, T_c and T_m at −53, −15, and 31 °C, respectively. The neat (P_{4444})(2-PyrA) and (P_{4444})(2,5-PyrA) exhibit only glass transitions at −57 °C and −55 °C, respectively.

The addition of 10 mol % of Li(3-PyrA) salt to (P_{4444})(3-PyrA) lead to a slight shift in the glass transition to −55 °C, however, both the crystallization and melting peaks disappeared, and the resulting electrolyte behaves as a pure glass-forming liquid. This dramatic change in the thermal behavior is associated with the smaller radius of Li^+, causing an increase in the ionic strength and/or ion-ion interactions leading to the disruption of crystallization and melting peaks.[40] A similar change in the glass transition is observed for (P_{4444})(2,5-PyrA) after doping with 10 mol % of the Li-salt.

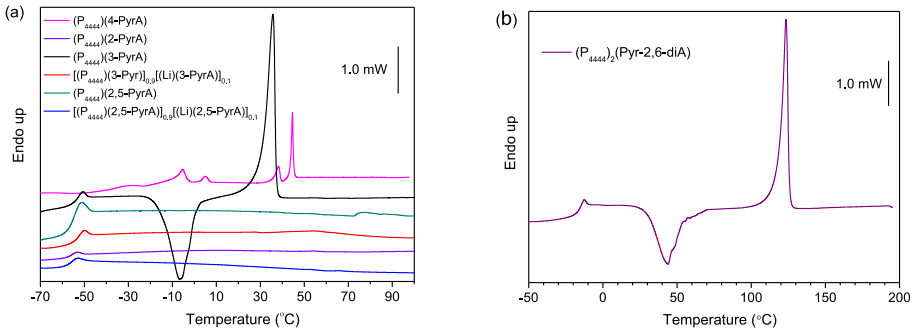

Figure 2. DSC traces for the neat ionic materials and the electrolytes.

Ionic Conductivity

Ionic conductivity is one of the key parameters to consider during design and optimization of IL electrolytes.[41,42] Ionic conductivities of the two neat RTILs and their electrolytes are measured over a temperature range from -20 to 100 °C and the values are plotted in the Arrhenius coordinates as shown in Figure 3. The neat (P_{4444})(3-PyrA) IL and its electrolyte

shows higher ionic conductivity over the whole temperature range as compared with the neat (P_{4444})(2,5-PyrA) IL and the corresponding electrolyte. The difference in ionic conductivity of these systems is linked to the simultaneous influence of electronic structures and flexibility of the ions generated by variations in the geometrical forms or steric hindrance. In the case of (P_{4444})(3-PyrA), the negative inductive and resonance effects in the anion reduces the ionic interactions and thus provide higher ionic conductivity than the (P_{4444})(2,5-PyrA) IL. The ionic conductivity of ILs is slightly decreased upon addition of the Li^+ ion due to the increase in the Coulombic interaction, leading to formation of aggregates consisting of Li^+ and the organic ions and result into reduced free volume and amount of charge carriers.[43] This behavior is previously observed for electrolytes containing $(P_{4444})^+$ cation and different anions. [16, 44]

The ionic conductivities are further analyzed by fitting the ionic conductivity data to the following Vogel-Fulcher-Tammann (VFT) equation.

$$\sigma = \sigma_0 \exp\left(\frac{-B}{(T - T_0)}\right) \quad (3)$$

Where σ_0 is a pre-exponential factor, B is an empirical material-dependent fitting parameter related to the dynamic T_g and activation/pseudo activation energy (E_σ) of the system. The reference temperature T_0 is attributed to the ideal vitreous transition temperature, at which configurational entropy vanishes.[45] T_0 is determined by fitting the temperature-dependent conductivity data to the VTF equation for the best linearity relationship. The E_σ value of (P_{4444})(2,5-PyrA) is slightly larger than the E_σ of (P_{4444})(3-PyrA) (Table S1), suggesting that a relatively larger thermal energy is required to achieve the same ion mobility. On the other hand, an increase in the E_σ values is observed for the electrolytes, which is yet another indication of the relatively stronger interactions between the Li^+ ion and the organic ions within the electrolytes. As expected, the T_0 values in all these systems are about 50 K smaller than the

glass transition temperatures T_g and agree well to the empirical approximation of ionic liquids-based electrolytes: $T_0/T_g \approx 0.75$.[46]

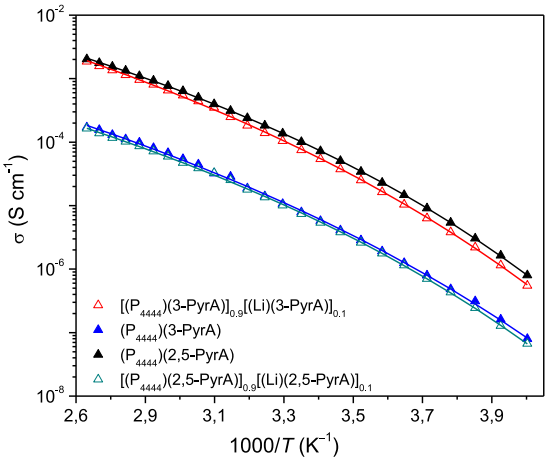

Figure 3. Ionic conductivity as a function of temperature for the neat ILs and the electrolytes. The solid lines indicate best fit of the data to the VFT equation.

NMR Diffusometry

PFG NMR diffusometry is used to better understand the ionic mobility and, in particular, the effect of Li^+ ion addition on the overall diffusivity of the IL-based electrolytes. It is observed that the diffusional decays (DDs) for the neat ILs and the IL-based electrolytes has a single exponential form (Equation 1) and are not affected by the diffusion time t_d. Experimental DDs are then fitted to Equation 1 to obtain the diffusion coefficients. Figure 3 depicts Arrhenius plots of the ion diffusion coefficients as a function of temperature. As expected, the diffusion coefficients of all the ions exhibit a monotonic increase as a function of temperature (Figure 4 and Table S1). The anion diffusivity is faster than the cation in their respective ILs across the whole studied temperature range, directly related to the ion sizes. A comparison of the two neat systems shows that the $(2,5\text{-PyrA})^-$ anion diffuses slower than the analogous $(3\text{-PyrA})^-$ anion,

which is due the presence of an extra nitrogen atom in the aromatic ring, not only increasing the ionic mass but also contribute towards stronger ionic interactions. The diffusivity of both cation and anion reduces after doping the neat ILs with lithium salts, indicating the formation of aggregates, facilitated by the relatively stronger ionic interactions of organic anions and the Li^+. Despite the lowest mass among these ions, Li^+ diffuses slower than both the organic ions particularly at lower temperatures, suggesting temperature dependent electrostatic interactions between the Li^+ and the organic anions.

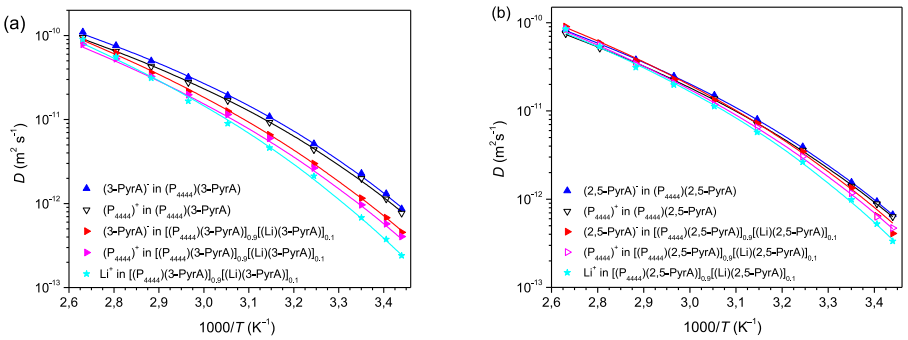

Figure 4. Diffusion coefficients of ions in the (a) neat (P_{4444})(3-PyrA) IL and its electrolyte and (b) neat (P_{4444})(2,5-PyrA) IL and its electrolyte. Symbols indicate experimental data and the solid lines represent the VFT fittings.

Because the temperature dependence of diffusion coefficients is in the non-linear convex form in Arrhenius coordinates, we applied VFT equation to fit the diffusivity data: [47,48]

$$D = D_0 \exp\left(\frac{-B}{(T - T_0)}\right) \tag{4}$$

where D_0, T_0, B are adjustable parameters. Energy of activation for diffusion is related with B as $E_D = B \times R$. We have described $D(T)$ by fitting D_0, T_0 and B. The results of fitting are shown

by solid lines in Figures 4 and the corresponding fitting parameters are presented in Table S2. It is clear that the VFT parameters are comparable for the cations and anions of these ILs but different for ions of the electrolytes. The comparable values of diffusion coefficients and activation energy of the cation and anion in these ILs might be explained by the fact that these diffusion processes occur in a homogeneous "matrix," where ion diffusivities are primarily determined by the "free volume".[49] However, the apparent activation energy for diffusion, E_D, changes slightly after doping the ILs with lithium salts, revealing a minimal role in the alteration of ionic diffusion when compared to D_0. T_0 values determined from ionic conductivity data are less than the T_0 values estimated from the diffusivity data. This is because the ion diffusion coefficients measured by PFG-NMR are average of the diffusion coefficients of the isolated, paired, clustered ions, and the neutral ion clusters, whereas the ionic conductivity is contributed by the mobility of electrochemically active ions.

^{7}Li and ^{31}P NMR Spectroscopy

Further insights into the dynamics and microscopic environment are gained from the variation in linewidths and chemical shifts of the electrolytes as a function of temperature analyzed by ^{7}Li and ^{31}P NMR spectroscopy (Figure. 5 Figure S. 22). As can be seen from Fig. 5a, the ^{7}Li linewidths of the electrolytes are sensitive to temperature. The quadrupole interactions are visible in the spectra of lower temperatures, which are averaged out at elevated temperatures. The ^{7}Li NMR line shape is narrowed at elevated temperatures and could be accurately fit with a Lorentzian line shape, which is common for ^{7}Li signals.[50]

The line widths initially increase with an increase in temperature and then decrease continuously over the whole studied temperature, suggesting a limited ion mobility at slightly elevated temperatures (Fig. 5a and Figure S. 22). This phenomenon is not entirely surprising because increased ion pairing, and ion aggregation is known to occur at higher temperatures.[51] Such an effect is expected to slightly immobilize the Li^+ cations resulting in broadening of the

line widths. However, the ion pairing is temperature-dependent and further increase in the temperature cause an ion dissociation and an increased ion mobility, such an exchange causes the ^{7}Li to experience an average environment leading to narrowing of the ^{7}Li resonance lines. ^{7}Li chemical shift values decrease with increase in the temperature, again suggesting ion aggregation and deshielding of Li^{+} ions at higher temperature. It is noteworthy that the line broadening at lower temperatures is more pronounced for $[(P_{4444})(2,5\text{-PyrA})]_{0.9}[(Li)(2,5\text{-PyrA})]_{0.1}$ electrolyte than the $[(P_{4444})(3\text{-PyrA})]_{0.9}[(Li)(3\text{-PyrA})]_{0.1}$ electrolyte, which might be due to the formation of thermodynamically stable clusters, which again can be explained due to the electronic effect of the nitrogen atom in the aromatic ring, facilitating stronger coordination of Li^{+} with the carboxylate group of $(3\text{-PyrA})^{-}$ anion. This agrees with the ionic conductivity data, as the addition of Li(3-PyrA) in RTIL lowered the conductivity to a larger extent than that obtained from the addition of Li(2,5-PyrA) in $(P_{4444})(2,5\text{-PyrA})$.

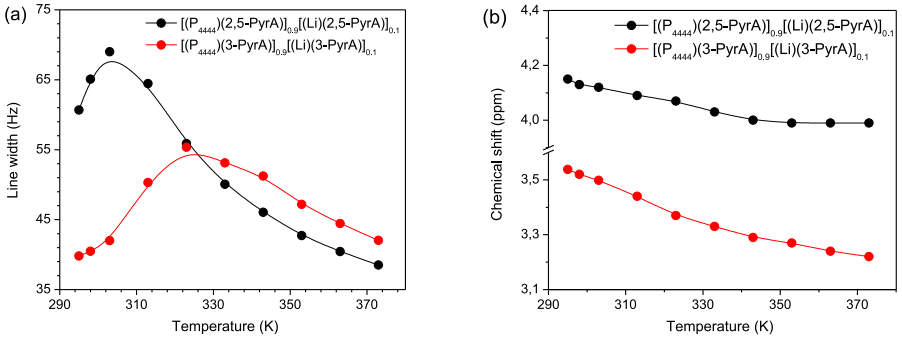

Figure 5. ^{7}Li NMR spectra of (a) $[(P_{4444})(3\text{-PyrA})]_{0.9}[(Li)(3\text{-PyrA})]_{0.1}$ and (b) $[(P_{4444})(2,5\text{-PyrA})]_{0.9}[(Li)(2,5\text{-PyrA})]_{0.1}$ electrolyte, and (c) the line width of these electrolytes as a function of temperature.

Electrochemical Stability

We employed both cathodic and anodic LSV experiments to determine the electrochemical stability window (ESW) of the neat ILs and their electrolytes (Figure 6 and Table S3). The

ESWs are found to be 3.57 and 2.82 V for (P_{4444})(3-PyrA) and (P_{4444})(2,5-PyrA), respectively, which are superior to the previously reported heterocyclic based halogen-free ILs.[52] The ESWs of the electrolytes are slightly wider by 10 mol % of the Li salt as compared with the neat ILs. For example, the ESWs of $[(P_{4444})(3\text{-PyrA})]_{0.9}[Li(3\text{-PyrA})]_{0.1}$ and $[(P_{4444})(2,5\text{-PyrA})]_{0.9}[Li(2,5\text{-diPyrA})]_{0.1}$ are 3.74 and 3.12 V, respectively, at 293 K. Such an improvement in the ESWs by doping Li salts is previously reported and can be attributed to the formation of passive layer on the surface of WE.[53,54]

The wider ESW of (P_{4444})(3-PyrA) IL than the (P_{4444})(2,5-PyrA) IL is explained by the extensive electron polarization and weaker ionic interactions of the $(3\text{-PyrA})^-$ anion with the counter $(P_{4444})^+$ cation, which can possibly house the incoming electrons and expand the anodic limit of this IL (Scheme 2). Another plausible reason for the relatively lower anodic limit of (P_{4444})(2,5-PyrA) IL might be due to the presence of two *N* atoms in the aromatic ring of $(2,5\text{-PyrA})^-$ anion, which are more susceptible to oxidation than the $(3\text{-PyrA})^-$ anion in (P_{4444})(3-PyrA) IL, the latter only has one *N* atom.[55]

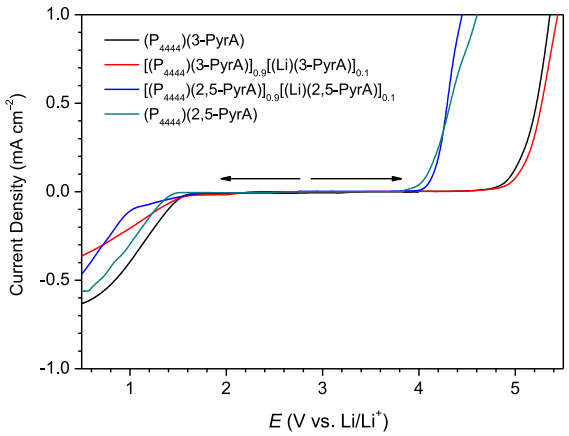

Figure 6. LSV curves of the neat ILs and the electrolytes using GC as the WE.

Table 1. Physiochemical properties of the synthesized ionic materials and the electrolytes.[a]

System	T_g (ºC)	T_c (ºC)	T_m (ºC)	$T_{s\text{-}s}$ (ºC)	T_d (ºC)	σ (S cm^{-1})
(P_{4444})(2-PyrA)	-57	---	---	---	291	---
(P_{4444})(3-PyrA)	-53	-15	31	---	332	1.00E^{-4}
(P_{4444})(4-PyrA)	-35	---	---	-9, 2, 36	317	---
(P_{4444})(2,5-PyrA)	-55	---	---	---	303	7.83 E^{-6}
$(P_{4444})_2$(Pyr-2,6-diA)	-16	31	118		245	---
$[(P_{4444})$(3-PyrA)$]_{0.9}$[Li(3-PyrA)$]_{0.1}$	-55	---	----	---	335	7.47E^{-5}
$[(P_{4444})$(2,5-PyrA)$]_{0.9}$[Li(2,5-PyrA)$]_{0.1}$	-57	---	---	---	330	7.73 E^{-6}

a=T_g: glass transition, T_c: cold crystallization, T_m: melting point, T_d: decomposition temperature, $T_{s\text{-}s}$: solid state transition, σ: ionic conductivity at 30 ºC.

Infrared Spectroscopy

FTIR spectroscopy is employed to further understand the ionic interactions in these ionic materials, and the possible role of Li^+ in these interactions (Figure 7 and Figure S23). The symmetric and asymmetric methyl and methylene stretching modes in the alkyl chains of the $(P_{4444})^+$ cation are attributed to the infrared bands between 3000 and 2800 cm^{-1}. The peaks appeared at 1600-1650 cm^{-1} and 1520-1590 cm^{-1} are assigned to the C=O (COO^-) asymmetrical stretching

and the C=C stretching, respectively. The C=N symmetric stretching, C=O symmetric stretching, and C-N stretching are responsible for the absorption peaks at 1430–1480, 1380–1420, and 1300–1330 cm^{-1}, respectively. The band at 1180–1140 cm^{-1} is designated to the C-O (COO^-) stretching peak. The peaks in the ranges 1030–1110 cm^{-1} and 650–820 cm^{-1} are attributed to the C-H in plane and out plane bending vibrations, respectively. The full range spectra are shown in Figure S23.

In the case of (P_{4444})(3-PyrA) and (P_{4444})(2,5-PyrA) ILs, the prominent single bands centered at 1603 cm^{-1} and 1615 cm^{-1} with shoulders on the right side, suggesting single mode of interaction, which is more similar to a carbonyl group interaction.[56] The symmetric stretching band of the carboxylate group appears as a single and symmetrical peak at *ca.* 1350 cm^{-1} for (P_{4444})(3-PyrA) and (P_{4444})(2,5-PyrA) ILs again indicates one kind of ionic interactions and justifying the low melting of these materials. For the other systems, (P_{4444})(2-PyrA), (P_{4444})(4-PyrA) and $(P_{4444})_2$(Pyr-2,6-diA) the asymmetric stretching bands appeared in the frequency range (1570–1650 cm^{-1}) and the symmetric stretching bands at (1320–1370 cm^{-1}), suggesting the presence of long range strong ionic interactions justifying their room temperature solid/semi-solid nature.

The modes of cation–anion interactions change upon doping of the neat ILs with the corresponding lithium salts. In the case of $[(P_{4444})(2,5\text{-PyrA})]_{0.9}[(Li)(2,5\text{-PyrA})]_{0.1}$ electrolyte, two new asymmetric stretching bands at 1380 and 1400 cm^{-1} appeared in addition to original peak at 1350 cm^{-1} (Figure 7d), while a significant broadening of the asymmetric band at 1615 cm^{-1} with distinct shoulders at both sides occurred. Similar spectral features are observed in the case of $[(P_{4444})(3\text{-PyrA})]_{0.9}[(Li)(3\text{-PyrA})]_{0.1}$ electrolyte. These drastic changes in the infrared absorption behavior clearly suggests the interaction of Li^+ ion with carboxylate groups of the anions.

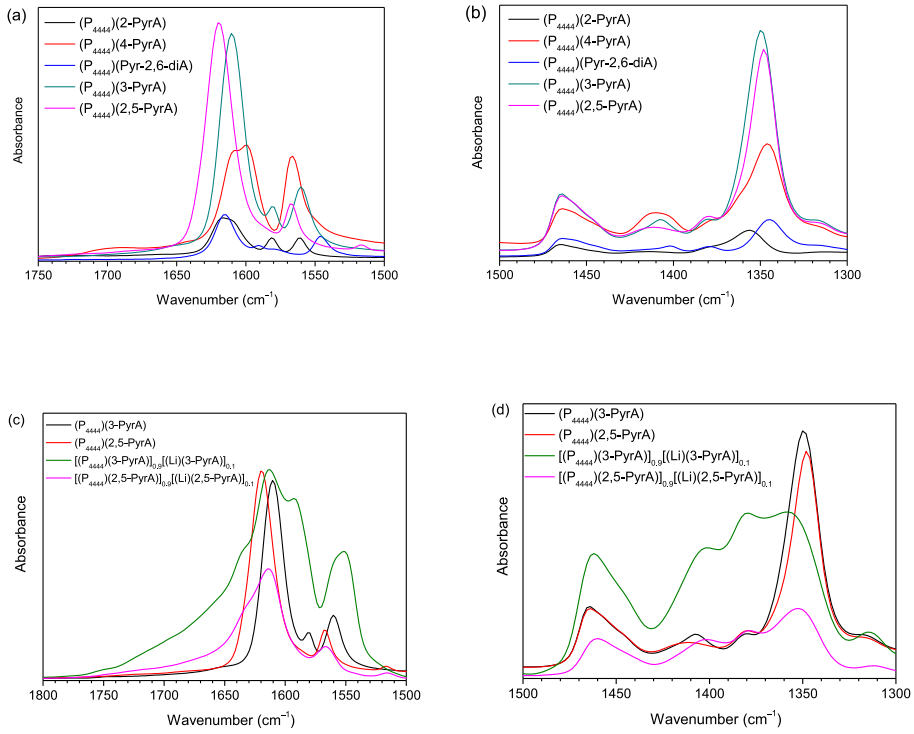

Figure 7. FTIR spectra of (a and b) the neat ILs and (c and d) the electrolytes.

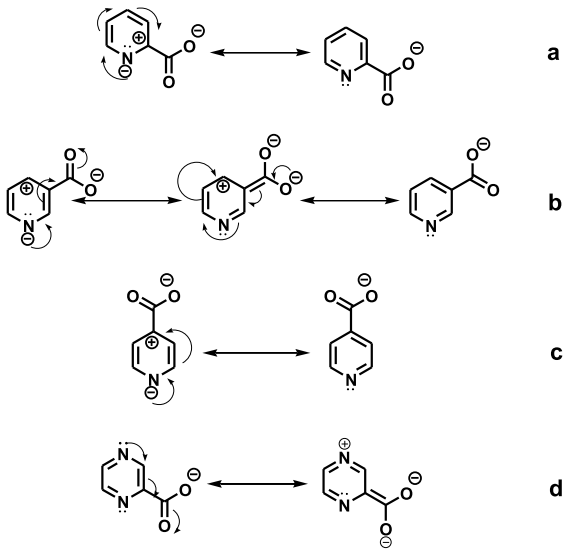

Scheme 2. Resonance structures of a) $(2\text{-PyrA})^-$, b) $(3\text{-PyrA})^-$, c) $(4\text{-PyrA})^-$ and $(2,5\text{-PyrA})^-$ anions.

Ion pair Interaction Energies and NBO

Starting with the ion-pair interactions, both the $(2\text{-PyrA})^-$ and the $(2,5\text{-PyrA})^-$ anions interact with Li^+ *via* both the ring nitrogen atom (N1) and the carboxylate group (Figure 8 and Figure S24), while the other two anions interact with the Li^+ ion only through the carboxylate oxygens. Overall, the interaction energies follow the order: $(2\text{-PyrA})^- > (2,5\text{-PyrA})^- > (3\text{-PyrA})^- > (4\text{-PyrA})^-$ indicating that the interaction of anion with Li^+ ion is strongest in $(2\text{-PyrA})^-$ and $(2,5\text{-PyrA})^-$. Stronger interactions between the Li^+ and anion leads to a decrease in the number of mobile ions and hence lower ionic conductivity and Li^+ ion diffusivity. Since $(2\text{-PyrA})^-$ and $(4\text{-PyrA})^-$ anions coupled with $(P_{4444})^+$ form room temperature solids/organic plastic crystals, therefore, $(3\text{-PyrA})^-$ and $(2,5\text{-pyrA})^-$ combined with $(P_{4444})^+$ cation can be used as potential liquid electrolytes for LIBs. $(3\text{-PyrA})^-$ has lower association energies which agrees well with the highest ionic conductivity provided by (P_{4444})(3-PyrA) IL.

In more detail, the stabilization energies and the NBO analysis foremost show strong interactions between the donor lone pairs (LP) of N1 and the antibonding acceptor π *C1-C2 (or C3-C4) orbitals within the aromatic ring for all anions (Tables S4-S7). The charge transfer from the aromatic ring to the carboxylate group is evident through σ C1-N1 → π* Ca=O1 delocalization. At the same time, the extension of delocalization of electrons in $(3\text{-PyrA})^-$ is evident through the significant σ C4 – C3 → π *Ca =O2 delocalization leading to a more polarizable structure (Table S6). Thus, σ-induction combined with π-delocalization results in significant push–pull effects on the electron density and delocalization.

Turning to the ion-pairs the electron delocalization within the aromatic ring, both σ C5–N1 → π* C1–C2 and σ C5–N1 → π*C4 –C5 increase significantly for Li^+–$(2\text{-PyrA})^-$ (Table S4). In contrast, the presence of an extra ring nitrogen atom in $(2,5\text{-PyrA})^-$ anion largely neutralizes the electron withdrawing effect of N1 and thereby stabilizes the anion, but again the ion-pair shows increased hyper-conjugative interactions (Table S8). The Li^+–$(3\text{PyrA})^-$ ion pair shows significantly higher σ C3– N1 → σ*C3 – C4 delocalization within the ring on Li^+ association compared to the other anions. Overall, comparing the two (P_{4444})(3-PyrA) and (P_{4444})(2,5-PyrA) RTILs, lower association energies of Li^+–$(3\text{-PyrA})^-$ anion and higher delocalization of negative charges compared to $(2,5\text{-PyrA})^-$ anion make it a better candidate as an electrolyte for LIBs.

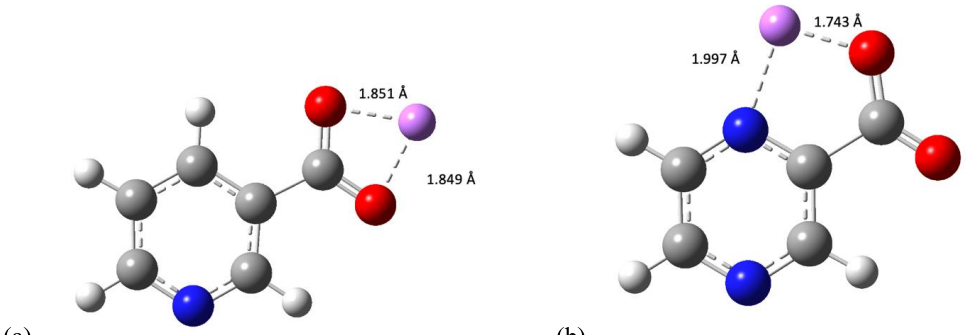

(a) (b)

Figure 8. Optimized geometries of (a) Li^+–(3-PyrA)$^-$ and (b) Li^+–(2,5-PyrA)$^-$ ion-pairs including coordination bond distances and association energies.

Conclusions

New ionic materials comprising aromatic heterocyclic analogous anions based on pyridine and pyrazine coupled to a common $(P_{4444})^+$ cation are investigated through experimental and theoretical studied. It is found that altering the position of nitrogen atom in the aromatic ring of the anion can dramatically affect the cation-anion interactions and influence the overall physiochemical properties of the ionic materials, ranging from RTILs and organic ionic plastic crystals. Comparing the RTILs, the neat (P_{4444})(3-PyrA) IL and its electrolyte exhibit much superior thermal and electrochemical stabilities, higher ionic conductivity and ion diffusivity. Among all the ions, Li^+ ions revealed slowest diffusivity in the electrolytes suggesting stronger electrostatic interactions leading to ion association. The combination of NMR (^{7}Li and ^{31}P) and FTIR spectroscopic data, and computational studies revealed the possible modes of ionic interactions between the aromatic anions and the $(P_{4444})^+$ and Li^+ cation. Overall, the neat (P_{4444})(3-PyrA) IL and its electrolyte, the anion of which is derived from niacin (a form of vitamin B_3), provided beneficial physical and electrochemical properties by reduced ionic interactions and can be used an electrolyte in lithium batteries.

Acknowledgment

The financial support from the Swedish Energy Agency (project number: 48194-1) is gratefully acknowledged.

References

(1) Li, M.; Lu, J.; Chen, Z.; Amine, K. 30 years of lithium-ion batteries. *Advanced Materials* **2018,** *30* (33), 1800561.

(2) Nagaura, T. Lithium ion rechargeable battery. *Progress in Batteries & Solar Cells* **1990,** *9*, 209.

(3) Tian, X.; Yi, Y.; Fang, B.; Yang, P.; Wang, T.; Liu, P.; Qu, L.; Li, M.; Zhang, S. Design strategies of safe electrolytes for preventing thermal runaway in lithium ion batteries. *Chemistry of Materials* **2020,** *32* (23), 9821.

(4) Navarra, M. A.; Tsurumaki, A.; Vitucci, F. M.; Paolone, A.; Palumbo, O.; Panero, S. A Novel Li+-Conducting Polymer Membrane Gelled by Fluorine-Free Electrolyte Solutions for Li-Ion Batteries. *Batteries & Supercaps* **2020,** *3* (10), 1112.

(5) Wang, Q.; Mao, B.; Stoliarov, S. I.; Sun, J. A review of lithium ion battery failure mechanisms and fire prevention strategies. *Progress in Energy and Combustion Science* **2019,** *73*, 95.

(6) Li, Q.; Chen, J.; Fan, L.; Kong, X.; Lu, Y. Progress in electrolytes for rechargeable Li-based batteries and beyond. *Green Energy & Environment* **2016,** *1* (1), 18.

(7) Zeng, Z.; Murugesan, V.; Han, K. S.; Jiang, X.; Cao, Y.; Xiao, L.; Ai, X.; Yang, H.; Zhang, J.-G.; Sushko, M. L. Non-flammable electrolytes with high salt-to-solvent ratios for Li-ion and Li-metal batteries. *Nature Energy* **2018,** *3* (8), 674.

(8) Pham, H. Q.; Lee, H.-Y.; Hwang, E.-H.; Kwon, Y.-G.; Song, S.-W. Non-flammable organic liquid electrolyte for high-safety and high-energy density Li-ion batteries. *Journal of power sources* **2018,** *404*, 13.

(9) Liu, X.; Shen, X.; Zhong, F.; Feng, X.; Chen, W.; Ai, X.; Yang, H.; Cao, Y. Enabling electrochemical compatibility of non-flammable phosphate electrolytes for lithium-ion batteries by tuning their molar ratios of salt to solvent. *Chemical Communications* **2020,** *56* (48), 6559.

(10) Ding, D.; Maeyoshi, Y.; Kubota, M.; Wakasugi, J.; Kanamura, K.; Abe, H. Non-flammable super-concentrated polymer electrolyte with "solvated ionic liquid" for lithium-ion batteries. *Journal of Power Sources* **2021,** *506*, 230099.

(11) von Aspern, N.; Leissing, M.; Wölke, C.; Diddens, D.; Kobayashi, T.; Börner, M.; Stubbmann-Kazakova, O.; Kozel, V.; Röschenthaler, G. V.; Smiatek, J. Non-Flammable Fluorinated Phosphorus (III)-Based Electrolytes for Advanced Lithium-Ion Battery Performance. *ChemElectroChem* **2020,** *7* (6), 1499.

(12) Kim, G.; Jeong, S.; Joost, M.; Rocca, E.; Winter, M.; Passerini, S.; Balducci, A. Use of natural binders and ionic liquid electrolytes for greener and safer lithium-ion batteries. *Journal of Power Sources* **2011,** *196* (4), 2187.

(13) Nakagawa, H.; Fujino, Y.; Kozono, S.; Katayama, Y.; Nukuda, T.; Sakaebe, H.; Matsumoto, H.; Tatsumi, K. Application of nonflammable electrolyte with room temperature ionic liquids (RTILs) for lithium-ion cells. *Journal of Power Sources* **2007,** *174* (2), 1021.

(14) Lee, H.; Yanilmaz, M.; Toprakci, O.; Fu, K.; Zhang, X. A review of recent developments in membrane separators for rechargeable lithium-ion batteries. *Energy & Environmental Science* **2014,** *7* (12), 3857.

(15) Wilken, S.; Xiong, S.; Scheers, J.; Jacobsson, P.; Johansson, P. Ionic liquids in lithium battery electrolytes: Composition versus safety and physical properties. *Journal of Power Sources* **2015,** *275*, 935.

(16) Shah, F. U.; Gnezdilov, O. I.; Khan, I. A.; Filippov, A.; Slad, N. A.; Johansson, P. Structural and ion dynamics in fluorine-free oligoether carboxylate ionic liquid-based electrolytes. *The Journal of Physical Chemistry B* **2020,** *124* (43), 9690.

(17) Ilyas, F.; Ishaq, M.; Jabeen, M.; Saeed, M.; Ihsan, A.; Ahmed, M. Recent trends in the benign-by-design electrolytes for zinc batteries. *Journal of Molecular Liquids* **2021,** *343*, 117606.

(18) Lei, Z.; Chen, B.; Koo, Y.-M.; MacFarlane, D. R. Introduction: ionic liquids. *Chemical Reviews* **2017,** *117* (10), 6633.

(19) Fan, Y.; Li, W.; Zhang, S.; Sun, S.; Yang, L. Vitamin B3-based protic ionic liquids as green solvents for the isolation of astilbin from rhizoma smilacis glabrae. *Industrial Crops and Products* **2020,** *152*, 112563.

(20) Wilson, R. A.; Fernandez, J.; Rocha, R. O.; Marroquin-Guzman, M.; Wright, J. D. Genetic evidence for Magnaporthe oryzae vitamin B3 acquisition from rice cells. *Microbiology* **2019,** *165* (11), 1198.

(21) Neale, A. R.; Murphy, S.; Goodrich, P.; Hardacre, C.; Jacquemin, J. Thermophysical and Electrochemical Properties of Ethereal Functionalised Cyclic Alkylammonium-based Ionic Liquids as Potential Electrolytes for Electrochemical Applications. *ChemPhysChem* **2017,** *18* (15), 2040.

(22) Blümich, B.; Wiley Online Library, 1995.

(23) Tanner, J. E. Use of the stimulated echo in NMR diffusion studies. *The Journal of Chemical Physics* **1970,** *52* (5), 2523.

(24) Zhao, Y.; Truhlar, D. G. Density functionals with broad applicability in chemistry. *Accounts of chemical research* **2008,** *41* (2), 157.

(25) Zhao, Y.; Schultz, N. E.; Truhlar, D. G. Design of density functionals by combining the method of constraint satisfaction with parametrization for thermochemistry, thermochemical kinetics, and noncovalent interactions. *Journal of chemical theory and computation* **2006,** *2* (2), 364.

(26) Frisch, M. e.; Trucks, G.; Schlegel, H.; Scuseria, G.; Robb, M.; Cheeseman, J.; Scalmani, G.; Barone, V.; Petersson, G.; Nakatsuji, H.; Gaussian, Inc. Wallingford, CT, 2016.

(27) Becke, A. D. A new mixing of Hartree–Fock and local density-functional theories. *The Journal of chemical physics* **1993,** *98* (2), 1372.

(28) Lee, C.; Yang, W.; Parr, R. G. Development of the Colle-Salvetti correlation-energy formula into a functional of the electron density. *Physical review B* **1988,** *37* (2), 785.

(29) Reed, A. E.; Curtiss, L. A.; Weinhold, F. Intermolecular interactions from a natural bond orbital, donor-acceptor viewpoint. *Chemical Reviews* **1988,** *88* (6), 899.

(30) Zhu, H.; Huang, G.; O'Dell, L. A.; Forsyth, M. New insights into decoupled cation and anion transport and dynamic heterogeneity in a diethyl (methyl)(isobutyl) phosphonium hexafluorophosphate organic ionic plastic crystal. *The Journal of Physical Chemistry Letters* **2021,** *12* (40), 9853.

(31) Makhlooghiazad, F.; Guazzagaloppa, J.; O'Dell, L. A.; Yunis, R.; Basile, A.; Howlett, P. C.; Forsyth, M. The influence of the size and symmetry of cations and anions on the physicochemical behavior of organic ionic plastic crystal electrolytes mixed with sodium salts. *Physical Chemistry Chemical Physics* **2018,** *20* (7), 4721.

(32) Das, S.; Mondal, A.; Reddy, C. M. Harnessing molecular rotations in plastic crystals: a holistic view for crystal engineering of adaptive soft materials. *Chemical Society Reviews* **2020,** *49* (24), 8878.

(33) Do Nascimento, A.; Caires, F.; Gomes, D.; Gigante, A.; Ionashiro, M. Thermal behaviour of nicotinic acid, sodium nicotinate and its compounds with some bivalent transition metal ions. *Thermochimica Acta* **2014,** *575*, 212.

(34) Marinković, A.; Drmanić, S.; Jovanović, B. Ž.; Misić-Vuković, M. Investigations of the reactivity of pyridine carboxylic acids with diazodiphenylmethane in protic and aprotic solvents, Part I: Pyridine mono-carboxylic acids. *Journal of the Serbian Chemical Society* **2005,** *70* (4), 557.

(35) Hallé, J.-C.; Lelievre, J.; Terrier, F. Solvent effect on preferred protonation sites in nicotinate and isonicotinate anions. *Canadian journal of chemistry* **1996,** *74* (4), 613.

(36) Khan, I. A.; Shah, F. U. Fluorine-free Ionic liquid-based electrolyte for supercapacitors operating at elevated temperatures. *ACS Sustainable Chemistry & Engineering* **2020,** *8* (27), 10212.

(37) Zhu, L.; Dong, J.; Ma, Y.; Jia, Y.; Peng, C.; Li, W.; Zhang, M.; Gong, K.; Wang, X. Synthesis and investigation of halogen-free phosphonium-based ionic liquids for lubrication applications. *Tribology Transactions* **2019,** *62* (6), 943.

(38) Macfarlane, D. R.; Meakin, P.; Sun, J.; Amini, N.; Forsyth, M. Pyrrolidinium imides: a new family of molten salts and conductive plastic crystal phases. *The Journal of Physical Chemistry B* **1999,** *103* (20), 4164.

(39) Shah, F. U.; Glavatskih, S.; Dean, P. M.; MacFarlane, D. R.; Forsyth, M.; Antzutkin, O. N. Halogen-free chelated orthoborate ionic liquids and organic ionic plastic crystals. *Journal of Materials Chemistry* **2012,** *22* (14), 6928.

(40) Girard, G. M.; Hilder, M.; Zhu, H.; Nucciarone, D.; Whitbread, K.; Zavorine, S.; Moser, M.; Forsyth, M.; Macfarlane, D. R.; Howlett, P. C. Electrochemical and physicochemical properties of small phosphonium cation ionic liquid electrolytes with high lithium salt content. *Physical chemistry chemical physics* **2015,** *17* (14), 8706.

(41) Park, M. J.; Choi, I.; Hong, J.; Kim, O. Polymer electrolytes integrated with ionic liquids for future electrochemical devices. *Journal of Applied Polymer Science* **2013,** *129* (5), 2363.

(42) Karuppasamy, K.; Theerthagiri, J.; Vikraman, D.; Yim, C.-J.; Hussain, S.; Sharma, R.; Maiyalagan, T.; Qin, J.; Kim, H.-S. Ionic liquid-based electrolytes for energy storage devices: A brief review on their limits and applications. *Polymers* **2020,** *12* (4), 918.

(43) Moreno, M.; Simonetti, E.; Appetecchi, G. B.; Carewska, M.; Montanino, M.; Kim, G.-T.; Loeffler, N.; Passerini, S. Ionic Liquid Electrolytes for Safer Lithium Batteries: I. Investigation Around Optimal Formulation. *ECS Transactions* **2016,** *73* (1), 67.

(44) Khan, I. A.; Gnezdilov, O. I.; Filippov, A.; Shah, F. U. Ion Transport and Electrochemical Properties of Fluorine-Free Lithium-Ion Battery Electrolytes Derived from Biomass. *ACS Sustainable Chemistry & Engineering* **2021**.

(45) Cohen, M. H.; Turnbull, D. Molecular transport in liquids and glasses. *The Journal of Chemical Physics* **1959,** *31* (5), 1164.

(46) Galiński, M.; Lewandowski, A.; Stępniak, I. Ionic liquids as electrolytes. *Electrochimica acta* **2006,** *51* (26), 5567.

(47) Fulcher, G. S. Analysis of recent measurements of the viscosity of glasses. *Journal of the American Ceramic Society* **1925,** *8* (6), 339.

(48) Tammann, G.; Hesse, W. Die Abhängigkeit der Viscosität von der Temperatur bie unterkühlten Flüssigkeiten. *Zeitschrift für anorganische und allgemeine Chemie* **1926,** *156* (1), 245.

(49) Filippov, A.; Munavirov, B.; Glavatskih, S.; Shah, F. U.; Antzutkin, O. N. Diffusion of ions in phosphonium orthoborate ionic liquids studied by 1H and 11B pulsed field gradient NMR. *Frontiers in chemistry* **2020,** *8*, 119.

(50) Hilder, M.; Gras, M.; Pope, C. R.; Kar, M.; MacFarlane, D. R.; Forsyth, M.; O'Dell, L. A. Effect of mixed anions on the physicochemical properties of a sodium containing alkoxyammonium ionic liquid electrolyte. *Physical Chemistry Chemical Physics* **2017,** *19* (26), 17461.

(51) Kakihana, M.; Schantz, S.; Torell, L. Raman spectroscopic study of ion–ion interaction and its temperature dependence in a poly (propylene-oxide)-based NaCF3SO3–polymer electrolyte. *The Journal of chemical physics* **1990,** *92* (10), 6271.

(52) Savateev, A.; Liedel, C.; Tröger-Müller, S.; de León, A. S.; Antonietti, M.; Dontsova, D. Halogen free 1, 2, 3-and 1, 2, 4-triazolide based ionic liquids: synthesis and properties. *Chemical Communications* **2017,** *53* (73), 10192.

(53) Girard, G. M.; Hilder, M.; Nucciarone, D.; Whitbread, K.; Zavorine, S.; Moser, M.; Forsyth, M.; MacFarlane, D. R.; Howlett, P. C. Role of Li concentration and the SEI layer in enabling high performance Li metal electrodes using a phosphonium bis (fluorosulfonyl) imide ionic liquid. *The Journal of Physical Chemistry C* **2017,** *121* (39), 21087.

(54) Girard, G. M.; Hilder, M.; Dupre, N.; Guyomard, D.; Nucciarone, D.; Whitbread, K.; Zavorine, S.; Moser, M.; Forsyth, M.; MacFarlane, D. R. Spectroscopic characterization of the SEI layer formed on lithium metal electrodes in phosphonium bis (fluorosulfonyl) imide ionic liquid electrolytes. *ACS applied materials & interfaces* **2018,** *10* (7), 6719.

(55) Soldatenkov, A.; Temesgen, A.; Kolyadina, N. Oxidation of heterocyclic compounds by permanganate anion. *Chemistry of Heterocyclic Compounds* **2004,** *40* (5), 537.

(56) Shah, F. U.; Holmgren, A.; Rutland, M. W.; Glavatskih, S.; Antzutkin, O. N. Interfacial behavior of orthoborate ionic liquids at inorganic oxide surfaces probed by NMR, IR, and raman spectroscopy. *The Journal of Physical Chemistry C* **2018,** *122* (34), 19687.

Supporting Information

Aromatic Heterocyclic Anion Based Ionic Liquids and Electrolytes

Mukhtiar Ahmed[1], Soniya Rao[2], Andrei Filippov[1], Patrik Johansson[2*], and Faiz Ullah Shah[1*]

[1]Chemistry of Interfaces, Luleå University of Technology, SE-971 87 Luleå, Sweden

[2]Department of Physics, Chalmers University of Technology, SE-412 96 Gothenburg, Sweden

[*]Corresponding authors:

patrik.johansson@chalmers.se

faiz.ullah@ltu.se

Synthesis and Characterization

(P_{4444})(3-PyrA): Transparent yellowish room temperature liquid. MS (ESI). $[C_{16}H_{36}P]^+$: Calcd m/z 259.2556. Found m/z 259.2555, $[C_6H_4NO_2]^-$: Calcd m/z 122.0247, Found m/z 122.0222. ^{1}H NMR (400.21 MHz, $CDCl_3$), $^\delta$(ppm): 9.19-9.20 (m, 1H), 8.47-8.49 (m, 1H), 8.28-8.21 (m, 1H),7.17-7.20 (m, 1H), 2.31-2.36 (m, 8H, P-CH_2-), 1.42-1.51 (m, 16H, -CH_2-), 0.93-0.96 (t, $3J_{HH}$ = 7.1 Hz, 12H, -CH_3) ppm. ^{13}C NMR (100.64 MHz, $CDCl_3$): 169.88, 151.33, 149.58, 136.97, 135.52, 122.60, 24.17, 24.02, 23.93, 23.88, 19.05, 18.58, 13.56 ppm. ^{31}P NMR (162.01 MHz, $CDCl_3$): 33.12 ppm.

(P_{4444})(4-PyrA): White solid, MS (ESI). $[C_{16}H_{36}P]^+$: Calcd m/z 259.2556. Found m/z 259.2562, $[C_6H_4NO_2]^-$: Calcd m/z 122.0247. Found m/z 122.0188.^{1}H NMR (400.21 MHz, $CDCl_3$), $^\delta$(ppm): 8.52-8.54 (m, 2H), 7.82-7.84 (m, 2H), 2.29-2.36 (m, 8H, P-CH_2-), 1.46-1.49 (m, 16H, -CH_2-), 0.90-0.93 (t, $3J_{HH}$ = 7.1 Hz, 12H, -CH_3) ppm. ^{13}C NMR (100.64 MHz, CDCl3): 169.77, 148.16, 123.72, 24.17, 24.02, 23.92, 23.87, 19.04, 18.58, 13.56 ppm. ^{31}P NMR (162.01 MHz, $CDCl_3$): 33.10 ppm.

(P_{4444})(2-PyrA): Yellowish gel. MS (ESI). $[C_{16}H_{36}P]^+$: Calcd m/z 259.2556. Found m/z 259.2535, MS (ESI). $[C_6H_4NO_2]^-$: Calcd m/z 122.0247, Found m/z 122.0212. ^{1}H NMR (400.21 MHz, $CDCl_3$), $^\delta$(ppm): 8.36-8.37 (m, 1H), 7.90-7.92 (m, 1H), 7.42-7.45 (m, ^{1}H), 6.95-6.98 (m, 1H), 2.19-2.27 (m, 8H, P-CH_2-), 1.25-1.34 (m, 16H, -CH_2-), 0.72-0.74 (t, $3J_{HH}$ = 7.1 Hz, 12H, -CH_3) ppm. ^{13}C NMR (100.64 MHz, $CDCl_3$): 170.56, 158.10, 148.48, 135.74, 123.94, 123.10, 24.21,24.12, 24.06, 19.10, 18.63, 13.65 ppm. ^{31}P NMR (162.01 MHz, $CDCl_3$): 33.08 ppm.

(P_{4444})(2,5-PyrA): Transparent yellow room temperature liquid. MS (ESI). $[C_{16}H_{36}P]^+$: Calcd m/z 259.2556. Found m/z 259.2562, MS (ESI). $[C_6H_4NO_2]^-$: Calcd m/z 123.0200, Found m/z 123.0146. ^{1}H NMR (400.21 MHz, $CDCl_3$), $^\delta$(ppm): 8.52-8.54 (m, 2H), 7.82-7.84 (m, 2H), 2.29-

2.36 (m, 8H, P-CH_2-), 1.46-1.49 (m, 16H, -CH_2-), 0.90-0.93 (t, 3J_{HH} = 7.1 Hz, 12H, -CH_3) ppm. ^{13}C NMR (100.64 MHz, $CDCl_3$): 168.78, 152.64, 146.21, 143.81, 143.39, 24.26, 24.10, 24.05, 19.17, 18.70, 13.65 ppm. ^{31}P NMR (162.01 MHz, $CDCl_3$): 33.19 ppm.

(P_{4444})(Pyr-2,6-diA): White crystalline solid. MS (ESI). $[C_{16}H_{36}P]^+$: Calcd m/z 259.2556. Found m/z 259.2562, $[C_7H_3NO_4]^{2-}$: Calcdm/z 165.10412, Found m/z 166.0146. Found m/z 389.157. ^{1}H NMR (400.21 MHz, $CDCl_3$), $^{\delta}$(ppm): 8.09-8.11 (m, 2H), 7.59-7.61 (m, 1H), 2.21-2.27 (m, 16H, P-CH_2-), 1.36-1.37 (m, 32H, -CH_2-), 0.84-0.87 (t, 3J_{HH} = 7.1 Hz, 24H, -CH_3) ppm. ^{13}C NMR (100.64 MHz, $CDCl_3$): 170.39, 155.85, 135.85, 124.22, 24.02, 23.99, 23.95, 23.87, 18.93, 18.46, 13.65 ppm. ^{31}P NMR (162.01 MHz, $CDCl_3$): 32.80 ppm.

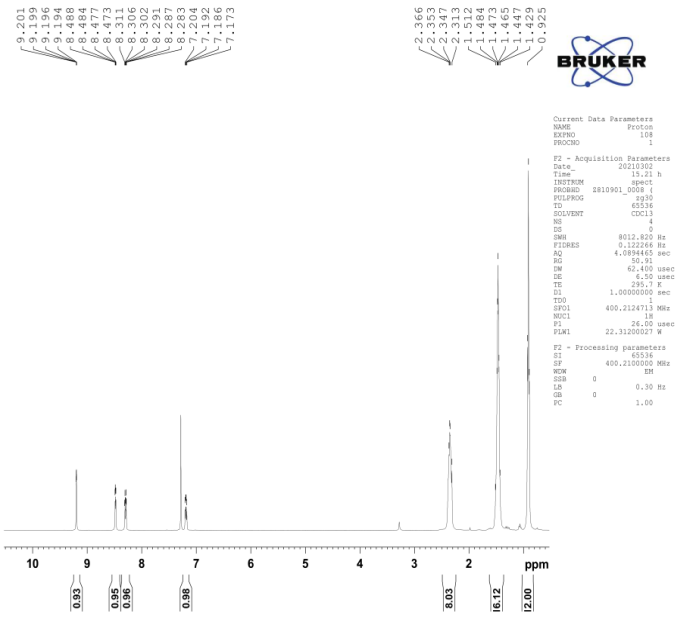

Figure S1. ^{1}H NMR spectrum of (P_{4444})(3-PyrA) in $CDCl_3$.

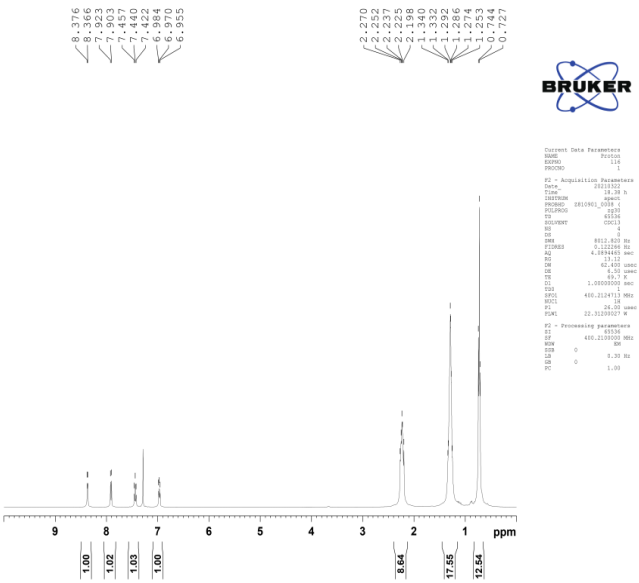

Figure S2. ^{1}H NMR spectrum of (P_{4444})(2-PyrA) in $CDCl_3$.

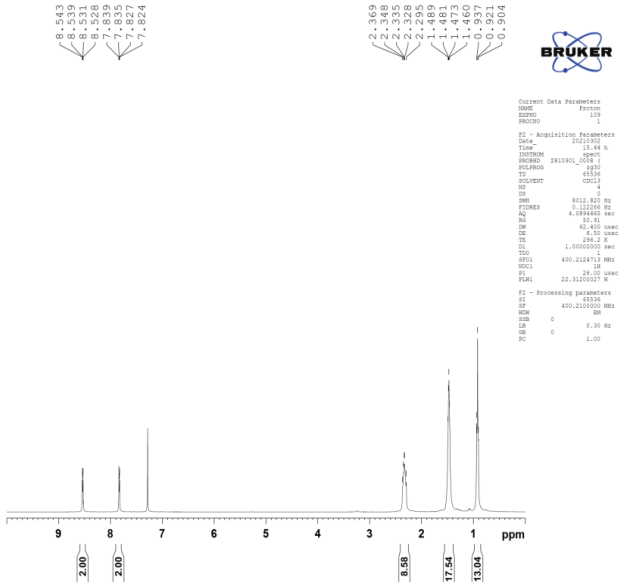

Figure S3. ^{1}H NMR spectrum of (P_{4444})(4-PyrA) in $CDCl_3$.

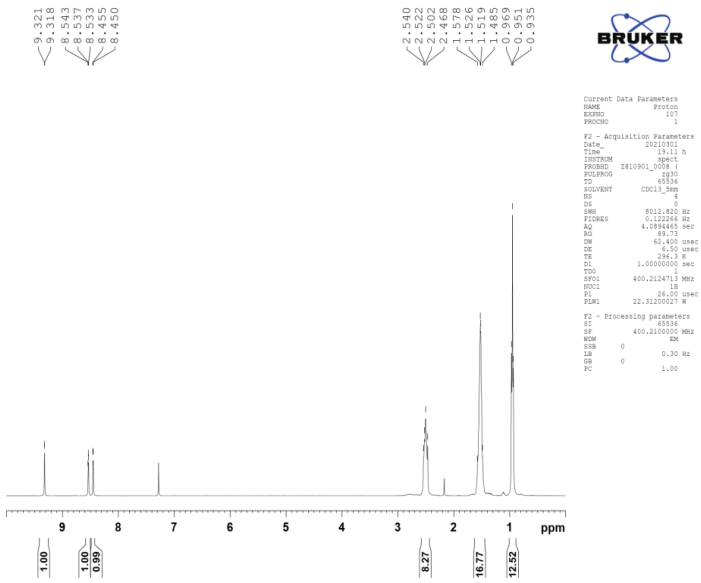

Figure S4. ^{1}H NMR spectrum of (P_{4444})(2,5-PyrA) in $CDCl_3$.

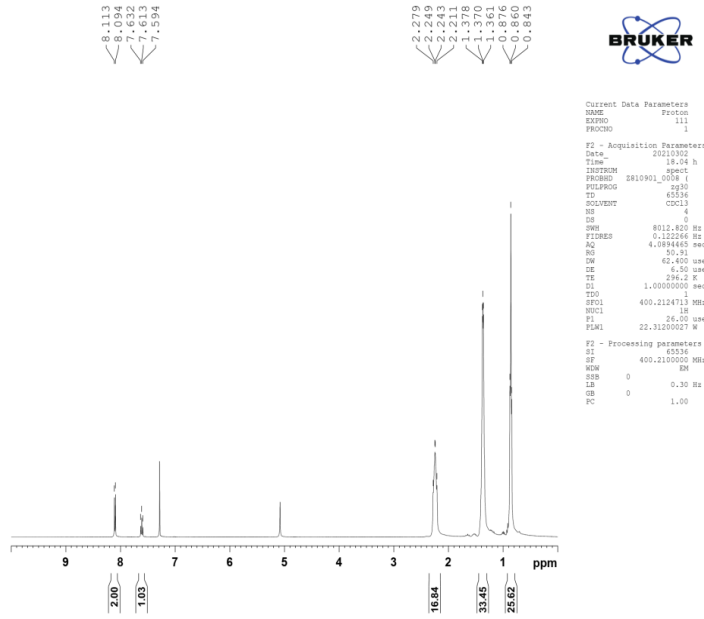

Figure S5. ^{1}H NMR spectrum of (P_{4444})(Pyr-2,6-diA) in $CDCl_3$.

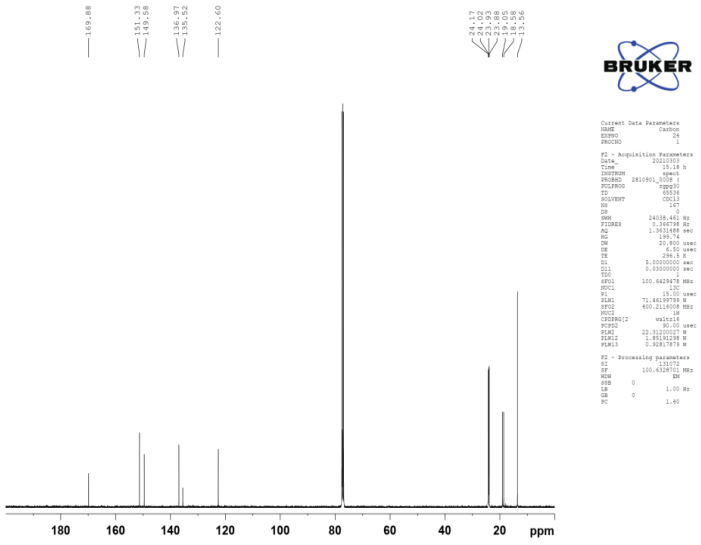

Figure S6. ^{13}C NMR spectrum of (P_{4444})(2-PyrA) in $CDCl_3$.

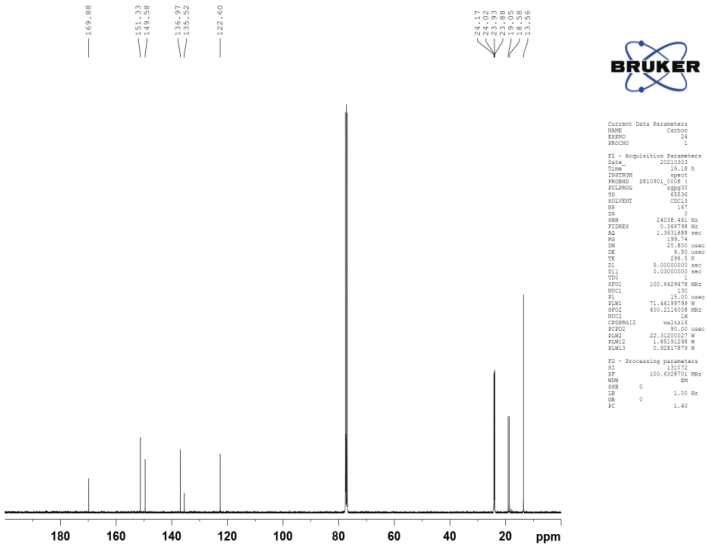

Figure S7. ^{13}C NMR spectrum of (P_{4444})(3-PyrA) in $CDCl_3$.

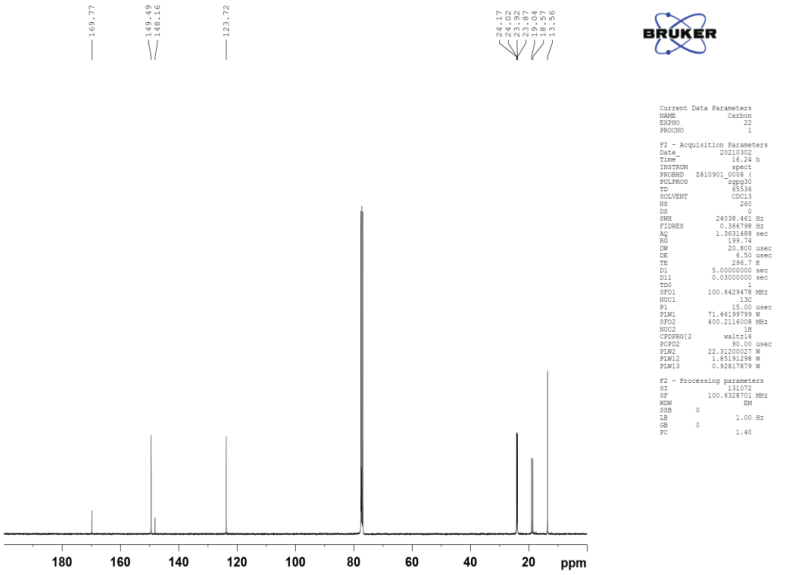

Figure S8. ^{13}C NMR spectrum of (P_{4444})(4-PyrA) in $CDCl_3$.

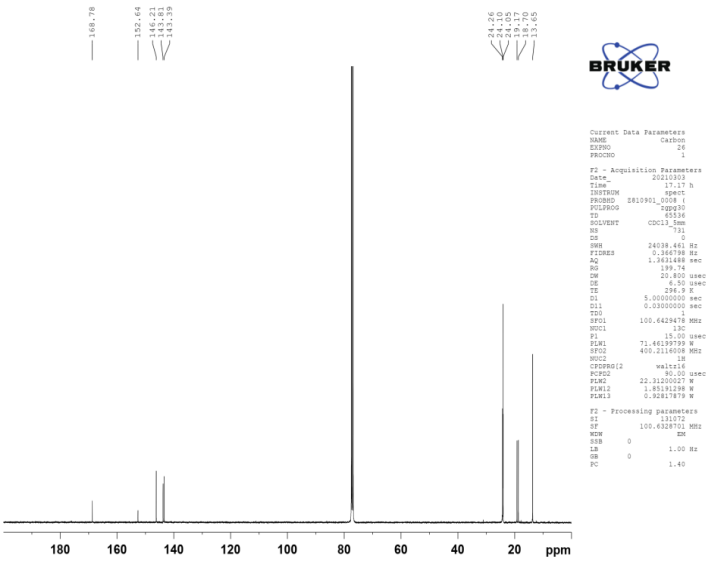

Figure S9. ^{13}C NMR spectrum of (P_{4444})(2,5-PyrA) in $CDCl_3$.

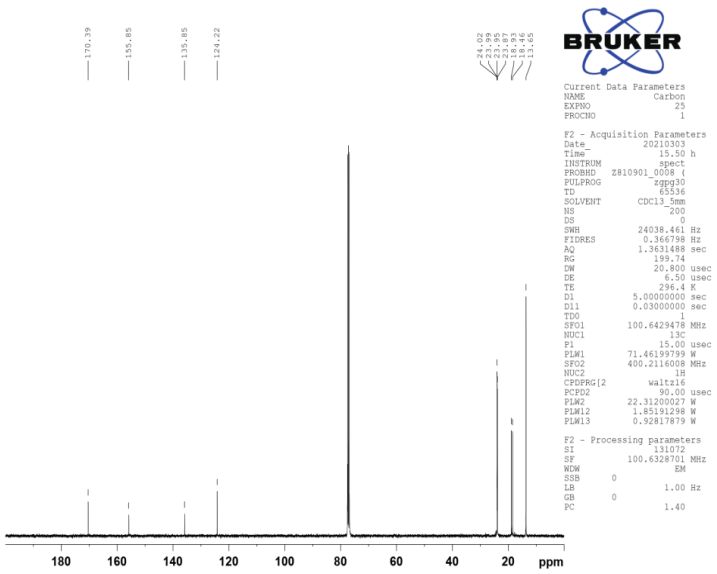

Figure S10. ^{13}C NMR spectrum of (P_{4444})(Pyr-2,6-diA) in $CDCl_3$.

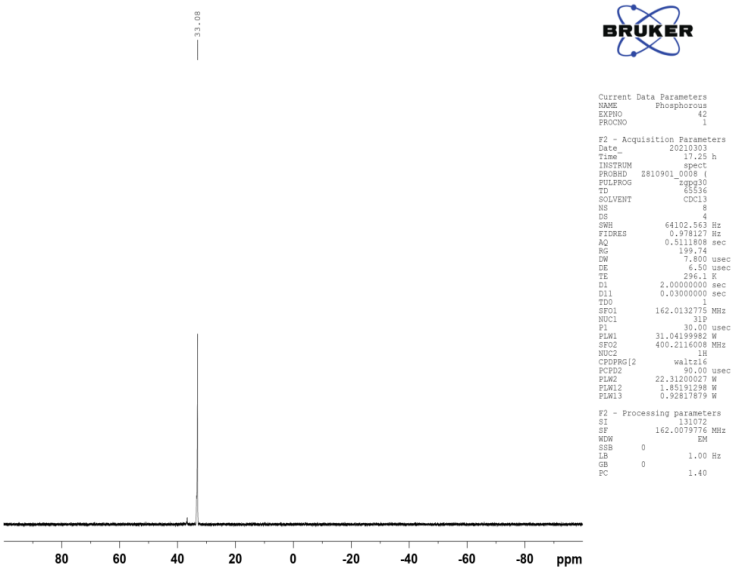

Figure S11. ^{31}P NMR spectrum of (P_{4444})(2-PyrA) in $CDCl_3$.

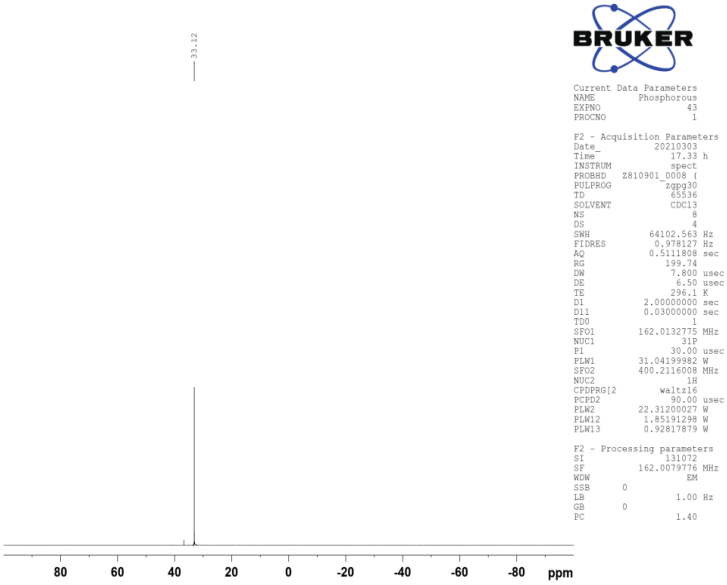

Figure S12. ^{31}P NMR spectrum of (P_{4444})(3-PyrA) in $CDCl_3$.

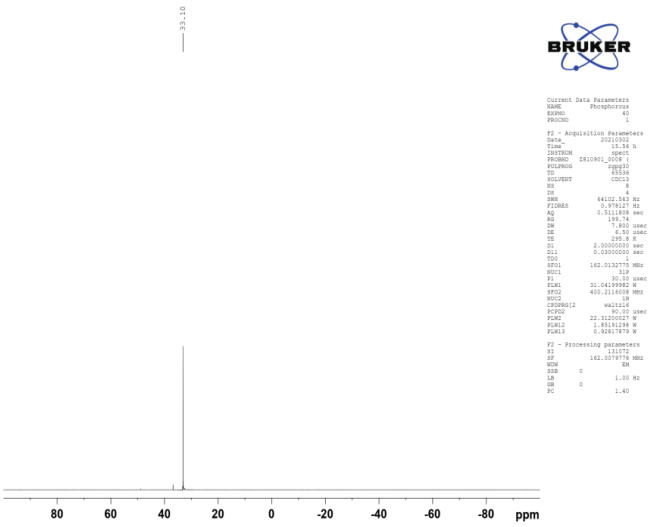

Figure S13. ^{31}P NMR spectrum of (P_{4444})(4-PyrA) in $CDCl_3$.

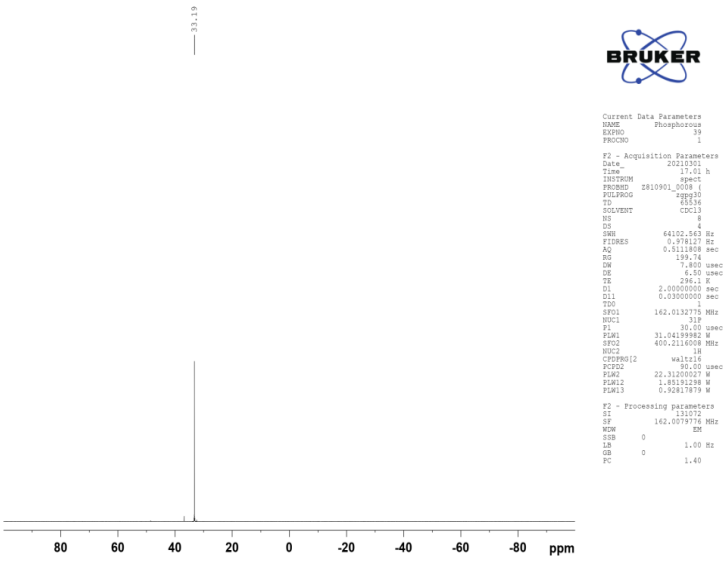

Figure S14. ^{31}P NMR spectrum of (P_{4444})(2,5-PyrA) in $CDCl_3$.

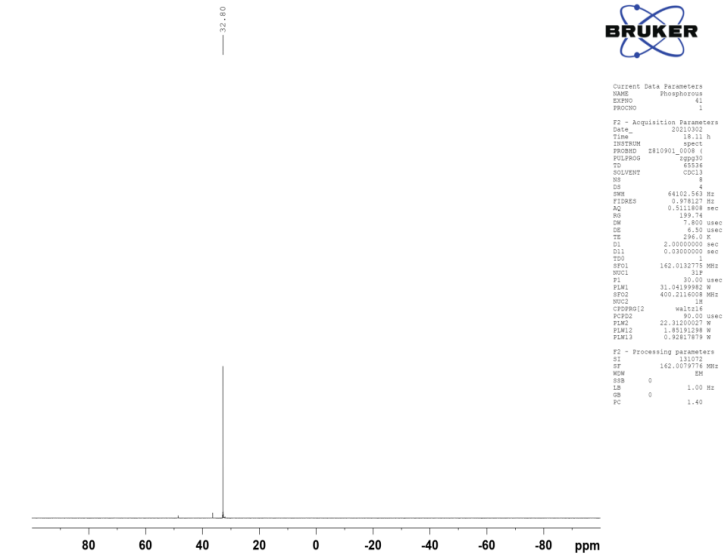

Figure S15. ^{31}P NMR spectrum of (P_{4444})(Pyr-2,6-diA) in $CDCl_3$.

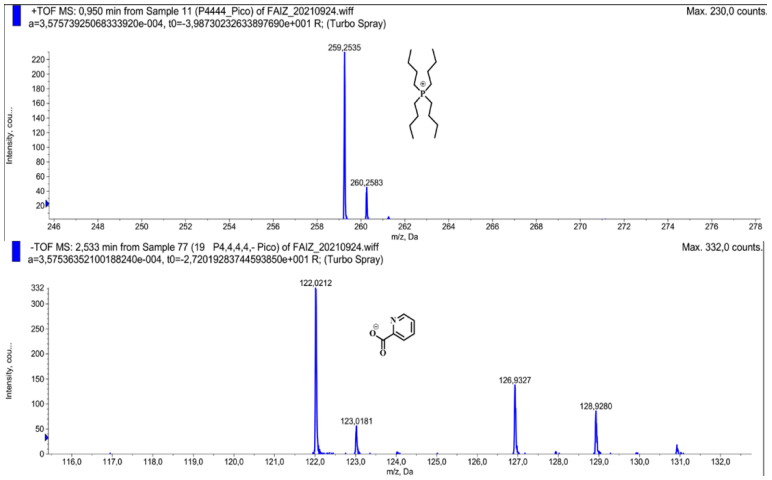

Figure S16. ESI-MS of (P_{4444})(2-PyrA)

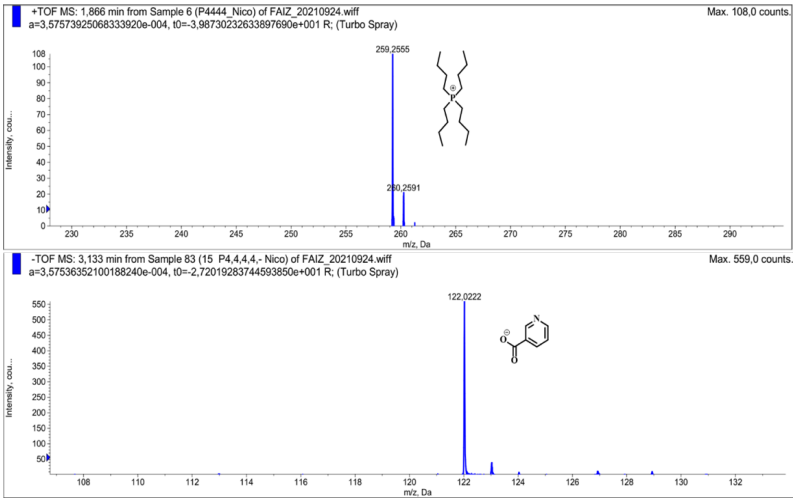

Figure S17. ESI-MS of (P_{4444})(3-PyrA)

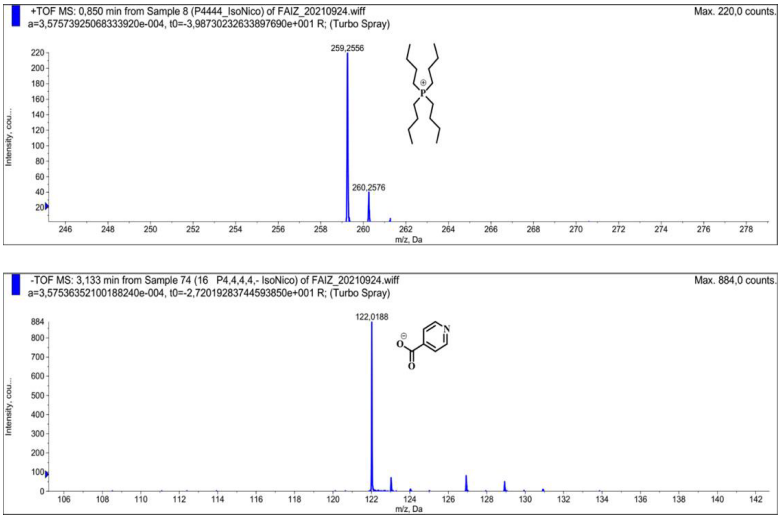

Figure S18. ESI-MS of (P_{4444})(4-PyrA)

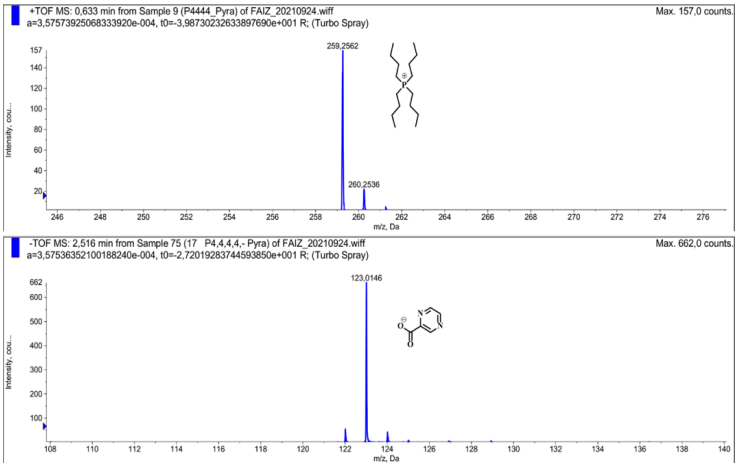

Figure S19. ESI-MS of (P_{4444})(2,5-PyrA)

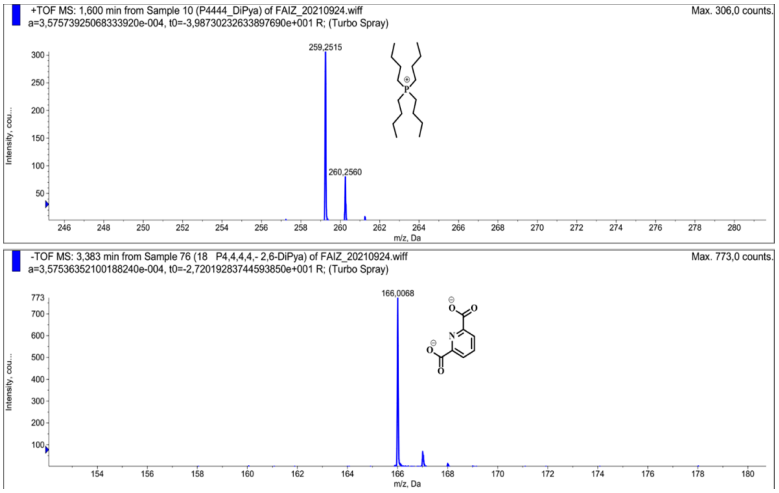

Figure S20. ESI-MS of (P_{4444})(Pyr-2,6-diA)

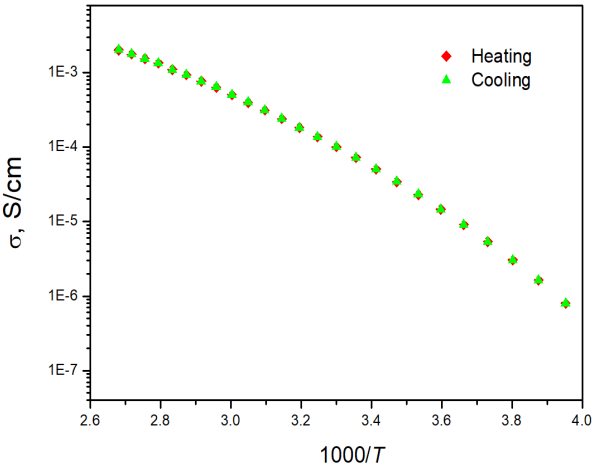

Figure S21. Heating and cooling cycles of the ionic conductivity of (P_{4444})(3-PyrA)

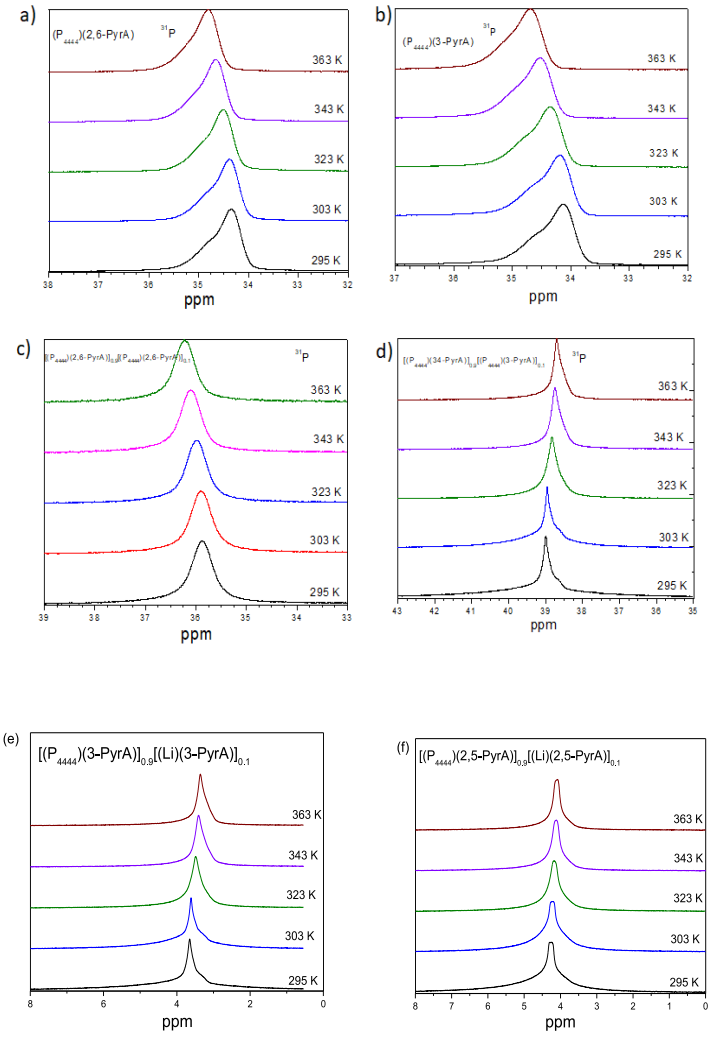

Figure S22. ^{31}P NMR spectra of (a) [(P_{4444})(2,5-PyrA)] (b) [(P_{4444})(3-PyrA)] (c) [(P_{4444})(2,5-PyrA)]$_{0.9}$[(Li)(2,6-PyrA)]$_{0.1}$ and (d) [(P_{4444})(3-PyrA)]$_{0.9}$[(Li)(3-PyrA)]$_{0.1}$ and ^{7}Li NMR (e) [(P_{4444})(3-PyrA)]$_{0.9}$[(Li)(3-PyrA)]$_{0.1}$ and (f) [(P_{4444})(2,5-PyrA)]$_{0.9}$[(Li)(2,5-PyrA)]$_{0.1}$ as a function of temperature.

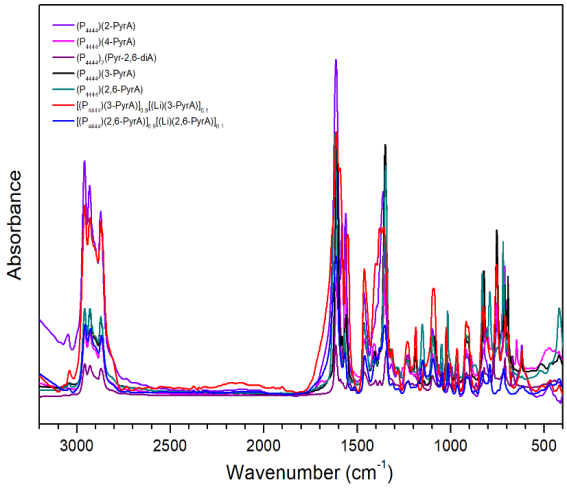

Figure S23. FTIR spectra of neat ILs and electrolytes

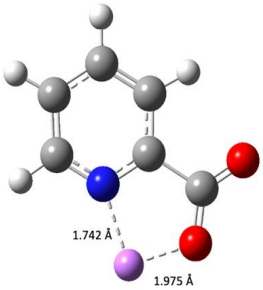

(a) 2-PyrA (-709 kJ mol^{-1})

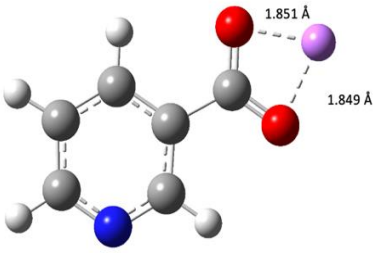

(b) 3-PyrA (-674 kJ mol^{-1})

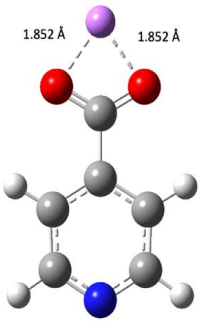

(c) 4-PyrA (-666 kJ mol^{-1})

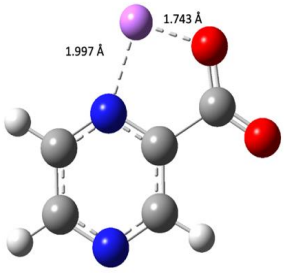

(d) 2,5-PyrA (-680 kJ mol^{-1})

Figure S24: Optimized geometries of the various Li^{+}– -PyrA ion-pairs for: (a) 2-PyrA (b) 3-PyrA, (c) 4-PyrA, and (d) 2,5-PyrA, including coordination bond distances and association energies.

Table S1. VFT equation parameters and apparent energies of activation of conductivity for ILs and electrolytes.

System	σ_0 mS/cm	B,K	T_0, K	$E\sigma$, kJ/(mol)
(P_{4444}) (3-PyrA)	1.218	1381	156	11.4
(P_{4444}) (2,5-PyrA)	0.135	1496	150	12.4
$[(P_{4444})(3\text{-PyrA})]_{0.9}$ $[Li(3\text{-PyrA})]_{0.1}$	2.352	1600	148	13.3
$[(P_{4444})$ (2,5-PyrA)$]_{0.9}$ $[Li(2,5\text{-PyrA})]_{0.1}$	0.216	1626	143	13.5

Table S2. VFT equation parameters and apparent energies of activation of diffusivity for ILs and electrolytes.

System	ion	$D_0 \times 10^{-8}$ m^2/s	B,K	T_0, K	E_D, kJ/(mol)
(P_{4444}) (3-PyrA)	(3-PyrA)$^-$	1.55	800	213	6.7
	$(P_{4444})^+$	1.49	826	211	6.9
$[(P_{4444})(3\text{-PyrA})]_{0.9}$ $[Li(3\text{-PyrA})]_{0.1}$	(3-PyrA)$^-$	5.07	1100	200	9.2
	$(P_{4444})^+$	3.36	1000	204	8.3
	Li^+	6.46	1124	205	9.3
(P_{4444}) (2,5-PyrA)	(2,5-PyrA)$^-$	1.53	853	210	7.1
	$(P_{4444})^+$	1.59	892	207	7.4
$[(P_{4444})$ (2,5-PyrA)$]_{0.9}$ $[Li(2,5\text{-PyrA})]_{0.1}$	(2,5-PyrA)$^-$	3.20	990	205	8.2
	$(P_{4444})^+$	3.03	998	205	8.3
	Li^+	3.50	1024	205	8.5

Table S3. Anodic and cathodic limits and electrochemical stability windows (ESWs) *vs*. Li/Li^+ of ILs and electrolytes at 0.10 mA cm^{-2} cut-off current density using GC as WE at 293 K.

System	E_A (V)	E_C (V)	*ESW* (V)
(P_{4444}) (3-PyrA)	4.97	1.39	3.57
$[(P_{4444})(3\text{-PyrA})]_{0.9}$ $[Li(3\text{-PyrA})]_{0.1}$	5.03	1.29	3.74
(P_{4444}) (2,5-PyrA)	4.09	1.27	2.82
$[(P_{4444})$ (2,5-PyrA)$]_{0.9}$ $[Li(2,5\text{-PyrA})]_{0.1}$	4.15	1.02	3.13

Table S4: Main interacting donor and acceptor NBOs and second order perturbation energy for the 2-PyrA anion and its Li^+ ion-pair.

From	To	2-PyrA	Li^+–2-PyrA
Donor NBO	Acceptor NBO	E (kcal/mol)	
σ C1 – N1	π^* C4 – C5	42.75	199.20
π C2 – C3	σ^* C1 – N1	33.50	44.21
π C2 – C3	π^*C4 – C5	26.45	25.74
π C4 – C5	σ^*C1 – N1	21.50	22.73
π C4 – C5	π^*C2 –C3	29.34	179.32
LP O2	π^*Ca –O1	134.73	27.61
σ C1 – N1	π^*Ca –O1	48.80	34.21
π C4 – C5	σ^*C1 – N1	161.29	22.73
π C4 – C5	σ^*C2 –C3	218.62	28.88
LP O 1	π^*Ca – O2	23.25	99.84
LP O1	σ^*C1 – Ca	26.24	15.46
LP O2	σ^*C1 – Ca	22.65	
LP N1	σ^*C4 – C5	11.31	8.50
LP N1	σ^*C1 –C2	10.70	9.48
σ C1 – N1	π^*C2 –C3	19.69	133.03
σ C1 – N1	π^*Ca–O2		34.21
σ C1 – N1	π^*C4 –C5	42.75	35.24

Table S5: Main interacting donor and acceptor NBOs and the second order perturbation energy E for the 3-PyrA anion and its Li^+ ion-pair.

From	To	3-PyrA	Li^+–3-PyrA
Donor NBO	Acceptor NBO	E kcal/mol	
σ C1 – N1	π*C4 – C5	38.10	
σ C 3 – C2	σ*C1 – N1	40.42	
σ C 3 – C2	π*C4 – C5	28.78	
π C4 – C5	σ*C1 –N1	22.84	
π C4 – C5	σ*C3– C2	27.78	
LP O1	π*C2 – Ca	22.86	18.41
LP O1	π*Ca – O2	142.82	18.89
LP O2	π*C2 – Ca	22.97	18.52
LP O2	π*Ca = O1	22.80	19.03
σ C1 – N1	σ*C3 – C2	124.99	
σ C4 – C3	π*Ca – O2	73.94	
σ C4 – C3	σ*C3 – C2	92.60	
LP N1	σ*C1– C2	9.70	
LP N1	σ*C1– H	4.61	
LP N1	σ*C1– C5	10.40	
LP N1	σ*C5– H	5.14	
σ C 5– N1	σ*C1 – C2		210.51
σ C3– N1	σ*C3 – C4		242.33
π C1– C2	σ*C5 – N1		24.35
π C1– C2	σ*C3 – C4		33.66
σ C3– C4	σ*C1– C2		23.89
σC3– C4	σ*C5– N1		40.90

Table S6: Main interacting donor and acceptor NBOs and the second order perturbation energy E for the 4-PyrA anion and its Li^+ ion-pair.

From	To	4-PyrA	Li^+–4-PyrA
Donor NBO	Acceptor NBO	E kcal/mol	
π C 1 – C2	σ*C4 – C3	29.99	32.27
π C 1 – C2	σ*C5 – N1	27.04	28.31
σ C4 – C3	π*C1 – C2	26.05	25.51
σ C4 – C3	σ*C5 – N1	45.80	36.67
σ C5 – N1	π*C 1 – C2	33.25	34.96
LP O2	σ*C3 – Ca	23.22	0.99
LP O2	σ*Ca – O1	22.57	18.95
LP O2	LP*Ca	244.22	206.27
LP O1	σ*C3 – Ca	23.22	18.79
LP O1	π*Ca – O2	22.57	18.96
π C 1 – C2	σ*C4 – C3	168.46	3.25
σ C5 – N1	π*C1 – C2	145.58	217.56
σ C5 – N 1	σ*C 4 – C3	90.27	256.64
LP N1	π*C1– C2	9.86	10.22
LP N1	σ*C1– H	4.98	5.15
LP N1	π*C4– C5	9.86	10.22
LP N1	σ*C5– H	4.98	5.15

Table S7: Main interacting donor and acceptor NBOs and the second order perturbation energy E for the 2,5-PyrA anion and its Li^+ ion-pair.

From	To	2,5-PyrA	Li^+–2,5-PyrA
Donor NBO	Acceptor NBO	E kcal/mol	
σ C1 – N1	σ* C 2 – N2	25.55	19.85
σ C1 – N1	σ* C3 – C4	37.33	31.59
σ C2 – N2	σ*C1 – N1	22.42	28.30
σ C2 – N2	π*C3 – C4	33.10	34.08
σ C3 – C4	σ* C1 – N1	24.15	27.60
σ C3 – C 4	σ* C2 – N2	26.38	26.37
LP O2	σ*C1 – Ca	23.08	26.34
LP O2	σ*Ca– O1	136.53	27.69
LP O1	σ*C1 – Ca	26.78	15.92
LP O1	σ*Ca – O2	23.23	99.57
σ C1 – N1	σ*Ca – O1	44.14	30.33
σ C2 – N2	σ*C1 – N1	225.77	218.96
π C3 – C4	σ*C1 – N1	155.98	174.89

Paper II

Oligoether Substituted Aromatic Carboxylate Ionic Liquids and Electrolytes

Mukhtiar Ahmed, Andrei Filippov, Patrik Johansson, and Faiz Ullah Shah

(*Manuscript*)

Oligoether Substituted Aromatic Carboxylate Ionic Liquids and Electrolytes

Mukhtiar Ahmed[1], Andrei Filippov[1], Patrik Johansson[2*] and Faiz Ullah Shah[1*]

[1]Chemistry of Interfaces, Luleå University of Technology, SE-971 87 Luleå, Sweden

[2]Materials Physics, Department of Physics, Chalmers University of Technology, SE-412 96 Gothenburg, Sweden

[*]Corresponding authors:
patrik.johansson@chalmers.se
faiz.ullah@ltu.se

Abstract

Here we designed and synthesized five new ionic liquids (ILs) with anions based on oligoether substituted aromatic carboxylates coupled to a common *n*- tetrabutylphosphonium $(P_{4444})^+$ cation. Electrolytes are created by doping two selected ILs with 10 mol % of lithium salts containing common anions. The nature and position of the attached oligoether chain to the phenyl ring influenced the physicochemical and electrochemical behavior, in particular thermal stability, phase behavior, ion transport, and inter-ionic interactions. The organic cations and anions diffused with the same diffusion coefficients as measured by pulsed field gradient nuclear magnetic resonance (PFG NMR) spectroscopy, however, the addition of lithium salts increased the strength of ionic interactions leading to cluster formation and reduced ionic diffusivity. The main reason for cluster formation is the interaction of Li^+ ion with the carboxylate group of anions as suggested by Fourier transform infrared (FTIR) spectroscopy.

Introduction

Among various electrochemical energy storage devices, rechargeable batteries, such as Li-ion batteries (LIBs), are considered the most promising power sources, because of their high energy density, low cost, and stable cyclability.[1-3] However, the safety issues associated with flammability of the conventional electrolytes currently being in LIBs have limited their application.[4,5] This drawback is progressively becoming a serious issue, as the number and size of LIBs are increasing for large scale applications including hybrid electric vehicles (HEVs) and energy storage systems (ESSs) for smart grids.[6] The electrolytes of LIBs composed of salt, mostly lithium hexafluorophosphate ($LiPF_6$) and/or sometimes lithium tetrafluoroborate ($LiBF_4$), dissolved in flammable carbonate-based organic solvents. There is an urge to identify non-flammable electrolytes that are thermally and electrochemically stable in order to improve safety of batteries.[7-9]

In this regard, room-temperature ionic liquids (RTILs), which are organic salts that remain liquid at room temperature, have attracted much attention due to their non-volatility and trifling "thermal sensitivity".[10,11] These salts usually consist of sterically demanding cations and/or anions with low charge densities and reduced noncovalent interactions, which eventually control the physicochemical and transport properties of RTILs.[12,13] Using design concepts based on the fundamental understanding noncovalent interactions, RTILs may be made as "task-specific" salts for a wide range of applications[14-16], particularly as electrolytes for batteries.[17,18] The most commonly studied IL-based electrolytes contain fluorinated anions are lithium hexafluorophosphate $LiPF_6$, bis(trifluoromethanesulfonyl)imide (TFSI)[19,20] and more recently bis(fluorosulfonyl)imide (FSI)[21]. Typically, these electrolytes are made by dissolving LiTFSI/LiFSI salts in their parent ILs with well-known cations such as phosphonium[22], pyrrolidinium[23], imidazolium[24], morpholinium[25] or piperidinium.[26] The use of fluorinated anions in batteries, however, makes these electrolytes less desirable due to their sensitivity to

moisture, corrosion of current collectors and potential health and environmental risks during recycling of used batteries.[27-29]

The number of studies on ILs and IL-based electrolytes has increased dramatically during the last two decades, however, most of these studies are focused on commercially available ILs[11,30] and relatively less number of studies have reported new ILs.[31-33] In the context of electrolytes, anion plays a crucial role not only in determining the physicochemical and electrochemical properties but also the overall performance as an electrolyte.[34] This is due to the fact that Li^+ ion directly interacts with the anion through electrostatic interactions and affect the properties of electrolytes.[35] As demonstrated by Brennecke *et al.*[36] the cation dependence is much smaller than the anions on the key physiochemical properties of ILs. Also, the solvation sphere, which transports Li^+ ions in the solvent matrix of an electrolyte and subsequently into the electrode structure significantly depend on the nature of anion.[37]

As the nature and chemical structure of an anion plays an important role in deciding the key properties of an electrolyte, in this study, we present new classes of fluorine-free aromatic carboxylate anions functionalized with oligoether chains, coupled with a common tetrabutylphosphonium $(P_{4444})^+$ cation. The anions are design with an aim to bring together the properties of aromaticity by incorporating phenyl ring and structural flexibility by substitution with oligoether chains in a single structure. All the ILs, synthesized using several steps synthetic protocol, are room temperature liquids. A systematic correlation between the anion chemistry and the key physicochemical properties with an emphasis on the ion transport behavior is established.

Experimental

Materials and Synthesis

Unless otherwise noted, all the commercial reagents were utilized without any additional purification. Salicylic acid (ACS reagents, >95 % purity), 4-toluenesulfonyl chloride (ACS

reagents, >97 % purity), 2-ethoxyethanol (>99 % purity), *iso*-propoxy ethanol (>99 % purity), diethylene glycol monoethyl ether (>99 % purity), an aqueous solution of tetrabutylphosphonium hydroxide (40 wt % in water) and lithium hydroxide monohydrate (ACS reagents, >98 % purity) were received from Sigma-Aldrich. Sodium sulphate, methanol, dichloromethane (DCM) and diethylether were purchased from VWR (BDH) chemicals. The synthesis and structural characterization of the intermediate and final products is described in detail in the supporting information (SI). The water content was measured by Karl Fischer titration (using Metrohm 917 Coulometer, Switzerland) and was determined to be less than 100 ppm for all synthesized ILs and the electrolytes.

Nuclear Magnetic Resonance Spectroscopy

The structures and purity of all the synthesized products were confirmed by using a Bruker Ascend Aeon WB 400 (Bruker BioSpin AG, Fallanden, Switzerland) nuclear magnetic resonance (NMR) spectrometer. $CDCl_3$ was used as a solvent. The working frequencies were 400.21 MHz for ^{1}H, 100.64 MHz for ^{13}C, and 162.01 MHz for ^{31}P. Data were processed using Bruker Topspin 3.5 software.

Thermal Analysis

Thermogravimetric analysis (TGA) was performed using a PerkinElmer TGA 8000 under N_2 gas at a heating rate of 10 °C per min. About 2-4 mg of sample was used for each experiment. The onset of decomposition temperature, T_{onset}, was calculated from the intersection of the baseline weight and the tangent of the weight versus temperature curve using the Pyris software. Differential scanning calorimetry (DSC) was performed using a PerkinElmer DSC 6000 on 2-5 mg of the sample placed in an aluminum pan. DSC data were collected at a scanning rate of 5 °C min^{-1} for both cooling and heating traces. To maintain an inert environment inside the sample chamber, dry N_2 gas was delivered at a constant flow rate of 20 mL min^{-1}. The glass

transition temperature (T_g) was determined by using the inflection mid-point of the initial *S*-shaped transition slope and determined from the onset with the aid of the Pyris software.

Electrochemical Characterization

The electrochemical stability and ionic conductivity were determined using a Metrohm Autolab PGSTAT302N electrochemical workstation with a FRA32M module for impedance measurements, all controlled by a Nova 2.02 software. A sealed Microcell HC from RHD instruments Germany was used to hold about 70 µL of the sample. To determine the electrochemical stability window (ESW), linear sweep voltammetry (LSV) was performed with a three-electrode setup: a Pt wire with a diameter of 0.25 mm as a working electrode (WE), a Pt crucible as counter electrode (CE) as well as a sample container, and an Ag wire coated with AgCl as a pseudo-reference electrode (RE). Both cathodic and anodic scans were recorded at a rate of 1 mV s^{-1}. The electrochemical potentials were calibrated using ferrocene (Fc) as an internal reference and shifted using $E_{Li/Li^+} \approx E_{Fc/Fc^+} + 3.2$ V.[37] The ESWs limits were defined by a 0.1 mA cm^{-2} cut-off current density.

The ionic conductivity was obtained from the impedance measurements performed in a frequency range from 1 Hz to 1 MHz with an AC voltage amplitude of 10 mV_{rms}. All the impedance spectra were measured during heating and cooling over a temperature range from –20 to 100 ± 0.1 °C. A two-electrode configuration was employed for ionic conductivity measurements, with a wire Pt as a WE and a 70 µL Pt crucible as a sample container as well as CE.

Prior to each CV and ionic conductivity measurement, both the electrodes were polished with a 0.25 m of Kemet diamond paste. The cell constant was calculated using a Metrohm 100 S cm^{-1} KCl standard solution (K_{cell} = 18.5396 cm^{-1}). The cell was thermally equilibrated for 10 minutes before recording the impedance spectra.

PFG NMR Diffusometry

Pulsed field gradient (PFG) NMR diffusometry measurements were performed using a Bruker Ascend/Aeon WB 400 (Bruker BioSpin AG) NMR spectrometer with a resonance frequency of 400.27 MHz for ^{1}H and 155.56 MHz for ^{7}Li. The PFG NMR measurements were performed with a PFG NMR probe Diff50 (Bruker) with a maximum amplitude of the magnetic field gradient pulse of 29.73 T m^{-1}. The samples were placed in a standard 5 mm NMR glass tube and closed with a plastic stopper to avoid contact with air. Prior to measurements, each sample was equilibrated at a specific temperature for 30 min. The details of the PFG NMR technique for measuring molecular diffusion coefficients are available elsewhere.[38] The diffusivity of a molecule is the diffusion decay (DD) of amplitude A of NMR spectral line, obtained by Fourier transformation of a descending half of stimulated-echo (StE), as a function of the amplitude of applied pulsed field gradient. For the stimulated echo pulse sequence used, diffusion decay of A in the case of simple non-associating molecular liquid can be described by the Eq.(1):[39]

$$A(g,\delta,t_d) = A(0)\exp(-\gamma^2 g^2 \delta^2 D t_d) \quad (1)$$

where $A(0)$ is the factor proportional to the proton content in the system, and to spin-lattice and spin-spin relaxation times, γ is the gyromagnetic ratio for a used nucleus; g and δ are the amplitude and duration of the gradient pulse; t_d is the diffusion time; and D is the self-diffusion coefficient. t_d was in the range 4-100 ms for ^{1}H diffusion and 5-15 ms for ^{7}Li diffusion. No diffusion time dependence was observed in these measurements.

FTIR Spectroscopy

The attenuated total reflection Fourier transform infrared (ATR-FTIR) spectra of samples were recorded using a Bruker IFS 80v spectrometer equipped with a deuterated triglycine sulfate (DTGS) detector and diamond ATR accessory, employing the double-side forward–backward acquisition mode. The total number of scans was 256, co-added and signal-averaged at an optical resolution of 4 cm^{-1}.

Results and Discussion

We start with synthesis and structural characterization of the ether functionalized ILs and their electrolytes, followed by assessing their phase and thermal behavior, before moving on to more LIB-relevant performance parameters such as ionic conductivity, electrochemical stability, and ion diffusion of the ILs and the electrolytes made. Finally, FTIR spectroscopy is employed to address the local interactions, coordination, and ion–ion interactions.

Synthesis and Characterization

A multistep synthetic protocol is used to create the ether functionalized acids and their ILs. A brief description of synthesis and characterization is provided below, and the details are given in the SI. We begin by tosylation of the alcohols to replace –OH by a better leaving group and make it acceptable for its use as an alkylating agent (Scheme S1a).

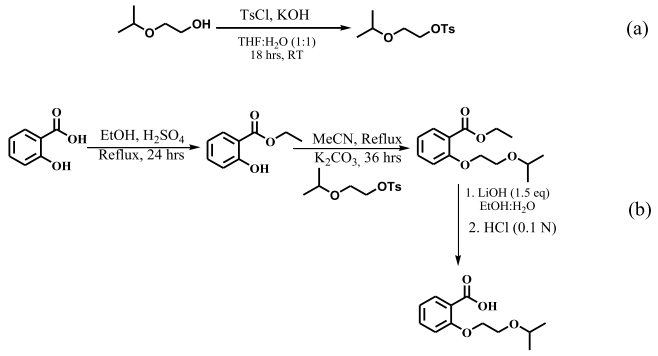

Scheme 1. (a) Tosylation of *iso*-propoxy ethanol (2-IE), (b) Synthetic rout for 2-(2-isopropoxyethoxy)benzoic acid (2-IEBA)

In second step, the tosylated alcohols are reacted with methyl esters in the presence of a mild base *i.e*; K_2CO_3 and acetonitrile as a reaction medium to obtain ether functionalized methylsalicylates. The esters are further converted into their corresponding acids *via* basic ester hydrolysis (Scheme S1b). Finally, the acids are converted into ILs *via* a simple neutralization reaction with *n*-tetrabutylphosphonium hydroxide. The structures and abbreviation of the ionic component of the synthesized ILs are shown in Figure 1.

The chemical structures of all the ILs agree well with the NMR spectroscopic analysis and the mass spectrometric data as shown in the SI. First, the ^{1}H NMR spectra of the ILs show characteristic resonance lines for the methylene protons of the ether chains in the anions in the range from 3.5 to 4.3 ppm. Second, the absence of the broad resonance line for the acidic proton and the appearance of distinct resonance lines in the aliphatic region; 0.90–1.0 ppm for the terminal methyl groups, the multiplet 1.46–1.54 ppm for the methylene protons, and another multiplet 2.39–2.46 ppm for the aliphatic alkyl chains attached to the $(P_{4444})^{+}$ cation corroborated the successful deprotonation of the corresponding acids and formation of the ILs (Figures S13-17). Third, the ^{13}C NMR spectra revealed resonance lines in the region 65–80 ppm attributed to the aliphatic carbon directly attached to the oxygen atoms in ether chains of the anions (Figures S23–26). In addition, the ^{13}C resonance lines for the carboxylate groups in the anions are found in the range 167–174 ppm. Finally, the ^{31}P NMR spectra indicate single resonance lines at *ca.* 33 ppm for each IL (Figures S81–22).

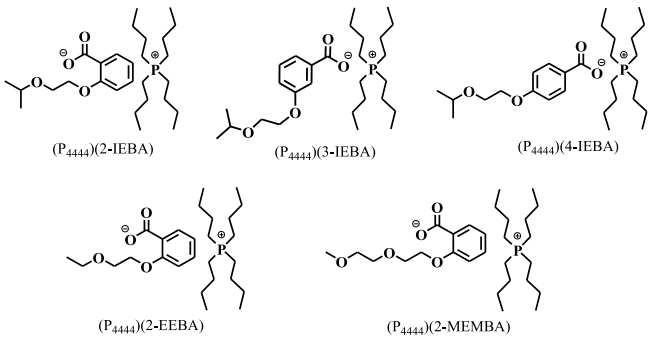

Figure 1. Chemical structures and abbreviations of the ionic components of the synthesized ILs.

Thermal properties

Figure 2 shows the TGA curves together with their derivative thermogravimetric analysis (DTG) for all the neat ILs and the electrolytes. All the systems show excellent dynamic thermal stability up to 280 °C, showing considerably higher thermal stability compared to any

traditional organic-solvent-based electrolyte.[40] It is important to note that the dynamic TGA analysis overestimate the thermal stability and should be complimented with the isothermal TGA to determine the precise thermal stability of IL-based electrolytes.[41] The (P_{4444})(3-IEBA) and (P_{4444})(4-IEBA) ILs show relatively higher thermal stability and one-stage decomposition. On the contrary, the (P_{4444})(2-IEBA), (P_{4444})(2-EEBA) and (P_{4444})(2-MEMBA) ILs present two-stage decomposition, with majority of the weight loss *ca.*70% comes from the first inflection, most probably due to the decomposition of the $(P_{4444})^+$ cation.[42]

The lower thermal stability of the ILs with ortho-substituted anions is due to the negative inductive and steric effects of the oxygen atom present in the oligoether chains. These effects decrease the electron density around carboxylate group of the anions leading to weaker ionic interactions. In the case of both meta- and para-substituted anions the positive inductive effect and the additional resonance effect of the meta-substitution cause an increase in the electron density around carboxylate centre. These effects enhance the polarity and subsequently increase the ionic interactions leading to higher thermal stability.

Doping the neat ILs with lithium salts brings an additional polarity and electrostatic interactions to the systems and, therefore, single steps decomposition occurred and further improvement in thermal stability is observed as well (Figure 2c), which is in agreement with the previously published reports on IL-based electrolytes.[25] The DTG curves (Figures 2b and 2d) show the rate of weight loss during the first decomposition step is much higher than the second decomposition step. In addition, the rate of weight loss is much lower for the electrolytes as compared with the neat ILs, which might be due the formation of stable lithium oxides. Overall, the thermal stability of these new ILs are comparable with the reported phosphonium-based ILs containing fluorine-free anions.[34,42]

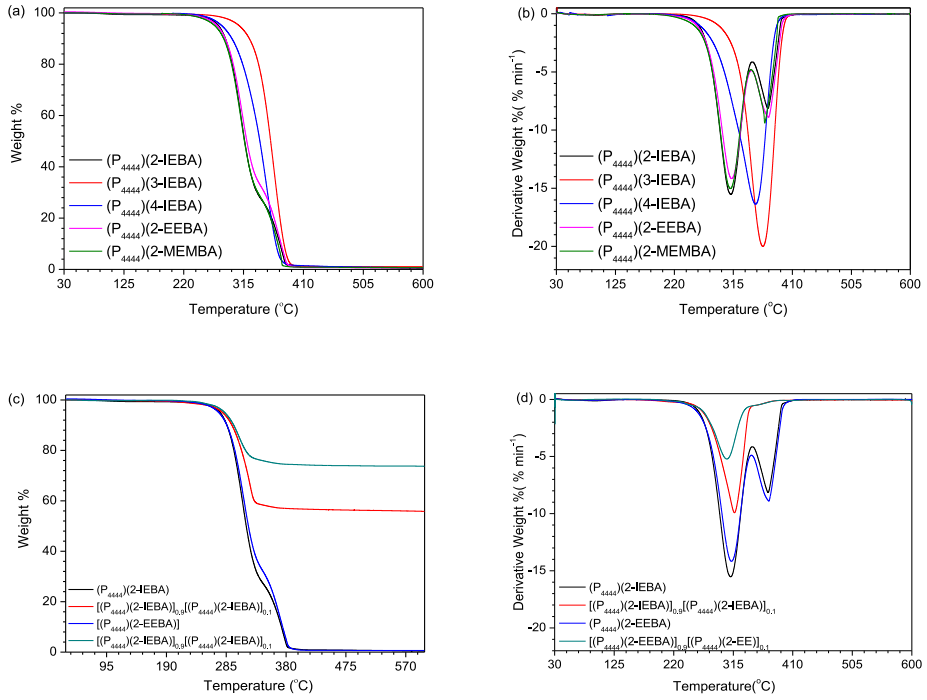

Figure 2. TGA thermograms (a and c), and DTG curves (b and d) of the neat ILs and the electrolytes.

DSC traces of the neat ILs and the electrolytes exhibit glass transition (T_g) in the temperature range from −62 °C to −58 °C, as shown in Figure 3 and the T_g values are tabulated in Table 1. In the case of IEBA-based ILs, changing the position of ether chain on the phenyl ring with respect to the carboxylate group is affecting T_g values – from ortho to meta to para, a gradual increase in T_g is observed. It suggests that the (P_{4444})(2-IEBA) IL with ortho substitution has the least ionic interactions as compared with the meta and para substituted ILs, (P_{4444})(3-IEBA) and (P_{4444})(4-IEBA). As expected from the structural flexibility, an increase in the ethoxy units of the ether chains decreases the T_g, however, branching in the ether chain lead to an increase in the T_g, suggesting efficient crystal packing and stronger ionic interactions.

Overall the T_g values of these ILs are higher than the previously reported non-aromatic ether-based (P_{4444})(MEEA) IL.[34] This is most probably due the contribution of the phenyl ring

providing additional pi-pi stacking and restricting the free low energy rotations of the ether chains.[43] As expected, doping of the ILs with lithium-salts slightly increase the T_g values (Table 1) of the electrolytes, thanks to the free low energy rotations of ether chains dominating over the increasing content of the "hard", dynamically cross-linking Li^+ ions.[44]

Table 1. Physiochemical properties of the synthesized ILs and the electrolytes.

System	T_g (ºC)	T_d (ºC)	σ (S cm^{-1})
(P_{4444})(2-IEBA)	-60	282	$1.9E^{-4}$
(P_{4444})(3-IEBA)	-58	330	$1.00E^{-4}$
(P_{4444})(4-IEBA)	-56	291	$5.6E^{-5}$
(P_{4444})(2-EEBA)	-58	282	$6.1E^{-5}$
(P_{4444})(2-MEMBA)	-62	284	$6.7E^{-5}$
$[(P_{4444})(2\text{-IEBA})]_{0,9}$ $[(Li)(2\text{-IEBA})]_{0,1}$	-62	288	$1.2E^{-4}$
$[(P_{4444})(2\text{-EEBA})]_{0,9}$ $[(Li)(2\text{-EEBA})]_{0,1}$	-60	289	$5.5E^{-5}$

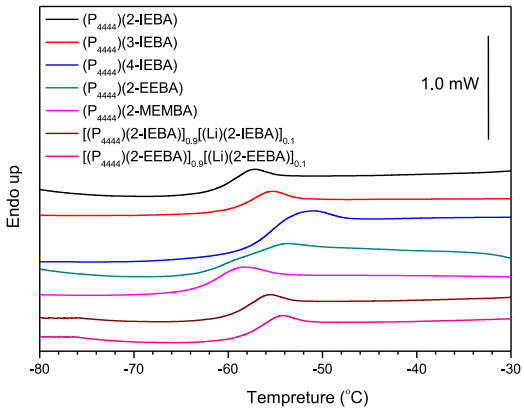

Figure 3. DSC traces for the neat ILs and the electrolytes. The traces are shifted along Y-axis for clarity.

Ionic Conductivity

Ionic conductivity is one of the most important feature to be considered when designing new electrolytes.[45] Here, it is observed that changing the position of the ether functionality can influence the ionic conductivity to a larger extent than changing length of the ether functional group (Figure 4). The (P_{4444})(2-IEBA) IL with ortho substitution shows the highest conductivity of 0.14 mS cm^{-1} at 20 °C , which is attributed to the reduced ionic interactions as a result of the repulsion between the terminal isopropyl group of the $(2\text{-IEBA})^-$ anion and alkyl chains of the $(P_{4444})^+$ cation. The para substituted (P_{4444})(4-IEBA) IL reveals the lowest ionic conductivity because the ether group is far from carboxylate group and there is no hindrance for the $(P_{4444})^+$ cation to approach the $(4\text{-IEBA})^-$ anion. The (P_{4444})(2-EEBA) IL with a shorter ether chain provide comparable ionic conductivity to the (P_{4444})(2-MEMBA) IL with a slightly longer ether chain, which is in accordance with the previous findings for ether functionalized cation-based ILs.[46]

The addition of Li^+ ions to the ILs lead to a slight decrease in the ionic conductivity of the electrolytes, which is primarily due the reduction of free volume as a result of stronger

electrostatic interactions (Figure 4b). It is quite expected because the incorporation of Li^+ ions into ILs is known to create clusters by simultaneous coordination with multiple anions, leading to dynamic cross-linking and thus reduce ionic mobility. The ionic conductivities are further analyzed by fitting the data to the Vogel-Fulcher-Tammann (VFT) equation.

$$\sigma = \sigma_0 \exp\left(\frac{-B}{(T - T_0)}\right) \quad (2)$$

Where σ_0 is a pre-exponential factor, B and T_0 are adjustable parameters, where the former is an empirical material-dependent fitting parameter related to the dynamic T_g and activation/pseudo activation energy (E_σ) of the system, and the latter is referred to the ideal vitreous transition temperature, at which configurational entropy vanishes, that can be determined by fitting the temperature-dependent conductivity data to the VTF equation.

The resulting VFT parameters show that the E_σ for IEBA-based neat ILs decreases in the order (P_{4444})(4-IEBA) > (P_{4444})(3-IEBA) > (P_{4444})(2-IEBA) (Table S1), which agrees well with the DSC data and again indicates that a higher thermal energy is required to reach the same ion mobility. As expected, the T_0 values for all these systems are about 60 K smaller than the glass transition temperatures T_g obtained from the DSC data and is in a accordance with the empirical approximation for IL-based electrolytes: $T_0/T_g \approx 0.75$.[47]

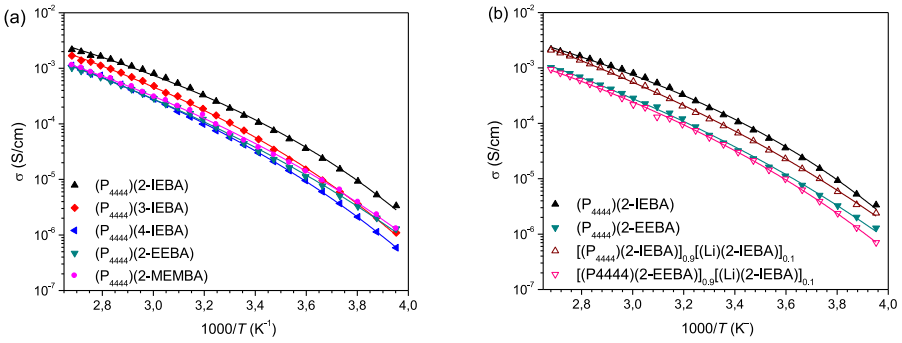

Figure 4. Ionic conductivity of the neat ILs (a) and the electrolytes (b) as a function of temperature. The solid lines indicate best fit of the data to the VFT equation.

Electrochemical stability

The electrochemical stability is assessed through LSV by recording both cathodic and anodic scans using GC as a working electrode at 20 °C (Figure 5). During cathodic scans, all the ILs and electrolytes reveal continuous reduction below 1 V (*vs* Li/Li^+), which is consistent with the previous reports on phosphonium-based ILs.[42,48,49] The low cathodic stability of phosphonium-based ILs is attributed to the presence of acidic alpha methylene protons of the phosphonium cations.[50] (P_{4444})(3-IEBA) shows improved cathodic potential as compared with the other neat ILs, which again might be related to the electron donating effect of the oxygen atom towards carboxylate group *via* resonance effect. On the anodic side, anions of the neat ILs are oxidizing between 3.50-4.00 V (*vs* Li/Li^+). An increase in the number of ethoxy units in the anions increases the anodic limit.

The neat (P_{4444})(2-IEBA) and (P_{4444})(2-EEBA) ILs doped with lithium salts reveal slightly narrower ESWs.

The $[(P_{4444})(2\text{-EEBA})]_{0.9}[(Li)(2\text{-EEBA})]_{0.1}$ electrolyte shows an oxidation peak at 3.79 V (*vs* Li/Li^+), which might be due to the oxidation of the ethoxy groups present in the anion.[34] In addition, two pronounced peaks C_1 and C_2 observed on the cathodic scan side at 1.30, and 0.75 *vs* Li/Li^+ V. The C_1 and C_2 peaks can be associated with the underpotential deposition (UPD) of lithium and partial decomposition of the $(P_{4444})^+$ cation on GC electrode.[51,52] The UPD layer formation can modify the nature of the GC working electrode surface, which is beneficial for the extended cathodic limits of the electrolytes, where the Li^+ ions can pass and prevent further reduction of the $(P_{4444})^+$ cation. Overall, the ESWs (*ca.* 3.14–3.57 V) of these novel ILs are comparable with the commonly studied imidazolium-[53] and phosphonium[54]-based ILs containing TFSI and other fluorinated anions. However, all of these ESWs should be regarded as the upper limits because we are utilizing a sweep approach and the ILs and the electrolytes are viscous at room temperature.

Table 2. Cathodic limit and anodic limit and ESWs of the neat ILs and the electrolytes at 20 °C using GC as a WE.

System	E_C (V vs Li/Li$^+$)	E_A (V vs Li/Li$^+$)	ESW
(P_{4444})(2-IEBA)	0.53	3.85	3.32
(P_{4444})(3-IEBA)	0.40	3.89	3.49
(P_{4444})(4-IEBA)	0.88	4.01	3.13
(P_{4444})(2-EEBA)	0.43	4.02	3.59
(P_{4444})(2-MEMBA)	1.12	4.20	3.08
[(P_{4444})(2-IEBA)]$_{0,9}$ [(Li)(2-IEBA)]$_{0,1}$	0.42	3.89	3.47
[(P_{4444})(2-EEBA)]$_{0,9}$ [(Li)(2-EEBA)]$_{0,1}$	1.39	3.68	2.29

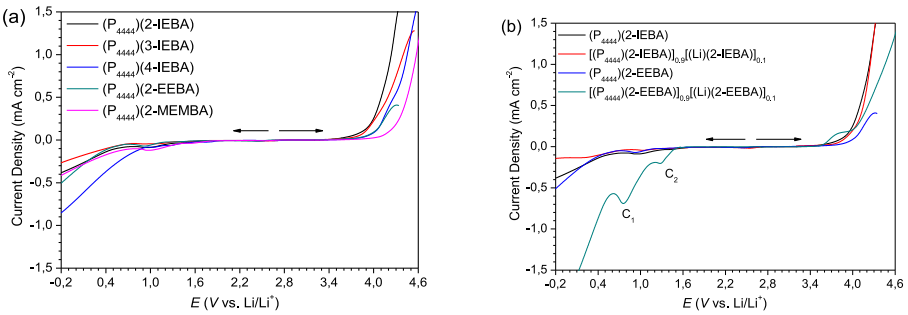

Figure 5. LSV curves of the neat ILs (a) and the electrolytes (b) using GC as the WE at 20 °C.

NMR Diffusometry

After establishing the overall ionic mobilities at a macroscopic level using DSC and impedance spectroscopy, ^{1}H and ^{31}P PFG NMR spectroscopy was used to gain deeper insights into the relative cation and anion mobility and further understand the transport properties at a molecular level. For all these studied systems, the diffusion coefficients of all species show a monotonous increase as a function of temperature and follows the VFT behavior (Figure 6a). It is interesting

to note that the self-diffusion coefficients of cation (D_{cation}) and anion (D_{anion}) in all the neat ILs measured by ^{1}H NMR is approximately same and cannot be separated, which is primarily due that their comparable molar masses. The D_{cation} were further measured by ^{31}P and the values match very well to the ones measured by ^{1}H (Figure 6b), confirming the simultaneous diffusivity of both cations and anions with the same diffusion coefficients.

The addition of lithium salts to the ILs lead to a decrease in diffusivity of both cations and anions due to additional electrostatic interactions in the systems leading ion clustering and thus reduced diffusivity (Figures 6c and 6d). The diffusivity of cations is suppressed by a large extent than the anions, which is unexpected because Li^+ generally interacts strongly anions due to opposite charges and thus reduce their diffusivity.[34] The clearly suggests that both the electrolytes possess freely moving anions, despite the addition of 10 mol % lithium salts. Although Li^+ has the smallest mass among these ions, it diffuses slowest and again the plausible reason is the formation ion aggregates. Li^+ ions are diffusing in the form of aggregates with larger sizes and masses, rather than individual ions.

In order to further analyze the comparative diffusivity of individual ions in the electrolytes, the apparent transference numbers of each ion is calculated from their diffusion coefficients using the equation 3.[55,56]

$$t_i = \frac{x_i D_i}{\sum i x_i D_i} \quad (3)$$

where t_i is the apparent transference number, x_i is the molar fraction of each individual ion, and D is the self-diffusion coefficient of an ion in $m^2\ s^{-1}$. The t_i for Li^+, $(P_{4444})^+$ and the anions as a function of temperature are shown in Figure 7. The t_i of the anions is found to be higher than both the $(P_{4444})^+$ cation and Li^+ ion, revealing a faster diffusion of the anions as compared with the cations. Among the three ions, t_i for Li^+ ion is the lowest throughout the studied temperature, again confirming that the ions are moving together in the form of clusters. An increase in temperature reveal a slight decrease in the t_i for anions, an increase in the t_i for

$(P_{4444})^+$ cation, while a little influence in seen on the t_i for Li^+ ion. It is important to note that PFG NMR diffusometry underestimate the diffusion coefficients of charged species because this technique averages the mobility of small ionic species and the larger aggregates, which are moving much slower than the individual ions. On the contrary, the transference numbers determined by electrochemical techniques are 2-3 fold larger than the numbers calculated from NMR experiments.[57] The lowest t_i for Li^+ ion compared to the organic ions in these electrolytes suggests that Li^+ ion is diffusing in the form of aggregates rather individual ions.

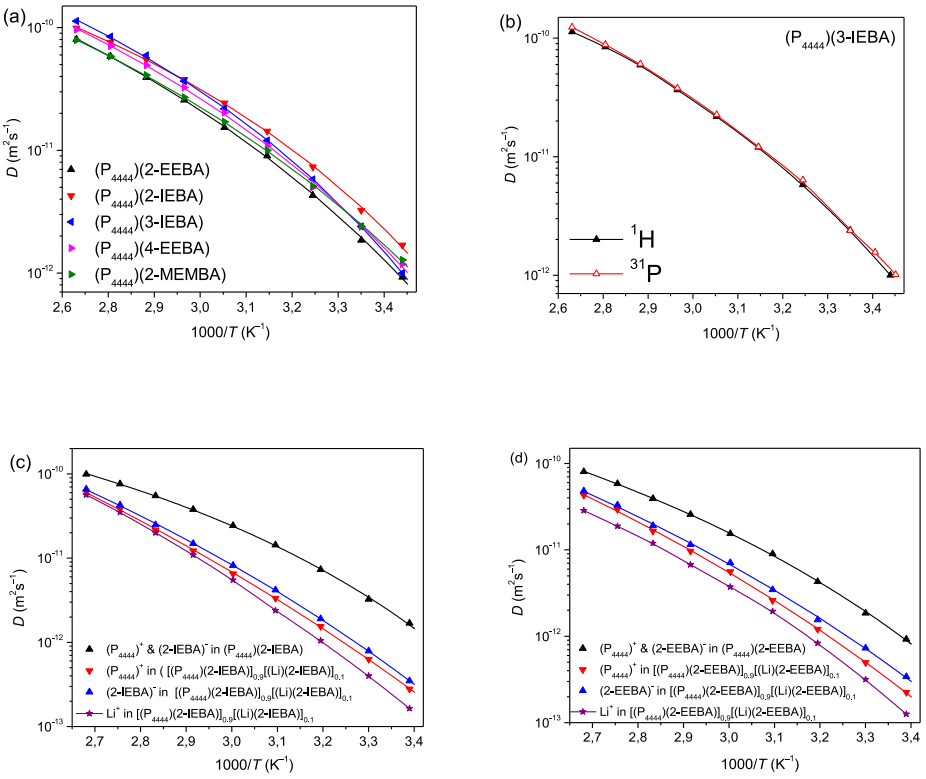

Figure 6. Diffusion coefficients of ions in the (a) neat ILs measured with ^1H NMR (b) the neat (P_{4444})(3-IEBA) IL measured with ^{31}P NMR, (c) the neat (P_{4444})(2-IEBA) IL and the electrolyte, and (d) the neat (P_{4444})(2-EEBA) IL and the electrolyte. Symbols indicate experimental data and the solid lines represent the VFT fittings.

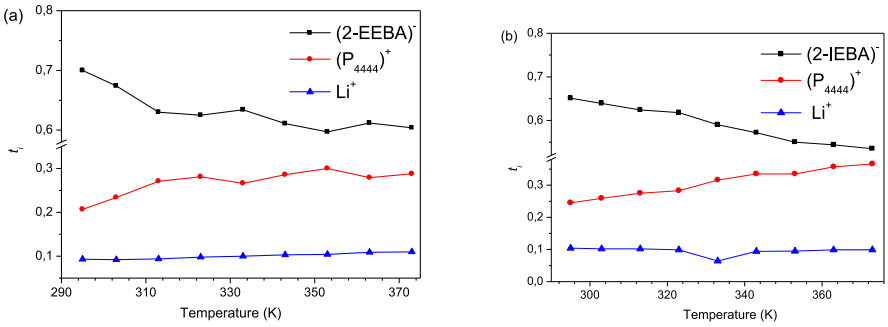

Figure 7. Apparent transfer numbers of ions in (a) $[(P_{4444})(2\text{-EEBA})]_{0.9}[(Li)(2\text{-EEBA})]_{0.1}$ and $[(P_{4444})(2\text{-IEBA})]_{0.9}[(Li)(2\text{-IEBA})]_{0.1}$ electrolytes calculated from the PFG NMR diffusion data.

Infrared Spectroscopy

FTIR spectroscopy is employed to better understand the ionic interactions in the neat ILs and the electrolytes, mainly focusing on the symmetric and asymmetric stretching of the carboxylate group, C–O stretching and CH_2 rocking bands of the anions (Figure 8). The full range spectra are shown in Figure S27. In the case of neat ILs, the asymmetric carbonyl stretching appears as a broad band at *ca.*1595 cm^{-1} with distinct satellite bands on both sides, indicating several different types of coordination/interaction active sites, whereas the symmetric stretching band appears as a single broad peak at *ca.* 1380 cm^{-1} pointing towards interactions of carboxylate group with the cation.[58] The symmetric stretching bands for (P_{4444})(3-IEBA) and (P_{4444})(4-IEBA) ILs shift slightly towards higher wavelength as compared to their structural isomer (P_{4444})(2-IEBA) IL, which is due to the electronic effect of the oxygen atom directly attached to the phenyl ring (Figure 8a).

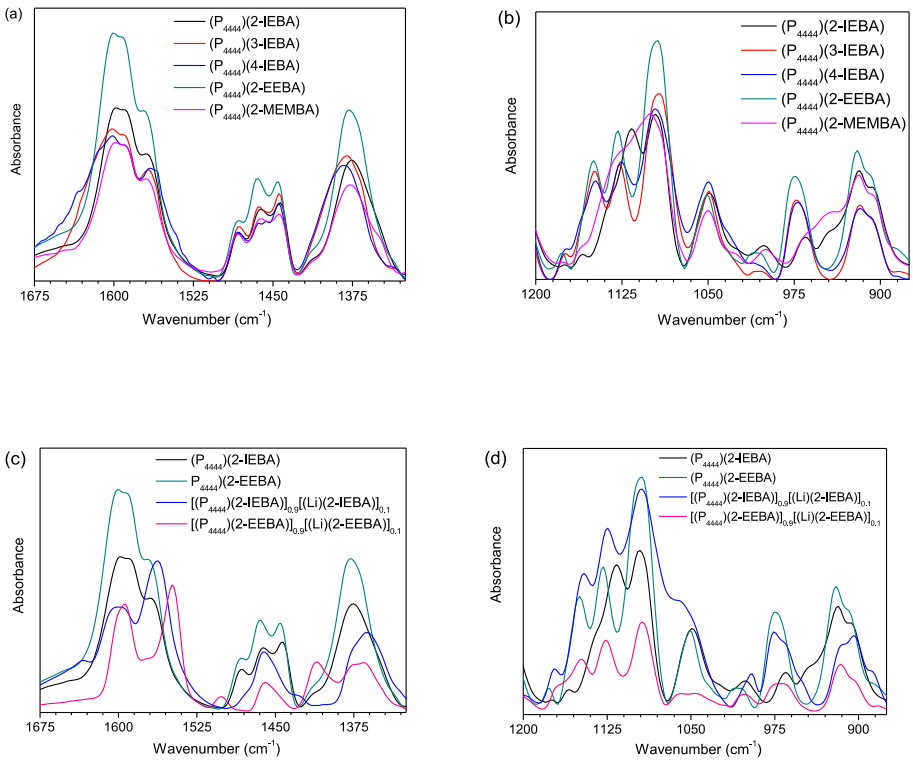

Figure 8. FTIR spectra of the neat ILs (a and b) and the electrolytes (c and d).

The spectral region between 1200 cm^{-1} and 800 cm^{-1} contains two main bands that correspond to the stretching of OCCO bonds (Figure 8b). The band at 1093 cm^{-1} is assigned to the OCCO antisymmetric stretching and the one at 920 cm^{-1} is associated to the combination of OCCO symmetric stretching and CH_2 rocking vibrations.[59] The distinct shoulder at the left side of the OCCO symmetric stretching and CH_2 rocking vibrations in the case of (P_{4444})(2-IEBA) and (P_{4444})(2-MEMBA) ILs indicates ionic interactions of the ethoxy units of anions with the aliphatic protons of the $(P_{4444})^+$ cation, which also agrees well with the relatively higher ionic conductivity of (P_{4444})(2-IEBA) IL compare to its structural isomers.

As expected, doping of the neat ILs with lithium salts changes the modes of interactions for both the electrolytes leading to splitting of the peak at 1595 cm^{-1} into two distinct bands,

confirming strong interactions of the Li^+ ion with the carboxylate group of the anions. This also brings similar changes in the symmetric stretching band at 1380 cm^{-1} (Figure 8c). In contrast, there are minimal changes in the spectral regions lower wavelengths indicating weak interactions of Li^+ ion with the ethoxy units of the ether chains (Figure 8de). This is most probably attributed to the electronic effect of the oxygen atom attached to the aromatic ring, donating electrons towards aromatic moiety that acquires partial positive charge leading to weaker coordination to the Li^+ ion.

Conclusion

Despite the structural similarities of these new classes of ether substituted ILs, (P_{4444})(2-IEBA) IL offered key beneficial properties including lower T_g, higher ionic conductivity and higher ion diffusivity. This IL, however, revealed lower dynamic thermal stability than its structural isomers (P_{4444})(3-IEBA) and (P_{4444})(4-IEBA) ILs. As quite expected, the addition of Li^+ ions to the ILs decrease ionic mobility and leading to reduced ionic conductivity and ion diffusivity, although a monotonous increase in both the ionic conductivity and ion diffusivity is seen as a function of temperature. The anions diffused faster within the electrolytes than the $(P_{4444})^+$ cation and Li^+ ion, in spite of the fact that FTIR revealed interactions between the Li^+ ions and the carboxylate group of the anions. Altogether, the nearly designed ILs and the electrolytes have promising properties to be used as electrolytes in next-generations batteries operating at elevated temperatures and over a wide potential range.

Acknowledgment

The financial support from the Swedish Energy Agency (project number: 48194-1) is gratefully acknowledged.

References

(1) Wu, F.; Maier, J.; Yu, Y. Guidelines and trends for next-generation rechargeable lithium and lithium-ion batteries. *Chemical Society Reviews* **2020,** *49* (5), 1569.

(2) Zhang, L.; Li, X.; Yang, M.; Chen, W. High-safety separators for lithium-ion batteries and sodium-ion batteries: advances and perspective. *Energy Storage Materials* **2021,** *41*, 522.
(3) Zheng, Y.; Yao, Y.; Ou, J.; Li, M.; Luo, D.; Dou, H.; Li, Z.; Amine, K.; Yu, A.; Chen, Z. A review of composite solid-state electrolytes for lithium batteries: fundamentals, key materials and advanced structures. *Chemical Society Reviews* **2020,** *49* (23), 8790.
(4) Chombo, P. V.; Laoonual, Y. A review of safety strategies of a Li-ion battery. *Journal of Power Sources* **2020,** *478*, 228649.
(5) Duan, J.; Tang, X.; Dai, H.; Yang, Y.; Wu, W.; Wei, X.; Huang, Y. Building safe lithium-ion batteries for electric vehicles: a review. *Electrochemical Energy Reviews* **2020,** *3* (1), 1.
(6) Etacheri, V.; Marom, R.; Elazari, R.; Salitra, G.; Aurbach, D. Challenges in the development of advanced Li-ion batteries: a review. *Energy & Environmental Science* **2011,** *4* (9), 3243.
(7) Wang, Q.; Jiang, L.; Yu, Y.; Sun, J. Progress of enhancing the safety of lithium ion battery from the electrolyte aspect. *Nano Energy* **2019,** *55*, 93.
(8) Deng, K.; Zeng, Q.; Wang, D.; Liu, Z.; Wang, G.; Qiu, Z.; Zhang, Y.; Xiao, M.; Meng, Y. Nonflammable organic electrolytes for high-safety lithium-ion batteries. *Energy Storage Materials* **2020,** *32*, 425.
(9) Zhang, S. S. A review on electrolyte additives for lithium-ion batteries. *Journal of Power Sources* **2006,** *162* (2), 1379.
(10) Lewandowski, A.; Świderska-Mocek, A. Ionic liquids as electrolytes for Li-ion batteries—An overview of electrochemical studies. *Journal of Power sources* **2009,** *194* (2), 601.
(11) Brutti, S.; Simonetti, E.; De Francesco, M.; Sarra, A.; Paolone, A.; Palumbo, O.; Fantini, S.; Lin, R.; Falgayrat, A.; Choi, H. Ionic liquid electrolytes for high-voltage, lithium-ion batteries. *Journal of Power Sources* **2020,** *479*, 228791.
(12) Benedetto, A.; Ballone, P. Room temperature ionic liquids meet biomolecules: a microscopic view of structure and dynamics. *ACS Sustainable Chemistry & Engineering* **2016,** *4* (2), 392.
(13) Fedorov, M. V.; Kornyshev, A. A. Ionic liquids at electrified interfaces. *Chemical reviews* **2014,** *114* (5), 2978.
(14) Rostamizadeh, S.; Zekri, N.; Tahershamsi, L. Nanosilica supported dual acidic ionic liquid as a recyclable catalyst for the rapid and green synthesis of polycyclic phenolic compounds. *Polycyclic Aromatic Compounds* **2014,** *34* (5), 542.
(15) Wu, J.; Xu, F.; Li, S.; Ma, P.; Zhang, X.; Liu, Q.; Fu, R.; Wu, D. Porous polymers as multifunctional material platforms toward task-specific applications. *Advanced Materials* **2019,** *31* (4), 1802922.
(16) Lee, S.-g. Functionalized imidazolium salts for task-specific ionic liquids and their applications. *Chemical Communications* **2006,** (10), 1049.
(17) Niu, H.; Wang, L.; Guan, P.; Zhang, N.; Yan, C.; Ding, M.; Guo, X.; Huang, T.; Hu, X. Recent advances in application of ionic liquids in electrolyte of lithium ion batteries. *Journal of energy storage* **2021,** *40*, 102659.
(18) Ilyas, F.; Ishaq, M.; Jabeen, M.; Saeed, M.; Ihsan, A.; Ahmed, M. Recent trends in the benign-by-design electrolytes for zinc batteries. *Journal of Molecular Liquids* **2021,** *343*, 117606.
(19) Karuppasamy, K.; Vikraman, D.; Hwang, I.-T.; Kim, H.-J.; Nichelson, A.; Bose, R.; Kim, H.-S. Nonaqueous liquid electrolytes based on novel 1-ethyl-3-methylimidazolium bis (nonafluorobutane-1-sulfonyl imidate) ionic liquid for energy storage devices. *Journal of Materials Research and Technology* **2020,** *9* (2), 1251.

(20) Elia, G. A.; Ulissi, U.; Jeong, S.; Passerini, S.; Hassoun, J. Exceptional long-life performance of lithium-ion batteries using ionic liquid-based electrolytes. *Energy & Environmental Science* **2016,** *9* (10), 3210.
(21) Liu, Q.; Hsu, C.-W.; Dzwiniel, T. L.; Pupek, K. Z.; Zhang, Z. A fluorine-substituted pyrrolidinium-based ionic liquid for high-voltage Li-ion batteries. *Chemical Communications* **2020,** *56* (53), 7317.
(22) Weng, W.; Zhang, Z.; Lu, J.; Amine, K. A disiloxane-functionalized phosphonium-based ionic liquid as electrolyte for lithium-ion batteries. *Chemical Communications* **2011,** *47* (43), 11969.
(23) McCallum, R.; Barghamadi, M.; Forsyth, C.; Hollenkamp, A. F.; Oldham, G.; Mahon, P. J.; Ruther, T. Comparing the Physicochemical, Electrochemical, and Structural Properties of Boronium versus Pyrrolidinium Cation-Based Ionic Liquids and Their Performance as Li-Ion Battery Electrolytes. *The Journal of Physical Chemistry C* **2021,** *125* (15), 8055.
(24) Sun, X.-G.; Liao, C.; Shao, N.; Bell, J. R.; Guo, B.; Luo, H.; Jiang, D.-e.; Dai, S. Bicyclic imidazolium ionic liquids as potential electrolytes for rechargeable lithium ion batteries. *Journal of power sources* **2013,** *237*, 5.
(25) Navarra, M. A.; Fujimura, K.; Sgambetterra, M.; Tsurumaki, A.; Panero, S.; Nakamura, N.; Ohno, H.; Scrosati, B. New Ether-functionalized Morpholinium-and Piperidinium-based Ionic Liquids as Electrolyte Components in Lithium and Lithium–Ion Batteries. *ChemSusChem* **2017,** *10* (11), 2496.
(26) Kim, K.; Cho, Y.-H.; Shin, H.-C. 1-Ethyl-1-methyl piperidinium bis (trifluoromethanesulfonyl) imide as a co-solvent in Li-ion batteries. *Journal of power sources* **2013,** *225*, 113.
(27) Yim, T.; Kwon, M. S.; Mun, J.; Lee, K. T. Room temperature ionic liquid-based electrolytes as an alternative to carbonate-based electrolytes. *Israel Journal of Chemistry* **2015,** *55* (5), 586.
(28) Thompson, D. L.; Hartley, J. M.; Lambert, S. M.; Shiref, M.; Harper, G. D.; Kendrick, E.; Anderson, P.; Ryder, K. S.; Gaines, L.; Abbott, A. P. The importance of design in lithium ion battery recycling–a critical review. *Green Chemistry* **2020,** *22* (22), 7585.
(29) Lisbona, D.; Snee, T. A review of hazards associated with primary lithium and lithium-ion batteries. *Process safety and environmental protection* **2011,** *89* (6), 434.
(30) Xu, C.; Yang, G.; Wu, D.; Yao, M.; Xing, C.; Zhang, J.; Zhang, H.; Li, F.; Feng, Y.; Qi, S. Roadmap on ionic liquid electrolytes for energy storage devices. *Chemistry–An Asian Journal* **2021,** *16* (6), 549.
(31) Armand, M.; Johansson, P.; Bukowska, M.; Szczeciński, P.; Niedzicki, L.; Marcinek, M.; Dranka, M.; Zachara, J.; Żukowska, G.; Marczewski, M. development of Hückel type anions: from molecular modeling to industrial commercialization. A success story. *Journal of The Electrochemical Society* **2020,** *167* (7), 070562.
(32) Hosseini-Bab-Anari, E.; Boschin, A.; Mandai, T.; Masu, H.; Moth-Poulsen, K.; Johansson, P. Fluorine-free salts for aqueous lithium-ion and sodium-ion battery electrolytes. *RSC advances* **2016,** *6* (88), 85194.
(33) Jankowski, P.; Wieczorek, W.; Johansson, P. Functional ionic liquids: cationic SEI-formers for lithium batteries. *Energy Storage Materials* **2019,** *20*, 108.
(34) Shah, F. U.; Gnezdilov, O. I.; Khan, I. A.; Filippov, A.; Slad, N. A.; Johansson, P. Structural and ion dynamics in fluorine-free oligoether carboxylate ionic liquid-based electrolytes. *The Journal of Physical Chemistry B* **2020,** *124* (43), 9690.
(35) Watanabe, M.; Thomas, M. L.; Zhang, S.; Ueno, K.; Yasuda, T.; Dokko, K. Application of ionic liquids to energy storage and conversion materials and devices. *Chemical reviews* **2017,** *117* (10), 7190.

(36) Shi, C.; Quiroz-Guzman, M.; DeSilva, A.; Brennecke, J. F. Physicochemical and electrochemical properties of ionic liquids containing aprotic heterocyclic anions doped with lithium salts. *Journal of The Electrochemical Society* **2013,** *160* (9), A1604.
(37) Neale, A. R.; Murphy, S.; Goodrich, P.; Hardacre, C.; Jacquemin, J. Thermophysical and Electrochemical Properties of Ethereal Functionalised Cyclic Alkylammonium-based Ionic Liquids as Potential Electrolytes for Electrochemical Applications. *ChemPhysChem* **2017,** *18* (15), 2040.
(38) Blümich, B.; Wiley Online Library, 1995.
(39) Tanner, J. E. Use of the stimulated echo in NMR diffusion studies. *The Journal of Chemical Physics* **1970,** *52* (5), 2523.
(40) Botte, G. G.; White, R. E.; Zhang, Z. Thermal stability of LiPF6–EC: EMC electrolyte for lithium ion batteries. *Journal of Power Sources* **2001,** *97*, 570.
(41) Shah, F. U.; Khan, I. A.; Johansson, P. Comparing the thermal and electrochemical stabilities of two structurally similar ionic liquids. *Molecules* **2020,** *25* (10), 2388.
(42) Khan, I. A.; Gnezdilov, O. I.; Filippov, A.; Shah, F. U. Ion Transport and Electrochemical Properties of Fluorine-Free Lithium-Ion Battery Electrolytes Derived from Biomass. *ACS Sustainable Chemistry & Engineering* **2021,** *9* (23), 7769.
(43) Girard, G. M.; Hilder, M.; Zhu, H.; Nucciarone, D.; Whitbread, K.; Zavorine, S.; Moser, M.; Forsyth, M.; Macfarlane, D. R.; Howlett, P. C. Electrochemical and physicochemical properties of small phosphonium cation ionic liquid electrolytes with high lithium salt content. *Physical chemistry chemical physics* **2015,** *17* (14), 8706.
(44) Gao, X.; Wu, F.; Mariani, A.; Passerini, S. Concentrated Ionic-Liquid-Based Electrolytes for High-Voltage Lithium Batteries with Improved Performance at Room Temperature. *ChemSusChem* **2019,** *12* (18), 4185.
(45) Ghandi, K. A review of ionic liquids, their limits and applications. *Green and sustainable chemistry* **2014,** *2014*.
(46) Fang, S.; Zhang, Z.; Jin, Y.; Yang, L.; Hirano, S.-i.; Tachibana, K.; Katayama, S. New functionalized ionic liquids based on pyrrolidinium and piperidinium cations with two ether groups as electrolytes for lithium battery. *Journal of Power Sources* **2011,** *196* (13), 5637.
(47) Silvester, D. S. Recent advances in the use of ionic liquids for electrochemical sensing. *Analyst* **2011,** *136* (23), 4871.
(48) Khan, I. A.; Gnezdilov, O. I.; Wang, Y.-L.; Filippov, A.; Shah, F. U. Effect of Aromaticity in Anion on the Cation–Anion Interactions and Ionic Mobility in Fluorine-Free Ionic Liquids. *The Journal of Physical Chemistry B* **2020,** *124* (52), 11962.
(49) Fraser, K. J.; MacFarlane, D. R. Phosphonium-based ionic liquids: an overview. *Australian journal of chemistry* **2009,** *62* (4), 309.
(50) Tsunashima, K.; Sugiya, M. Physical and electrochemical properties of low-viscosity phosphonium ionic liquids as potential electrolytes. *Electrochemistry Communications* **2007,** *9* (9), 2353.
(51) Wibowo, R.; Jones, S. E. W.; Compton, R. G. Investigating the electrode kinetics of the Li/Li+ couple in a wide range of room temperature ionic liquids at 298 K. *Journal of Chemical & Engineering Data* **2010,** *55* (3), 1374.
(52) Gasparotto, L.; Borisenko, N.; Bocchi, N.; El Abedin, S. Z.; Endres, F. In situ STM investigation of the lithium underpotential deposition on Au (111) in the air-and water-stable ionic liquid 1-butyl-1-methylpyrrolidinium bis (trifluoromethylsulfonyl) amide. *Physical Chemistry Chemical Physics* **2009,** *11* (47), 11140.
(53) Kazemiabnavi, S.; Zhang, Z.; Thornton, K.; Banerjee, S. Electrochemical stability window of imidazolium-based ionic liquids as electrolytes for lithium batteries. *The Journal of Physical Chemistry B* **2016,** *120* (25), 5691.

(54) De Vos, N.; Maton, C.; Stevens, C. V. Electrochemical stability of ionic liquids: general influences and degradation mechanisms. *ChemElectroChem* **2014,** *1* (8), 1258.
(55) Fromling, T.; Kunze, M.; Schonhoff, M.; Sundermeyer, J.; Roling, B. Enhanced lithium transference numbers in ionic liquid electrolytes. *The Journal of Physical Chemistry B* **2008,** *112* (41), 12985.
(56) Gélinas, B.; Natali, M.; Bibienne, T.; Li, Q. P.; Dollé, M. l.; Rochefort, D. Electrochemical and transport properties of ions in mixtures of electroactive ionic liquid and propylene carbonate with a lithium salt for lithium-ion batteries. *The Journal of Physical Chemistry C* **2016,** *120* (10), 5315.
(57) Martins, V. L.; Sanchez-Ramirez, N.; Ribeiro, M. C.; Torresi, R. M. Two phosphonium ionic liquids with high Li+ transport number. *Physical Chemistry Chemical Physics* **2015,** *17* (35), 23041.
(58) Shah, F. U.; Holmgren, A.; Rutland, M. W.; Glavatskih, S.; Antzutkin, O. N. Interfacial behavior of orthoborate ionic liquids at inorganic oxide surfaces probed by NMR, IR, and raman spectroscopy. *The Journal of Physical Chemistry C* **2018,** *122* (34), 19687.
(59) Frech, R.; Huang, W. Conformational changes in diethylene glycol dimethyl ether and poly (ethylene oxide) induced by lithium ion complexation. *Macromolecules* **1995,** *28* (4), 1246.

Supporting Information

Oligoether Substituted Aromatic Carboxylate Ionic Liquids and Electrolytes

Mukhtiar Ahmed[1], Andrei Filippov[1], Patrik Johansson[2*] and Faiz Ullah Shah[1*]

[1]Chemistry of Interfaces, Luleå University of Technology, SE-971 87 Luleå, Sweden

[2] Materials Physics, Department of Physics, Chalmers University of Technology, SE-412 96 Gothenburg, Sweden

[*]Corresponding authors:

patrik.johansson@chalmers.se

faiz.ullah@ltu.se

Synthesis

The synthesis procedure for 2-(2-isopropoxyethoxy)benzoic acid (2-IEBA) is described in detail, all other acids are synthesized using the same procedure. All the acids are synthesized using a two-steps reaction.

Synthesis of 2-(2-isopropoxyethoxy)benzoic acid (2-IEBA)

Step 1: Synthesis of 2-isopropoxyethyl 4-methylbenzenesulfonate

Tosylation of the corresponding alcohols was performed by the following the literature procedure with slight modifications [REF]. The 4-toluenesulfonyl chloride (1.1 g, 5.7 mmol, 1 equiv.) was dissolved in THF (500 ml) at room temperature making a solution "**A**". Solution of potassium hydroxide (0.38 g, 6.9 mmol, 1.2 equiv.) in water (20 mL) was dropped into the *iso*-propoxy ethanol (0.9 g, 8.6 mmol, 1.5 equiv.) over 5 minutes and after complete addition the mixture was further stirred for 10 minutes. Then the solution "**A**" was dropped into the mixture under vigorous stirring. The mixture was stirred at room temperature for 24 hours. 250 mL of water was added and the reaction mixture was extracted with DCM (3 x 100 mL). The organic layer was dried over Na_2SO_4, gravity filtered, and the solvent was removed by rotary evaporation, a pale-yellow liquid was obtained and used in the next step without further purification.

Step 2: Synthesis aromatic acids

A solution of 2-isopropoxyethyl 4-methylbenzenesulfonate (38.7 g, 0.15 moles, 1.5 equiv. in 100 ml of dry acetonitrile), methyl salicylate (15.2g, 0.1 moles, 1 equiv.) and potassium carbonate (69 g, 0.5 moles, 5 equiv.) in a dry acetonitrile (250 mL) was heated at 70 °C under N_2 and continuous stringing for 48 hours. The yellow suspension was filtered off and the solid was washed with 60 mL of acetonitrile. The extract and washes were concentrated *via* rotary evaporation. The residue was extracted with DCM (3 x 50 mL). The organic phase was washed with water (6 x 150 mL). The organic layer was dried over Na_2SO_4, gravity filtered, and the solvent was removed by a rotary evaporation to afford the product **B2** as a yellow oil. **B2** was dissolved in THF:MeOH (1:1, 50 mL) and dropped into the aqueous solution of $LiOH.H_2O$ (3 equiv.), stirred at room temperature for 12 hrs, neutralized with 0.1 M HCl and extracted with DCM (3 x 25 mL). The organic phase was washed with water (6 x 150 mL), dried over Na_2SO_4, gravity filtered, and the solvent was removed by rotary evaporation to afford the product 2-(2-isopropoxyethoxy)benzoic acid (2-IEBA) as a dark yellow liquid. All the acids were separated in good yields *ca.* 60%.

2-(2-isopropoxyethoxy)benzoic acid (2-IEBA): Dark yellow liquid. ^{1}H NMR (400.21 MHz, $CDCl_3$), $^{\delta}$(ppm): 10.34 (*b*, 1H), 8.16-8.14 (*d*, $^3J_{HH}$ = 8.2 Hz 1H), 7.56-7.52 (*d*, $^3J_{HH}$ = 8.1 Hz,

1H), 7.11-7.03 (*t*, $^{3}J_{HH}$ = 8.3 Hz 1H), 4.37-4.34 (*t*, $^{3}J_{HH}$ = 4.3 Hz, 2H, O-CH_2-), 3.84-3.82 (*t*, $^{3}J_{HH}$ = 4.5 Hz, 2H, -CH_2-O), 3.72-3.66 (*sept*, $^{3}J_{HH}$ = 6.1 Hz, 1H, -CH), 1.21-1.20 (*d*, $^{3}J_{HH}$ = 6.1 Hz, 6H, -CH_3) ppm. ^{13}C NMR (100.64 MHz, $CDCl_3$): 171.20, 163.58, 132.43, 121.78, 114.56, 72.47, 68.12, 66.45, 22.19.

3-(2-isopropoxyethoxy)benzoic acid (3-IEBA):: Dark yellow liquid. ^{1}H NMR (400.21 MHz, $CDCl_3$), $^{\delta}$(ppm): 11.66 (*b*, 1H), 7.73-7.71 (*d*, $^{3}J_{HH}$ = 7.6 Hz 1H), 7.66 (*s*, 1H),7.40-7.36 (*t*, $^{3}J_{HH}$ = 8.0 Hz 1H), 7.19-7.18 (*t*, $^{3}J_{HH}$ = 8.0 Hz 1H), 4.20-4.17 (*t*, $^{3}J_{HH}$ = 4.8 Hz, 2H, O-CH_2-), 3.85-3.82 (*t*, $^{3}J_{HH}$ = 4.7 Hz, 2H, -CH_2-O), 3.76-3.69 (*sept*, $^{3}J_{HH}$ = 6.7 Hz, 1H, -CH), 1.24-1.23 (*d*, $^{3}J_{HH}$ = 6.2 Hz, 6H, -CH_3) ppm. ^{13}C NMR (100.64 MHz, $CDCl_3$): 171.20, 163.58, 132.43, 121.78, 114.56, 72.47, 68.12, 66.45, 22.19.

4-(2-isopropoxyethoxy)benzoic acid (4-IEBA):: Dark yellow liquid. ^{1}H NMR (400.21 MHz, $CDCl_3$), $^{\delta}$(ppm): 8.07-8.05 (*d*, $^{3}J_{HH}$ = 8.6 Hz, 2H), 7.99-7.97 (*d*, $^{3}J_{HH}$ = 8.6 Hz, 2H), 4.21-4.18 (*t*, $^{3}J_{HH}$ = 4.6 Hz, 2H, O-CH_2-), 3.83-3.81 (*t*, $^{3}J_{HH}$ = 5.2 Hz, 2H, -CH_2-O), 3.81-3.68 (*sept*, 3J_{HH} = 6.0 Hz, 1H, -CH), 1.24-1.22 (*d*, $^{3}J_{HH}$ = 6.1 Hz, 6H, -CH_3) ppm. ^{13}C NMR (100.64 MHz, $CDCl_3$): 171.20, 163.58, 132.43, 121.78, 114.56, 72.47, 68.12, 66.45, 22.19.

2-(2-ethoxyethoxy)benzoic acid (2-EEBA): Dark yellow liquid. ^{1}H NMR (400.21 MHz, $CDCl_3$), $^{\delta}$(ppm): 10.81 (*b*, 1H), 8.14-8.12 (*d*, $^{3}J_{HH}$ = 7.9 Hz 1H), 7.55-7.51 (*t*, $^{3}J_{HH}$ = 7.6 Hz, 1H), 7.13-7.11 (*d*, $^{3}J_{HH}$ = 7.5 Hz 1H), 7.10-7.03 (*t*, $^{3}J_{HH}$ = 8.3 Hz, 1H), 4.37-4.34 (*t*, $^{3}J_{HH}$ = 4.3 Hz, 2H, O-CH_2-), 3.84-3.82 (*t*, $^{3}J_{HH}$ = 4.2 Hz, 2H, -CH_2-O), 3.62-3.56 (*t*, $^{3}J_{HH}$ = 6.9 Hz, 2H, -CH_2-O), 1.25-1.21 (*d*, $^{3}J_{HH}$ = 6.9 Hz, 3H, -CH_3) ppm. ^{13}C NMR (100.64 MHz, $CDCl_3$): 165.85, 157.64, 134.93, 133.71, 122.62, 118.74, 113.75, 69.48, 67.86, 67.09, 15.03.

2-(2-(2-methoxyethoxy)ethoxy)benzoic acid (2-MEMBA): Dark yellow liquid. ^{1}H NMR (400.21 MHz, $CDCl_3$), $^{\delta}$(ppm): 10.91 (*b*, 1H), 8.18-8.16 (*d*, $^{3}J_{HH}$ = 8.0 Hz 1H), 7.55-7.52 (*d*, $^{3}J_{HH}$ = 8.1 Hz, 1H),7.14-7.06 (*t*, $^{3}J_{HH}$ = 8.1 Hz 1H), 4.40-4.37 (*t*, $^{3}J_{HH}$ = 4.6 Hz, 2H, O-CH_2-), 3.95-3.92 (*t*, $^{3}J_{HH}$ = 4.9 Hz, 2H, -CH_2-O), 3.64-3.62 (*t*, $^{3}J_{HH}$ = 4.3 Hz, 2H, -CH_2-O), 3.54-3.53 (*t*, $^{3}J_{HH}$ = 5.2 Hz, 2H, -CH_2-O), 1.20 (*t*, $^{3}J_{HH}$ = 5.1 Hz, 3H, -CH_3) ppm. ^{13}C NMR (100.64 MHz, $CDCl_3$): 165.71, 157.57, 134.92, 133.81, 122.65, 118.70, 113.57, 71.05, 69.93, 69.33, 68.83, 66.87, 15.23.

Synthesis of ionic liquids

An aqueous solution of the tetrabutylphosphonium hydroxide (13.82 g, 50 mmol) was added dropwise into the stirred aqueous solution of the acid (50 mmol in 50 ml of water). The reaction mixture was stirred at room temperature for 4 hours and progress of the reaction was monitored *via* thin layer chromatography (TLC) and upon completion of the reaction water was removed under reduced pressure using a rotary evaporator. The products were washed three times with

50 ml of diethyl ether before being dissolved in dichloromethane and dried over anhydrous Na_2SO_4. Finally, the solution was filtered, residual solvent was removed under reduced pressure, and the final products were dried in a vacuum oven at 80 °C for more than 4 days. All the products were separated in quantitative yields.

(P_{4444})(2-IEBA): Pale yellow liquid. MS (ESI). $[C_{16}H_{36}P]^+$: Calcd m/z 259.2556. Found m/z 259.2565, $[C_{12}H_{15}O_4]^-$: Calcd m/z 223.0975, Found m/z 223.1071. ^{1}H NMR (400.21 MHz, $CDCl_3$), $^\delta$(ppm): 7.45-7.44 (*d*, $^3J_{HH}$ = 6 Hz 1H), 7.09-7.07 (*d*, $^3J_{HH}$ = 7.5 Hz, 1H), 6.85-6.82 (*m*, 2H), 4.18-4.16 (*t*, $^3J_{HH}$ = 5.6 Hz, 2H, O-CH_2-), 3.76-3.73 (*t*, $^3J_{HH}$ = 5.1 Hz, 2H, -CH_2-O), 3.61-3.58 (*sept*, $^3J_{HH}$ = 5.1 Hz, 1H, -CH), 2.41-2.34 (*m*, 8H, P-CH_2-), 1.48-1.46 (*m*, 16H, -CH_2-), 1.21-1.20, (*d*, $^3J_{HH}$ = 6.1 Hz, 6H, -CH_3) ppm. 0.84-0.87 (t, $3J_{HH}$ = 7.1 Hz, 12H, -CH_3) ppm. ^{13}C NMR (100.64 MHz, $CDCl_3$): 171.20, 163.58, 132.43, 121.78, 114.56, 72.47, 68.12, 66.45, 22.19. ^{31}P NMR (162.01 MHz, $CDCl_3$): 33.00 ppm.

(P_{4444})(3-IEBA): Pale yellow liquid. MS (ESI). $[C_{16}H_{36}P]^+$: Calcd m/z 259.2556. Found m/z 259.2569, , $[C_{12}H_{15}O_4]^-$: Calcd m/z 223.0975, Found m/z 223.0934. ^{1}H NMR (400.21 MHz, $CDCl_3$), $^\delta$(ppm): 7.67-7.65 (*m*, 2H), 7.20-7.16 (*m*,1H), 6.90-6.88 (*m*, 1H), 4.17-4.13 (*t*, $^3J_{HH}$ = 5.0 Hz, 2H, O-CH_2-), 3.78-3.75 (*t*, $^3J_{HH}$ = 6.11 Hz, 2H, -CH_2-O), 3.72-3.67 (*sept*, $^3J_{HH}$ = 6.6 Hz, 1H, -CH), 2.45-2.38 (*m*, 8H, P-CH_2-), 1.52-1.47 (*m*, 16H, -CH_2-), 1.20-1.18, (*t*, $^3J_{HH}$ = 5.2 Hz, 6H, -CH_3) ppm. 0.98-0.92 (t, $3J_{HH}$ = 3.5 Hz, 12H, -CH_3) ppm. ^{13}C NMR (100.64 MHz, $CDCl_3$): 171.48, 158.57, 142.61, 128.08, 122.25, 116.48, 114.71, 72.06, 67.86, 66.83, 24.21, 24.07, 24.06, 24.03, 22.27, 19.18, 18.17, 13.60. ^{31}P NMR (162.01 MHz, $CDCl_3$): 33.03 ppm.

(P_{4444})(4-IEBA): Pale yellow liquid. MS (ESI). $[C_{16}H_{36}P]^+$: Calcd m/z 259.2556. Found m/z 259.2565, , $[C_{12}H_{15}O_4]^-$: Calcd m/z 223.0975, Found m/z 223.0934. ^{1}H NMR (400.21 MHz, $CDCl_3$), $^\delta$(ppm): 7.99-7.97 (*d*, $^3J_{HH}$ = 8.4 Hz, 2H), 6.82-6.80 (*d*, $^3J_{HH}$ = 8.4 Hz, 2H), 4.10-4.08 (*t*, $^3J_{HH}$ = 4.9 Hz, 2H, O-CH_2-), 3.77-3.64 (*m*, 2H), 1.42-1.40 (*m*, 16H, -CH_2-), 1.20-1.18, (*t*, $^3J_{HH}$ = 5.2 Hz, 6H, -CH_3) ppm. 0.98-0.92 (t, $3J_{HH}$ = 3.5 Hz, 12H, -CH_3) ppm. ^{13}C NMR (100.64 MHz, $CDCl_3$): 171.82, 160.00, 132.72, 131.14, 113.37, 116.48, 72.25, 67.77, 66.67, 24.10, 23.95, 23.89, 23.85, 22.19, 19.00, 18.53, 13.54. ^{31}P NMR (162.01 MHz, $CDCl_3$): 32.96 ppm.

(P_{4444})(2-EEBA): Pale yellow liquid. MS (ESI). $[C_{16}H_{36}P]^+$: Calcd m/z 259.2556. Found m/z 259.2565, $[C_{12}H_{15}O_4]^-$: ^{1}H NMR (400.21 MHz, $CDCl_3$), $^\delta$(ppm): 7.45-7.43 (*d*, $^3J_{HH}$ = 7.2 Hz 1H), 7.09-7.05 (*d*, $^3J_{HH}$ = 7.9 Hz, 1H), 6.85-6.81 (*m*, 2H), 4.19-4.16 (*t*, $^3J_{HH}$ = 5.4 Hz, 2H, O-CH_2-), 3.76-3.73 (*t*, $^3J_{HH}$ = 5.3 Hz, 2H, -CH_2-O), 3.57-3.51 (*t*, $^3J_{HH}$ = 6.9 Hz, 2H), 2.39-2.36 (*m*, 8H, P-CH_2-), 1.46-1.44 (*m*, 16H, -CH_2-), 1.19-1.17, (*d*, $^3J_{HH}$ = 7 Hz, 3H, -CH_3) ppm. 0.84-0.87 (t, $3J_{HH}$ = 7.1 Hz, 12H, -CH_3) ppm. ^{13}C NMR (100.64 MHz, $CDCl_3$): 172.67, 155.29, 134.71,

129.02, 127.54, 120.93, 114.18, 69.32, 68.93, 66.88, 24.18, 24.03, 23.98, 19.01, 18.54, 15.41, 13.66. ^{31}P NMR (162.01 MHz, $CDCl_3$): 33.03 ppm.

(P_{4444})(2-MEMBA): Pale yellow liquid. MS (ESI). $[C_{16}H_{36}P]^+$: Calcd m/z 259.2556. Found m/z 259.2552, $[C_{13}H_{17}O_5]^-$: Calcd m/z 253.1081, Found m/z 253.1321. ^{1}H NMR (400.21 MHz, $CDCl_3$), $^{\delta}$(ppm): 7.43-7.41 (*m,* 1H), 7.08-7.04 (*m*, 1H), 6.83-6.79 (*m*, 2H), 4.17-4.15 (*t*, $^3J_{HH}$ = 5.2 Hz, 2H, O-CH_2-), 3.82-3.79 (*t*, $^3J_{HH}$ = 5.3 Hz, 2H, -CH_2-O), 3.68-3.66 (*t*, $^3J_{HH}$ = 4.3 Hz, 2H), 3.56-3.45 (*m*, 8H) 2.33-2.30 (*m*, 8H, P-CH_2-), 1.46-1.44 (*m*, 16H, -CH_2-), 1.19-1.17, (*d*, $^3J_{HH}$ = 7 Hz, 6H, -CH_3) ppm. 0.84-0.87 (t, 3J_{HH} = 7.1 Hz, 12H, -CH_3) ppm. ^{13}C NMR (100.64 MHz, $CDCl_3$): 172.78, 155.29, 134.42, 128.93, 127.67, 120.84, 114.51, 77.59, 77.28, 76.96, 70.77, 69.97, 68.88, 66.68, 24.13, 23.98, 23.95, 23.90 18.96, 18.49, 15.27, 13.61. ^{31}P NMR (162.01 MHz, $CDCl_3$): 33.04 ppm.

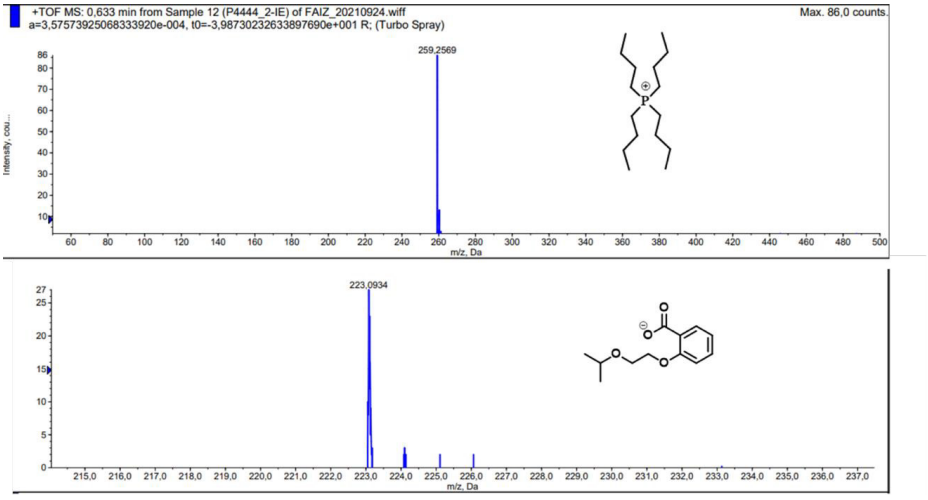

Figure S1. ESI-MS of (P_{4444})(2-IEBA)

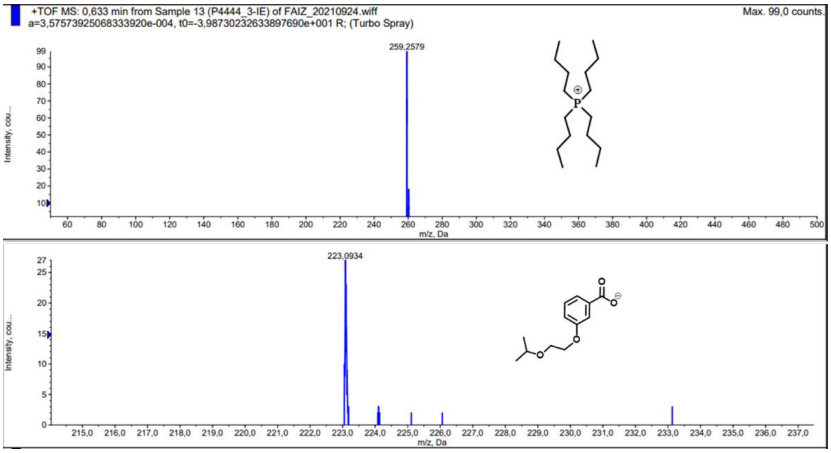

Figure S2. ESI-MS of (P_{4444})(3-IEBA)

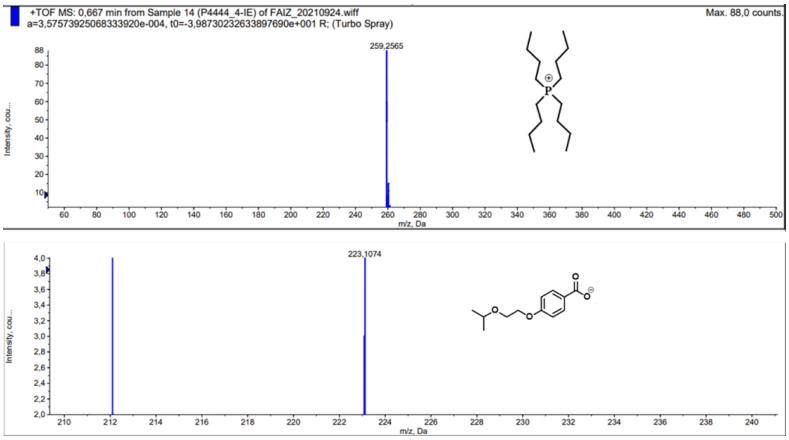

Figure S3. ESI-MS of (P_{4444})(4-IEBA)

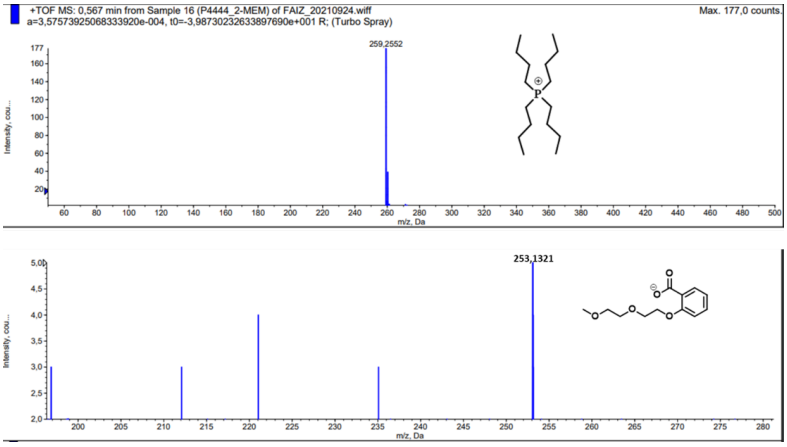

Figure S4. ESI-MS of (P_{4444})(2-MEMBA)

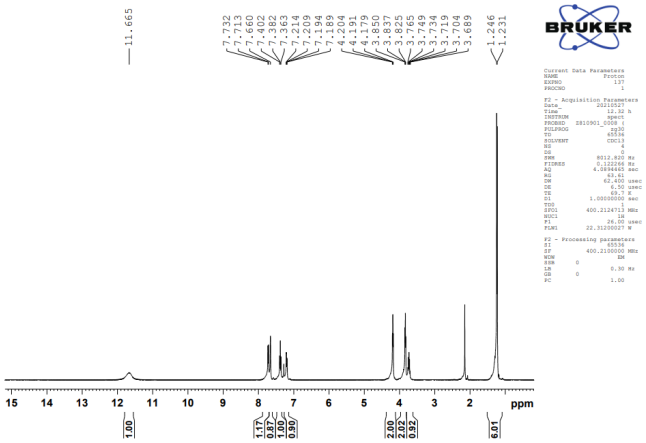

Figure S5. ^{1}H NMR spectrum of (3-IEBA)

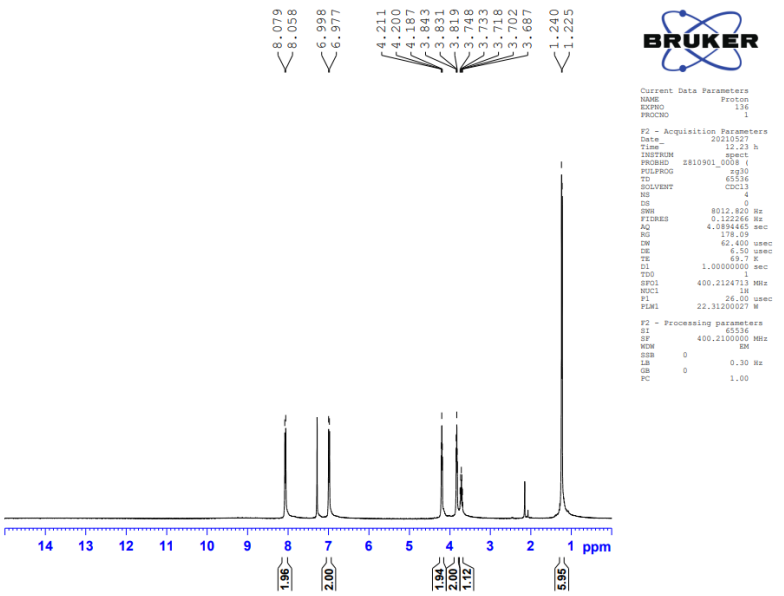

Figure S6. [1]H-NMR spectrum of (4-IEBA)

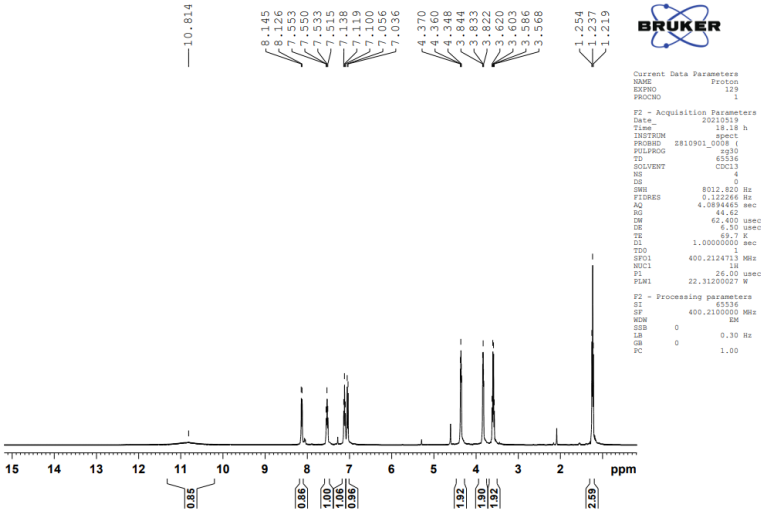

Figure S7. [1]H-NMR spectrum of (2-EEBA)

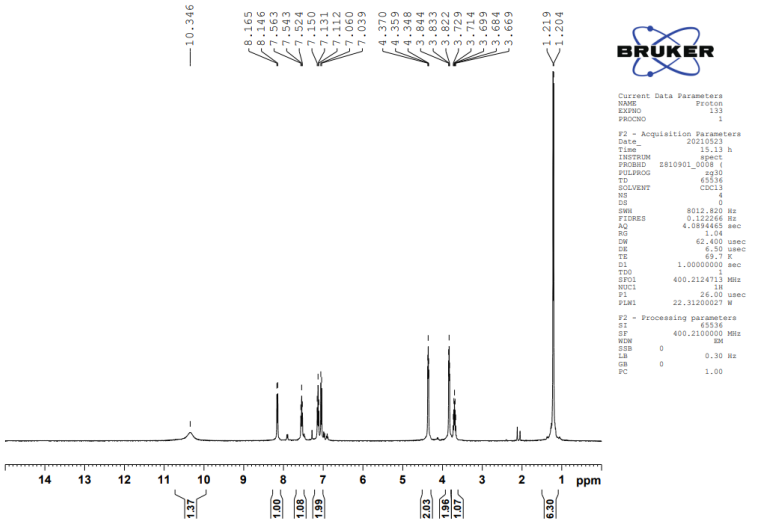

Figure S8. [1]H-NMR spectrum of (2-IEBA)

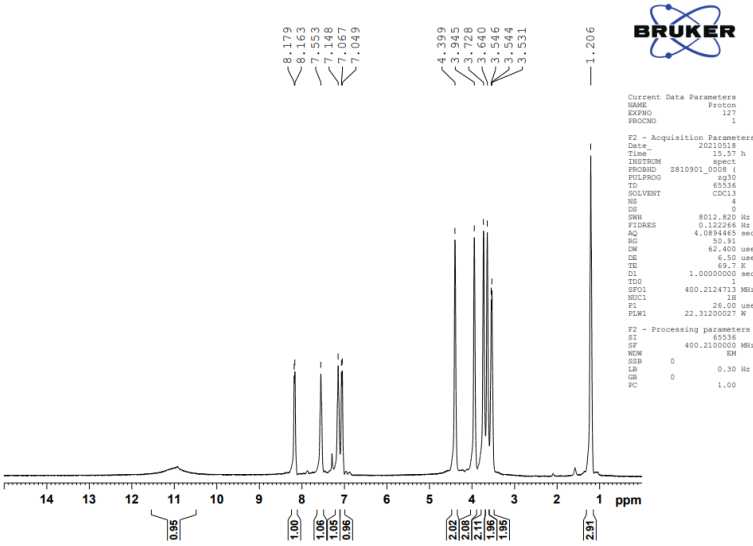

Figure S9. [1]H-NMR spectrum of (2-MEMBA)

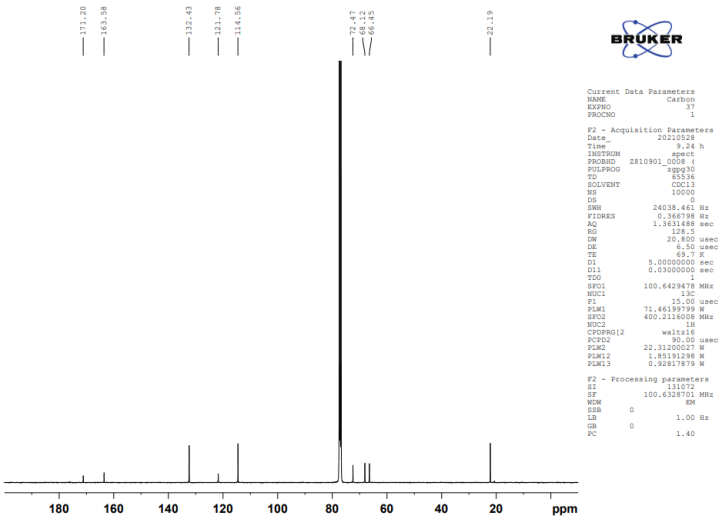

Figure S10. ^{13}C-NMR spectrum of (4-IEBA)

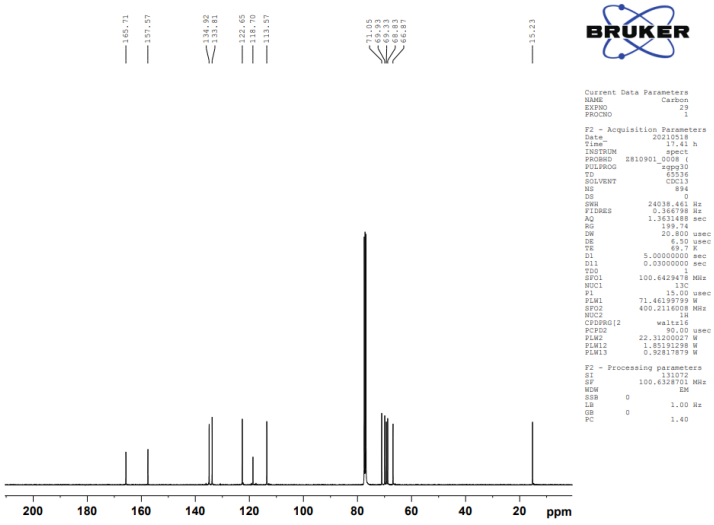

Figure S11. ^{13}C-NMR spectrum of (2-MEMBA)

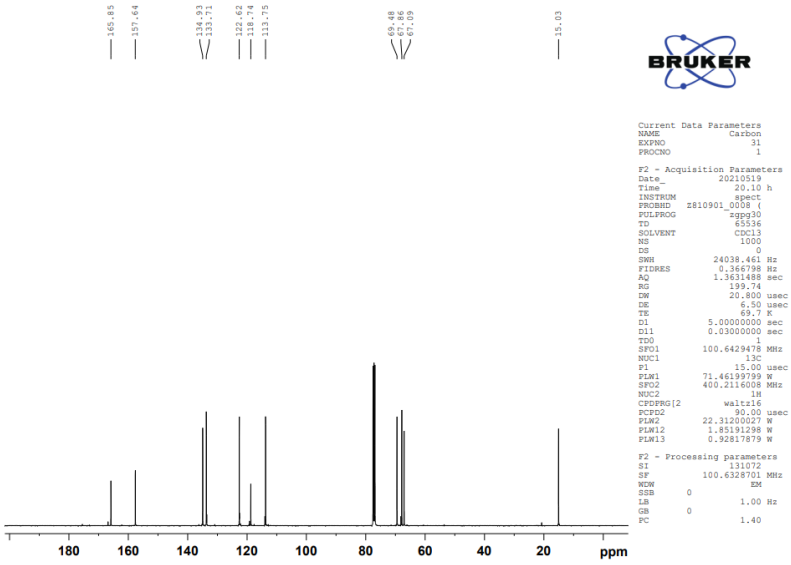

Figure S12. ^{13}C-NMR spectrum of (2-EEBA)

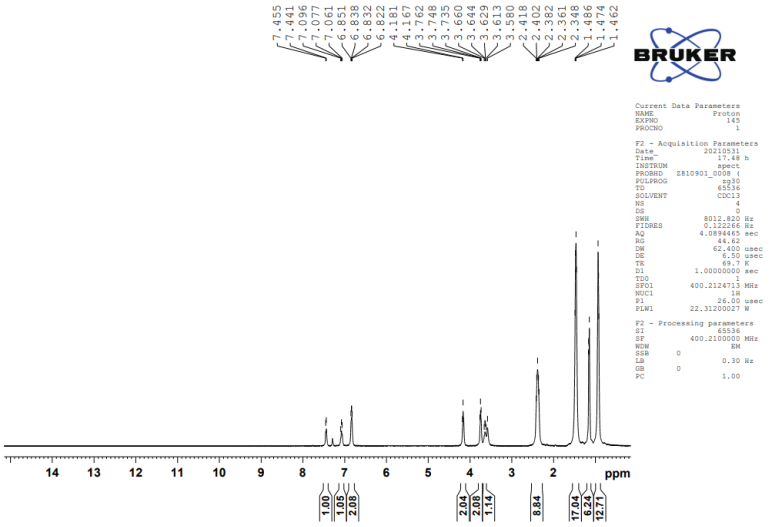

Figure S13. ^{1}H-NMR spectrum of (P_{4444})(2-IEBA)

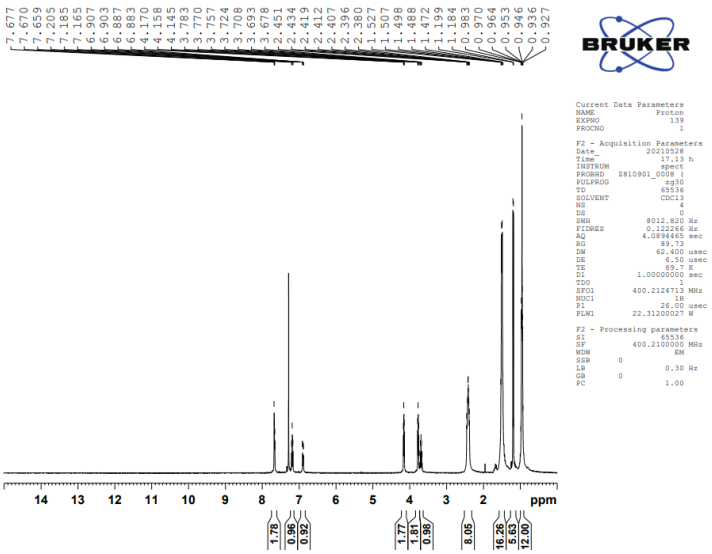

Figure S14. ^{1}H-NMR spectrum of (P_{4444})(3-IEBA)

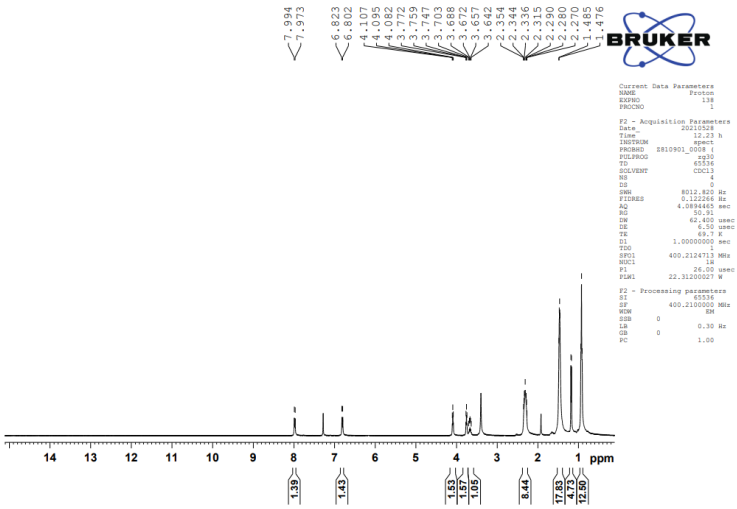

Figure S15. ^{1}H-NMR spectrum of (P_{4444})(4-IEBA)

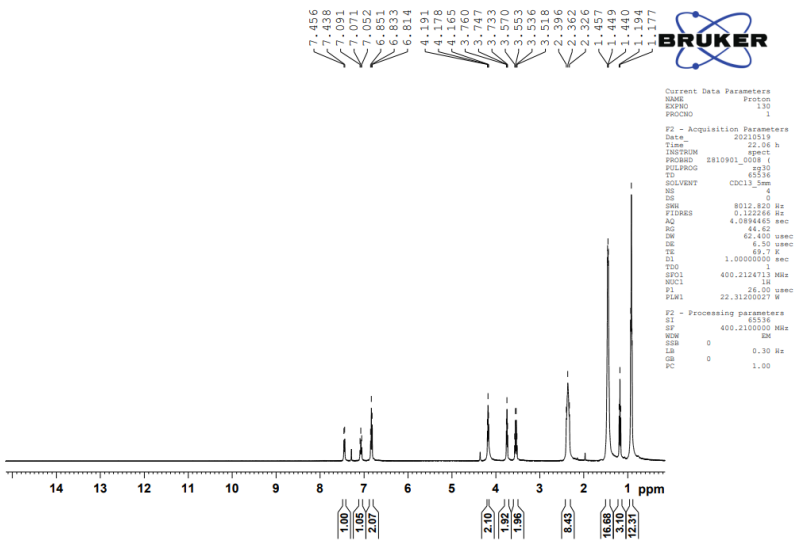

Figure S16. ^{1}H-NMR spectrum of (P_{4444})(2-EEBA)

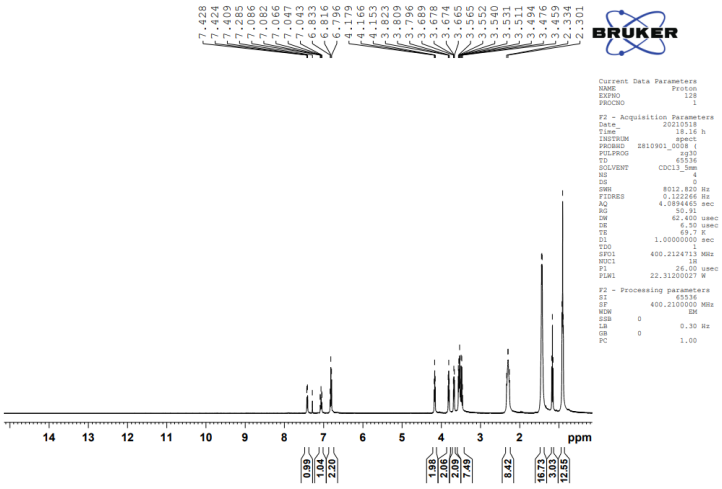

Figure S17. ^{1}H-NMR spectrum of (P_{4444})(2-MEMBA)

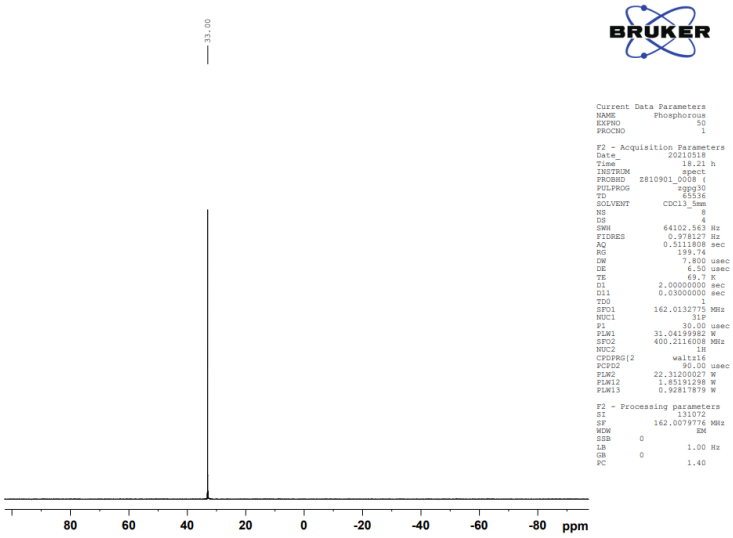

Figure S18. ^{31}P-NMR spectrum of (P_{4444})(2-IEMBA)

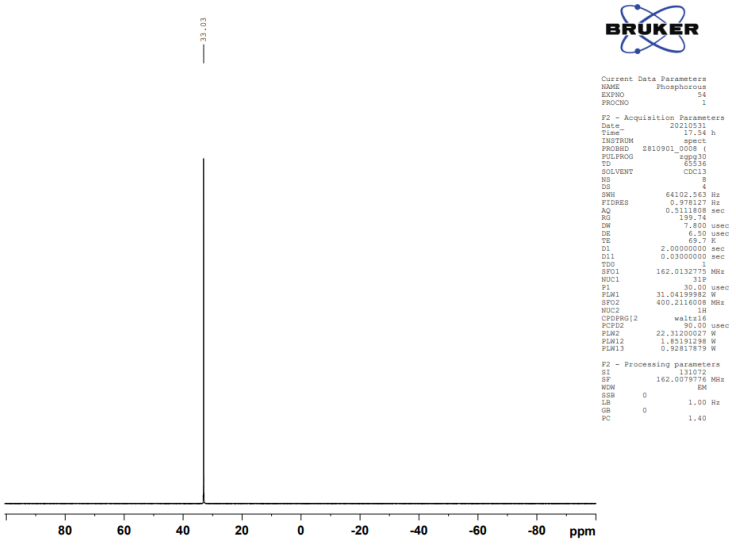

Figure S19. ^{31}P-NMR spectrum of (P_{4444})(3-IEMBA)

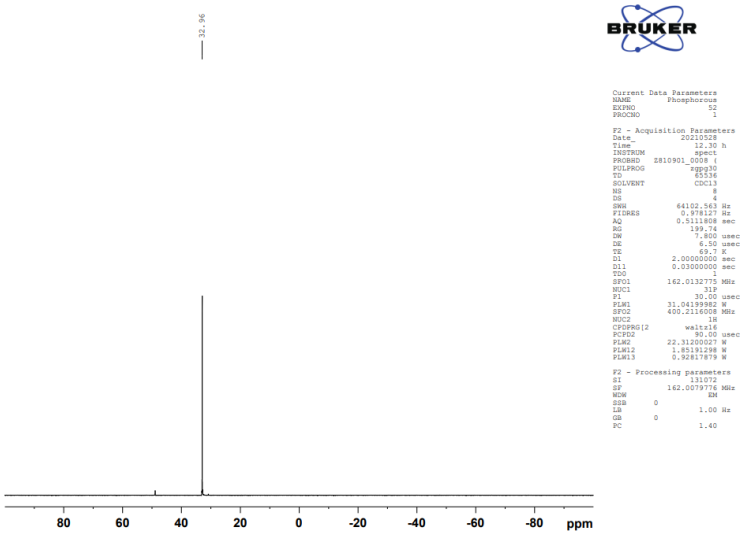

Figure S20. ^{31}P-NMR spectrum of (P_{4444})(4-IEMBA)

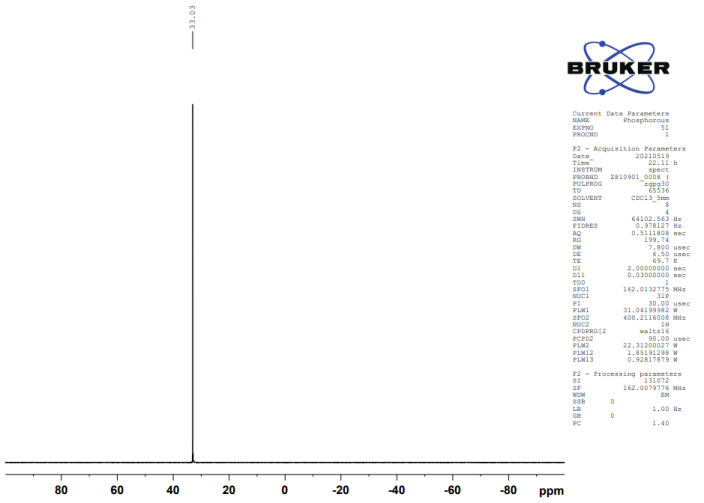

Figure S21. ^{31}P-NMR spectrum of (P_{4444})(2-EEMBA)

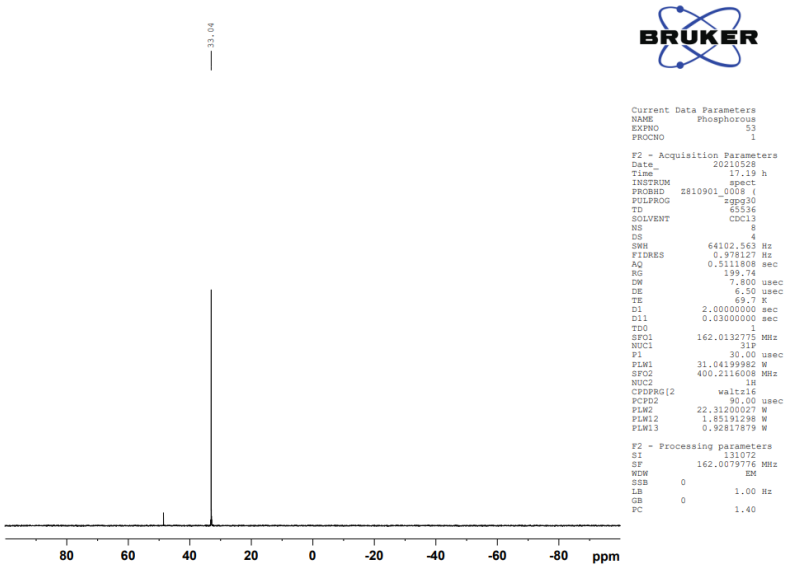

Figure S22. ^{31}P-NMR spectrum of (P_{4444})(2-MEMBA)

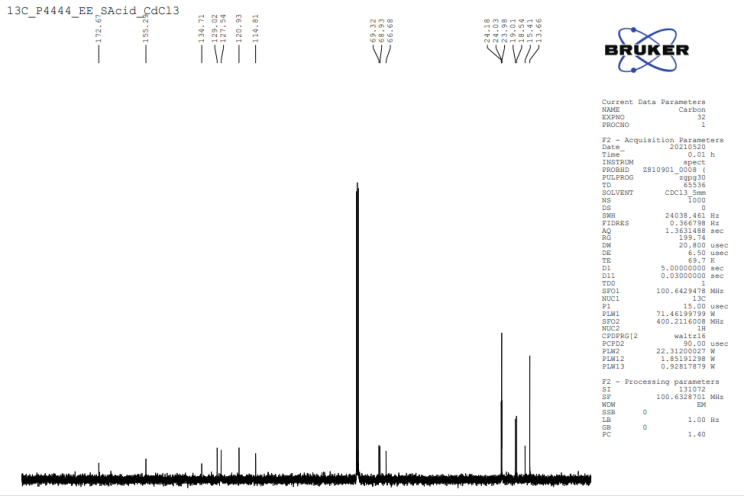

Figure S23. ^{13}C-NMR spectrum of (P_{4444})(2-EEBA)

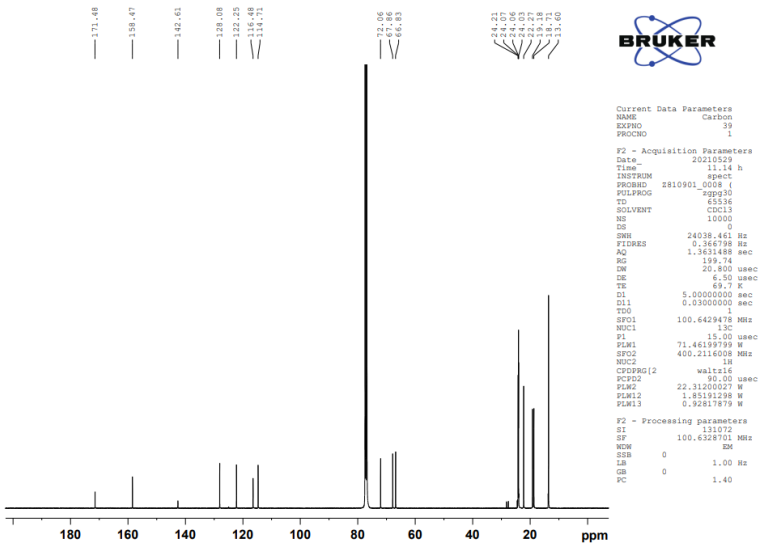

Figure S24. ^{13}C-NMR spectrum of (P_{4444})(3-IEBA)

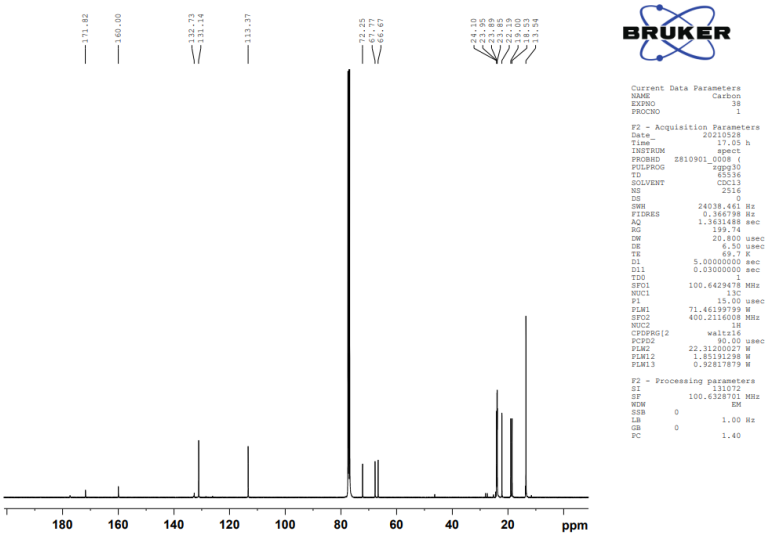

Figure S25. ^{13}C-NMR spectrum of (P_{4444})(4-IEBA)

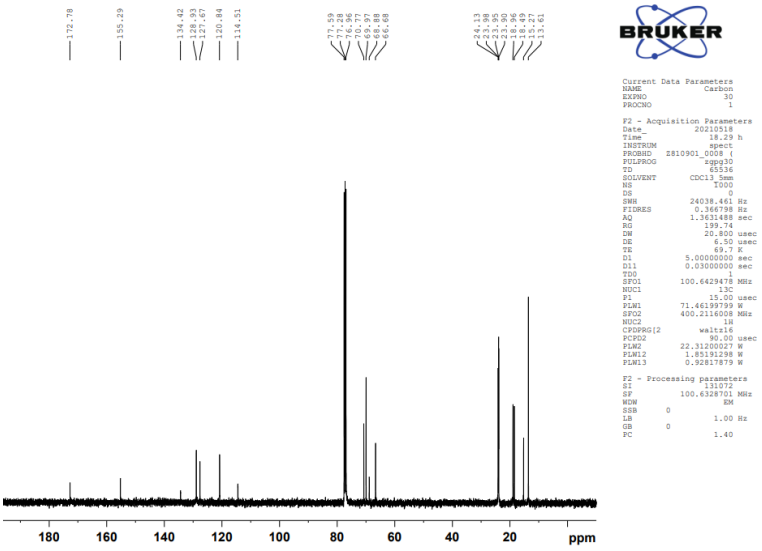

Figure S26. ^{13}C-NMR spectrum of (P_{4444})(2-MEMBA)

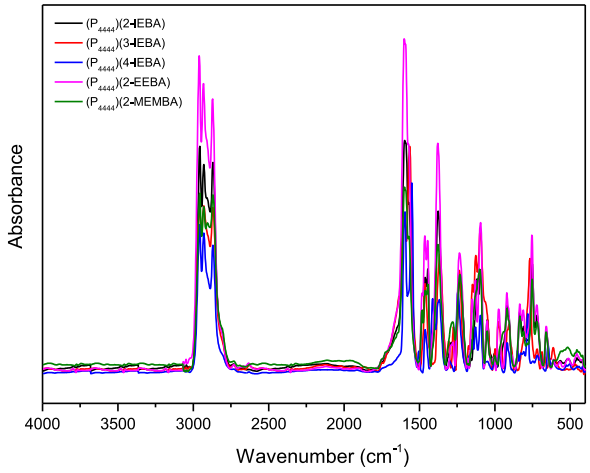

Figure S27. FTIR spectra of the neat ILs

Table S1. VFT equation parameters and apparent energies of activation of conductivity for ionic liquids.

System	σ_0 (Scm^{-1})	B (K)	T_0 (K)	E_σ(kJmol^{-1})
(P_{4444})(2-IEBA)	0.293	993	167	8.3
(P_{4444})(3-IEBA)	0.616	1254	159	10.4
(P_{4444})(4-IEBA)	2.45	1690	132	14.1
(P_{4444})(2-EEBA)	0.933	1609	135	13.4
(P_{4444})(2-MEMBA)	0.556	1416	144	11.8
[(P_{4444})(2-IEBA)]$_{0.9}$ [(Li)(2-IEBA)]$_{0.1}$	0.678	1422	151	11.8
[(P_{4444})(2-EEBA)]$_{0.9}$ [(Li)(2-EEBA)]$_{0.1}$	0.376	1331	152	11.1

Table S2. VFT equation parameters and apparent activation energy of diffusivity for the neat ILs and the electrolytes calculated from temperature dependences of diffusion coefficients presented in Figure 6.

System	Ion	$D_0\times10^{-8}$ (m^{2}s^{-1})	B (K)	T_0 (K)	E_σ(kJmol^{-1})
(P_{4444})(2-EEBA)	(P_{4444})$^+$	1.96	949	200	7.9
	(2-EEBA)$^-$	1.96	949	200	7.9
[(P_{4444})(2-EEBA)]$_{0.9}$ [(Li)(2-EEBA)]$_{0.1}$	(P_{4444})$^+$	27.3	1810	166	15.0
	(2-EEBA)$^-$	14.6	1638	169	13.6
	Li$^+$	2.73	1216	196	10.1
(P_{4444})(2-IEBA)	(P_{4444})$^+$	66.6	658	216	5.5
	(2-IEBA)$^-$	66.6	658	216	5.5
[(P_{4444})(2-IEBA)]$_{0.9}$ [(Li)(2-IEBA)]$_{0.1}$	(P_{4444})$^+$	179.0	2349	145	19.5
	(2-IEBA)$^-$	3.96	1812	165	15.1
	Li$^+$	199.0	2268	156	18.9
(P_{4444})(2-MEMBA)	(P_{4444})$^+$	1.68	952	195	7.9
	(2-MEMBA)$^-$	1.68	952	195	7.9
(P_{4444})(3-IEBA)	(P_{4444})$^+$	1.53	771	215	6.4
	(3-IEBA)$^-$	1.53	771	215	6.4
(P_{4444})(4-IEBA)	(P_{4444})$^+$	1.73	868	205	7.2
	(4-IEBA)$^-$	1.73	868	205	7.2

Paper III

Fluorine-Free Ionic Liquids and Concentrated Electrolytes

Mukhtiar Ahmed, Andrei Filippov, Patrik Johansson, and Faiz Ullah Shah

(*Manuscript*)

Fluorine-Free Ionic Liquids and Concentrated Electrolytes

Mukhtiar Ahmed[1], Andrei Filippov[1], Patrik Johansson[2*]and Faiz Ullah Shah[1*]

[1]Chemistry of Interfaces, Luleå University of Technology, SE-971 87 Luleå, Sweden
[2]Materials Physics, Department of Physics, Chalmers University of Technology, SE-412 96 Gothenburg, Sweden

[*]Corresponding authors:
patrik.johansson@chalmers.se
faiz.ullah@ltu.se

Abstract

We introduce new classes of fluorine-free oligoether functionalized ionic liquids (ILs) and their concentrated electrolytes. The physicochemical and electrochemical properties of ILs with two different cations, imidazolium and pyrrolidinium, coupled to the two oligoether anions, 2-(2-methoxyethoxy)acetate, $(MEA)^-$ and 2-[2-(2-methoxyethoxy)ethoxy]acetate $(MEEA)^-$. These ILs exhibit quite different thermal properties but comparable ion transport behaviors. For the ILs with $(MEEA)^-$ anions, the solubility of the lithium salts in the parent ILs is very high *ca.* 80 mol%, and currently we are studying the detailed physiochemical properties of these high concerted IL electrolytes.

Introduction

The liquid electrolytes used in conventional lithium-ion batteries (LIBs) are made by dissolving a lithium salt, usually lithium hexafluorophosphate ($LiPF_6$) and in some cases lithium tetrafluoroborate ($LiBF_4$), in flammable organic solvents such as ethylene carbonate (EC) combined with linear aliphatic carbonates including dimethyl and/or diethyl carbonates (DMC and DEC).[1,2] The electron-withdrawing effect of the fluoride atoms facilitate the distribution of negative charges, thus decreasing the lattice energy of the salt and promoting ion dissociation leading to improved salt dissolution in organic solvents.[3] This electrolyte solution has undoubtedly contributed to the tremendous commercial success of LIBs over the last 25 years, and it is undoubtedly an excellent system for small-scale portable electronic devices. However, for large-scale applications such as EVs, raise valid issues about safety of such electrolytes containing non-negligible amounts of flammable organic solvents.[4]

These organic solvent-based liquid electrolytes are flammable by nature, and the electrolyte salt contain *ca.* 75% fluorine by weight, which has been proven to decomposition at elevated temperatures to produce PF_5 and LiF, the former rapidly reacts with traces of water to release highly toxic hydrofluoric acid (HF) and a reactive intermediate phosphoryl fluoride (POF_3) that will either react with other organic materials or with water finally generating HF. Judging from its chlorine analogy $POCl_3$, POF_3 may even be more toxic than HF.[5] These decomposition products are extremely reactive towards both cathode and anode, adversely affecting the performance of a battery cell[6] and also create enormous health and environmental problems during battery recycling process. Fluorine appears to be unavoidable in traditional battery systems, not only as part of the electrolyte but also widely used as a component of binder in the form of polyvinylidene difluoride (PVdF).[7] Taken altogether, this urges for extensive research to develop thermally and electrochemically stable, but still performant, electrolytes to replace the conventional organic solvent-based electrolytes.

Oligoethers (also referred as “glymes”) are a group of organic compounds with the general chemical formula [R-(OCH_2CH_2)$_n$-OR] referred by the abbreviation G_n, where "*n*" stands for the number of repeating units and indicated by the letters monoglyme (G_1), diglyme (G_2), triglyme (G_3), tetraglyme (G_4), etc. This class of solvents is intensively examined during the past two decades, mostly because of their attractive physicochemical features.[8-10] Glymes can even dissolve an equimolar amount of some lithium salts *via* an ether multidentate coordination functionality, making complexes known as solvate ionic liquids (SILs) as they mimic ionic liquids (ILs) with high thermal and electrochemical stabilities.[11] The Lewis acidity of Li^+ is substantially decreased as a result of the complex formation, which is equivalent to the production of weakly Lewis-basic anions such as PF_6^- and BF_4^- with the interaction of a Lewis acid.[12] Compared to carbonate-based organic solvents, glymes have higher flash points and better solubility of lithium salts[13] but due to presence of oxygen lone pairs they suffer from instability at high redox potentials.[14]

In this study, we combine the characteristics of glyme solvents with those of ILs containing most popular small organic cations such as pyrrolidinium and imidazolium. Undoubtedly, electrolytes based on ILs offer a range of suitable advantages including low volatility and high thermal and electrochemical stabilities and can additionally be made fluorine-free and task-specific with synthetic diversity.[15-17] In general, their physicochemical properties are determined by the sizes of ions and the interactions between the cations and anions, which can be functionalized due to the vast freedom in structural design to reduce these interactions and enhance also the ion mobilities.[18-20] The main objective of combining oligoether-based anions with small pyrrolidinium and imidazolium cations is achieve better solubility, thermal electrochemical and electrochemical stabilities, and improved ion transport properties of the electrolytes.

Experimental

Materials and Synthesis

Unless otherwise stated, all the commercial reagents were utilized without any additional purification. 1,2-dimethylimidazole (ACS reagents, >97 % purity), *n*-methylpyrrolidine (ACS reagents, >97 % purity), 1-bromobutane (>99 % purity), Silver(I) oxide (>99.9 % purity), 2-[2-(2-methoxyethoxy)ethoxy]acetic acid (>97 % purity), 2-(2-methoxyethoxy)acetic acid (>97 % purity), an aqueous solution of tetrabutylphosphonium hydroxide (40 wt % in water) and lithium hydroxide monohydrate (ACS reagents, >98 % purity) were received from Sigma-Aldrich. Sodium sulphate, methanol, dichloromethane (DCM) and diethylether were purchased from VWR (BDH) chemicals. The synthesis and structural characterization of the products is described in detail in the supporting information (SI).

The electrolytes were made by dissolving 80 mol % lithium salts in the neat ILs to obtained the concentrated electrolytes. All the samples were kept in a vacuum oven at 80 °C for at least four days before any measurement. The water content was measured by Karl Fischer titration (using Metrohm 917 Coulometer, Switzerland) and was determined to be less than 100 ppm for all synthesized ILs.

Nuclear Magnetic Resonance Spectroscopy

The structures and purity of all the synthesized products were confirmed by using a Bruker Ascend Aeon WB 400 (Bruker BioSpin AG, Fallanden, Switzerland) nuclear magnetic resonance (NMR) spectrometer. $CDCl_3$ was used as a solvent. The working frequencies were 400.21 MHz for ^{1}H, 100.64 MHz for ^{13}C, and 162.01 MHz for ^{31}P. Data were processed using Bruker Topspin 3.5 software.

Thermal Analysis

Thermogravimetric analysis (TGA) was performed using a PerkinElmer TGA 8000 under N_2 gas at a heating rate of 10 °C per min. About 2-4 mg of sample was used for each experiment. The onset of decomposition temperature, T_{onset}, was calculated from the intersection of the baseline weight and the tangent of the weight versus temperature curve using the Pyris software. Differential scanning calorimetry (DSC) was performed using a PerkinElmer DSC 6000 on 2-5 mg of the sample placed in an aluminum pan. DSC data were collected at a scanning rate of 5 °C min^{-1} for both cooling and heating traces. To maintain an inert environment inside the sample chamber, dry N_2 gas was delivered at a constant flow rate of 20 mL min^{-1}. The glass transition temperature (T_g) was determined by using the inflection mid-point of the initial *S*-shaped transition slope and determined from the onset with the aid of the Pyris software.

Electrochemical Characterization

The electrochemical stability and ionic conductivity were determined using a Metrohm Autolab PGSTAT302N electrochemical workstation with a FRA32M module for impedance measurements, all controlled by a Nova 2.02 software. A sealed Microcell HC from RHD instruments Germany was used to hold about 70 µL of the sample. To determine the electrochemical stability window (ESW), linear sweep voltammetry (LSV) was performed with a three-electrode setup: a Pt wire with a diameter of 0.25 mm as a working electrode (WE), a Pt crucible as counter electrode (CE) as well as a sample container, and an Ag wire coated with AgCl as a pseudo-reference electrode (RE). Both cathodic and anodic scans were recorded at a rate of 1 mV s^{-1}. The electrochemical potentials were calibrated using ferrocene (Fc) as an internal reference and shifted using $E_{Li/Li^+} \approx E_{Fc/Fc^+} + 3.2$ V.[21] The ESWs limits were defined by a 0.1 mA cm^{-2} cut-off current density.

The ionic conductivity was obtained from the impedance measurements performed in a frequency range from 1 Hz to 1 MHz with an AC voltage amplitude of 10 mV_{rms}. All the impedance spectra were measured during heating and cooling over a temperature range from −20 to 100 ± 0.1 °C. A two-electrode configuration was employed for ionic conductivity measurements, with a wire Pt as a WE and a 70 μL Pt crucible as a sample container as well as CE.

Prior to each CV and ionic conductivity measurement, both the electrodes were polished with a 0.25 m of Kemet diamond paste. The cell constant was calculated using a Metrohm 100 S cm^{-1} KCl standard solution (K_{cell} = 18.5396 cm^{-1}). The cell was thermally equilibrated for 10 minutes before recording the impedance spectra.

PFG NMR Diffusometry

Pulsed field gradient (PFG) NMR diffusometry measurements were performed using a Bruker Ascend/Aeon WB 400 (Bruker BioSpin AG) NMR spectrometer with a resonance frequency of 400.27 MHz for ^{1}H and 155.56 MHz for ^{7}Li. The PFG NMR measurements were performed with a PFG NMR probe Diff50 (Bruker) with a maximum amplitude of the magnetic field gradient pulse of 29.73 T m^{-1}. The samples were placed in a standard 5 mm NMR glass tube and closed with a plastic stopper to avoid contact with air. Prior to measurements, each sample was equilibrated at a specific temperature for 30 min. The details of the PFG NMR technique for measuring molecular diffusion coefficients are available elsewhere.[22] The diffusivity of a molecule is the diffusion decay (DD) of amplitude *A* of NMR spectral line, obtained by Fourier transformation of a descending half of stimulated-echo (StE), as a function of the amplitude of applied pulsed field gradient. For the stimulated echo pulse sequence used, diffusion decay of *A* in the case of simple non-associating molecular liquid can be described by the Eq.(1):[23]

$$A(g,\delta,t_d) = A(0)\exp(-\gamma^2 g^2 \delta^2 D t_d) \quad (1)$$

where $A(0)$ is the factor proportional to the proton content in the system, and to spin-lattice and spin-spin relaxation times, γ is the gyromagnetic ratio for a used nucleus; g and δ are the amplitude and duration of the gradient pulse; t_d is the diffusion time; and D is the self-diffusion coefficient. t_d was in the range 4-100 ms for ^{1}H diffusion and 5-15 ms for ^{7}Li diffusion. No diffusion time dependence was observed in these measurements.

FTIR Spectroscopy

The attenuated total reflection Fourier transform infrared (ATR-FTIR) spectra of samples were recorded using a Bruker IFS 80v spectrometer equipped with a deuterated triglycine sulfate (DTGS) detector and diamond ATR accessory, employing the double-side forward–backward acquisition mode. The total number of scans was 256, co-added and signal-averaged at an optical resolution of 4 cm^{-1}.

Result and Discussion

We start with synthesis and structural characterization of the oligoether functionalized ILs, and their electrolytes, followed by assessing their thermal properties, and then proceeding to electrochemical assessments and ion transport properties such ionic conductivity, and ion self-diffusion of the ILs and the electrolytes made.

Synthesis and Characterization

A multistep synthetic protocol is used to synthesize the new oligoether functionalized ILs. A brief description of the synthesis and characterization is provided below and the details are given in the SI. We begin with synthesis of the imidazolium hydroxide (MMBImOH) and pyrrolidinium hydroxide (MBPyrrOH) from their bromide salts (Scheme S1). Bromide salts were treated with silver oxide (Ag_2O) in the presence of water at room temperature, the silver

bromide so formed was filtered. The hydroxide salts were further converted into ILs by a direct neutralization reaction with acids.

The chemical structures of all the ILs ionic liquids (Figure 1) agree well with the NMR spectroscopic data. First, the ^{1}H NMR spectra of the ILs (Figure. S1-4) show characteristic resonance lines for the butyl chain, methylene protons alpha to the charged nitrogen atom appear in the range of 4.1 to 4.5 ppm for imidazolium and 3.5 to 3.7 ppm for pyrrolidinium based ILs, and methyl protons with distinct triplet appear at 0.9 to 1 ppm for both systems. Second, the ^{1}H resonance lines in the range from 3.5 to 4.3 ppm are attributed to the methylene protons of the ether chains in anions and absence of any broad peak above 7 ppm and the presence of the signals at *ca.* 7.35 and 7.65 for aromatic groups of the imidazolium systems, corroborated the successful deprotonation of the corresponding acids and formation of the ILs. Finally, the ^{13}C NMR spectra revealed resonance lines in the region 65–80 ppm attributed to the aliphatic carbon directly attached to the oxygen atoms in ether chains of the anions (Figures S5–8). In addition, the ^{13}C resonance lines for the carboxylate groups in the anions are found at *ca.* 175 ppm.

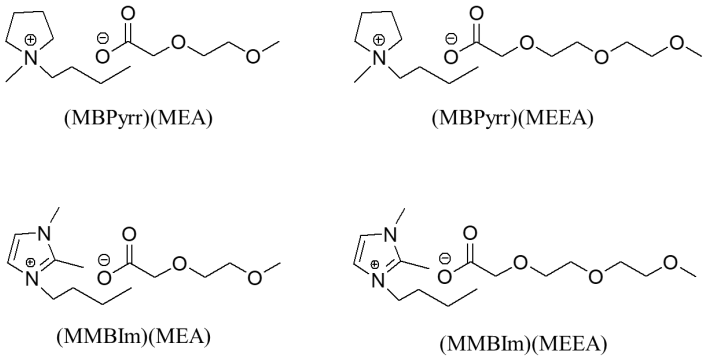

Figure 1. Chemical structures and the abbreviations of ionic components of the ILs employed in this study.

Thermal properties

All the neat ILs show excellent dynamic thermal stability >200 °C as revealed by the TGA curves (Figure 2), which is considerably higher thermal stability as compared with the traditional organic-solvent-based electrolyte.[24] It is worth noting that the dynamic TGA analysis overestimate the thermal stability and should be complimented with the isothermal TGA to determine the precise thermal stability of IL-based electrolytes.[25] It is clear that keeping the anion constant, The thermal decompositions of the imidazolium ILs proceed over wider temperature regions than those of the pyrrolidinium analogs, which is consistent with the literature[26]. The IL with a bulkier oligoether anion is somewhat thermally more stable than the IL with a smaller anion, which is contradictory to the ILs with oligoether derived cations.[27]

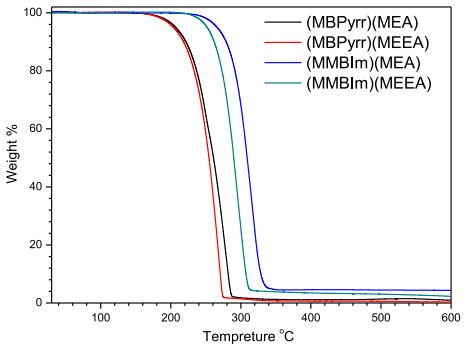

Figure 2. TGA thermograms of the neat ILs.

The corresponding DSC traces reveal that all the neat ILs are glass-forming liquids, that is, they all exhibit glass transitions (Figure 3 and Table 1). It is clear that pyrrolidinium-based ILs provide much higher glass transition (T_g) temperatures than the corresponding imidazolium-based ILs. This suggest that imidazolium-based ILs have weaker ion–ion interactions, and thus, a lower thermal energy would be required to reach the same ionic mobility as for pyrrolidinium.

As expected, a slight decrease in the T_g values with an increase in the ethylene oxide units in the anions is observed.

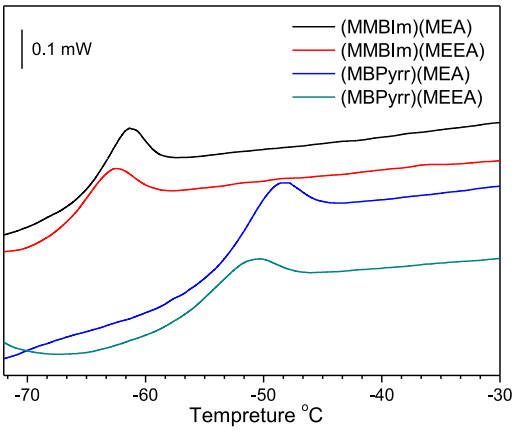

Figure 3. DSC traces for the neat ILs. The traces are shifted along Y-axis for clarity.

Ionic Conductivity

Ionic conductivity as a function of temperature for the neat ILs that are liquid at room temperature is presented in Figure 2. Ionic conductivity of all the neat ILs is comparable throughout the whole studied temperature range, the molecular masses of the ions are quite different. As it is clear from the DSC data that the pyrrolidinium based ILs have much lower T_g indicating weaker ionic interactions, however, ionic conductivity is not much influenced by the ionic interactions. The ionic conductivities are further analyzed by fitting the data to the following Vogel-Fulcher-Tammann (VFT) equation.[28]

$$\sigma = \sigma_0 \exp\left(\frac{-B}{(T - T_0)}\right) \qquad (2)$$

Where σ_0 is a pre-exponential factor, B is an empirical material-dependent fitting parameter related to the dynamic T_g and activation/pseudo activation energy (E_σ) of the system. The

reference temperature T_0 is attributed to the ideal vitreous transition temperature, at which configurational entropy vanishes.[29] T_0 is determined by fitting the temperature-dependent conductivity data to the VTF equation for the best linearity relationship. The E_σ values for all the neat ILs are comparable (Table S1), suggesting that a relatively same thermal energy is required to achieve the same ion mobility. As expected, the T_0 values in all these systems are about 50 K smaller than the glass transition temperatures T_g and agree well to the empirical approximation of ionic liquids-based electrolytes: $T_0/T_g \approx 0.75$.[30]

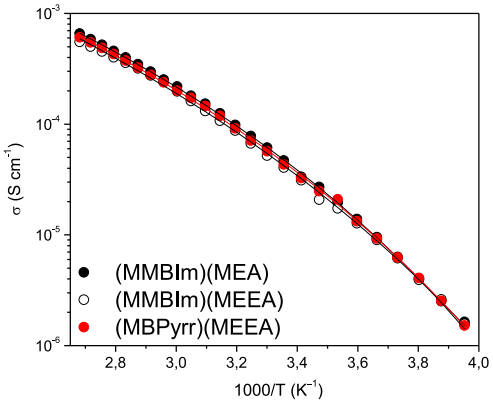

Figure 4. Ionic conductivity as a function of temperature for neat ILs. The solid lines indicate the best fit of data using the VFT equation.

Electrochemical Stability

Applicability of ionic liquid electrolytes in the LIBs is profoundly governed by their ability to withstand the working potential range. A relatively reliable means to detect the potential range of stability is by performing either linear sweep or cyclic voltammetry.[31] In the present text, to evaluate ESW of neat ILs and electrolytes, both cathodic and anodic LSV experiments were performed on glassy carbon (GC) electrode, LSV curves at 20 °C are shown in Figure 5 and

detailed in Table 1. The ESWs are revealed to be wider for imidazolium-based ILs than for the pyrrolidinium-based ILs. These ESWs are comparable with the commonly studied ammonium- and -pyrrolidinium-based ILs containing non-fluorinated anions.[2]

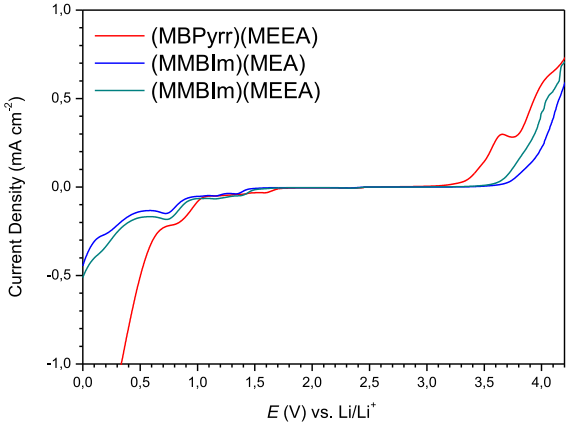

Figure 5. LSV curves of the neat ILs.

Table 1. Physiochemical properties of the synthesized ILs[a]

System	T_g (ºC)	T_d (ºC)	σ (S cm^{-1})	ESW
(MBPyrr)(MEA)	-62	262	---	---
(MBPyrr)(MEEA)	-64	266	3.26E^{-05}	2.47
(MMBIm)(MEA)	-48	302	3.34E^{-05}	3.02
(MMBIm)(MEEA)	-52	315	3.11E^{-5}	2.87

a=T_g: glass transition, T_d: decomposition temperature, σ: ionic conductivity at 20 ºC.

NMR Diffusometry

^{1}H PFG NMR diffusometry was employed to acquire deeper insights into the relative mobility of cations and anions in the neat ILs and to better comprehend the transport characteristics at a molecular level. The diffusion coefficients of all the ions exhibit a monotonous increase as a function of temperature and follow the VFT trend (Figure 6). It is important to mention that these diffusion coefficients are averaged out and have not resolved yet. From the initial studies, it shows that the diffusion coefficients of the pyrrolidinium-based IL are slightly faster at lower temperatures but comparable at higher temperatures. Overall, the diffusivity of ions in all these neat ILs are comparable and consistent with the ionic conductivity data.

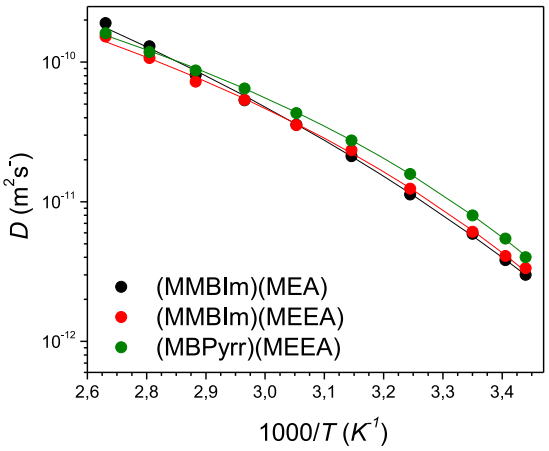

Figure 6. Diffusion coefficients of ions in the neat ILs.

Conclusions

The physiochemical and electrochemical properties of the newly synthesized four new ILs comprising two different oligoether anions coupled to a common imidazolium and pyrrolidinium cations are comparable. The pyrrolidinium-based ILs revealed lower thermal

stability but at the same time exhibit lower glass transition temperatures than the corresponding imidazolium-based ILs. It was found that the solubility of the Li salts is quite high in the parent ILs. Overall, the transport properties including ionic conductivity and ion diffusivity of the neat ILs are comparable over the whole studied temperature range. Further investigations on the performance of the electrolytes is under process and will be added to this manuscript later.

References

(1) Smart, M.; Ratnakumar, B.; Surampudi, S. Electrolytes for low-temperature lithium batteries based on ternary mixtures of aliphatic carbonates. *Journal of the Electrochemical Society* **1999,** *146* (2), 486.

(2) Kalhoff, J.; Eshetu, G. G.; Bresser, D.; Passerini, S. Safer electrolytes for lithium-ion batteries: state of the art and perspectives. *ChemSusChem* **2015,** *8* (13), 2154.

(3) Von Aspern, N.; Röschenthaler, G. V.; Winter, M.; Cekic-Laskovic, I. Fluorine and lithium: ideal partners for high-performance rechargeable battery electrolytes. *Angewandte Chemie International Edition* **2019,** *58* (45), 15978.

(4) Liu, M.; Vatamanu, J.; Chen, X.; Xing, L.; Xu, K.; Li, W. Hydrolysis of LiPF6-containing electrolyte at high voltage. *ACS Energy Letters* **2021,** *6* (6), 2096.

(5) Larsson, F.; Andersson, P.; Blomqvist, P.; Mellander, B.-E. Toxic fluoride gas emissions from lithium-ion battery fires. *Scientific reports* **2017,** *7* (1), 1.

(6) Han, J. G.; Kim, K.; Lee, Y.; Choi, N. S. Scavenging materials to stabilize LiPF6-containing carbonate-based electrolytes for Li-ion batteries. *Advanced Materials* **2019,** *31* (20), 1804822.

(7) Zou, F.; Manthiram, A. A review of the design of advanced binders for high-performance batteries. *Advanced Energy Materials* **2020,** *10* (45), 2002508.

(8) Shah, F. U.; Gnezdilov, O. I.; Khan, I. A.; Filippov, A.; Slad, N. A.; Johansson, P. Structural and ion dynamics in fluorine-free oligoether carboxylate ionic liquid-based electrolytes. *The Journal of Physical Chemistry B* **2020,** *124* (43), 9690.

(9) Brouillette, D.; Perron, G.; Desnoyers, J. E. Apparent molar volume, heat capacity, and conductance of lithium bis (trifluoromethylsulfone) imide in glymes and other aprotic solvents. *Journal of solution chemistry* **1998,** *27* (2), 151.

(10) Frech, R.; Huang, W. Conformational changes in diethylene glycol dimethyl ether and poly (ethylene oxide) induced by lithium ion complexation. *Macromolecules* **1995,** *28* (4), 1246.

(11) Angell, C. A.; Ansari, Y.; Zhao, Z. Ionic liquids: past, present and future. *Faraday discussions* **2012,** *154*, 9.

(12) Ueno, K.; Yoshida, K.; Tsuchiya, M.; Tachikawa, N.; Dokko, K.; Watanabe, M. Glyme–lithium salt equimolar molten mixtures: concentrated solutions or solvate ionic liquids? *The Journal of Physical Chemistry B* **2012,** *116* (36), 11323.

(13) Fang, S.; Wang, G.; Qu, L.; Luo, D.; Yang, L.; Hirano, S.-i. A novel mixture of diethylene glycol diethylether and non-flammable methyl-nonafluorobutyl ether as a safe electrolyte for lithium ion batteries. *Journal of Materials Chemistry A* **2015,** *3* (42), 21159.

(14) Jache, B.; Binder, J. O.; Abe, T.; Adelhelm, P. A comparative study on the impact of different glymes and their derivatives as electrolyte solvents for graphite co-intercalation electrodes in lithium-ion and sodium-ion batteries. *Physical Chemistry Chemical Physics* **2016,** *18* (21), 14299.

(15) Nakazawa, T.; Ikoma, A.; Kido, R.; Ueno, K.; Dokko, K.; Watanabe, M. Effects of compatibility of polymer binders with solvate ionic liquid electrolytes on discharge and charge reactions of lithium-sulfur batteries. *Journal of Power Sources* **2016,** *307*, 746.

(16) Ishikawa, M.; Sugimoto, T.; Kikuta, M.; Ishiko, E.; Kono, M. Pure ionic liquid electrolytes compatible with a graphitized carbon negative electrode in rechargeable lithium-ion batteries. *Journal of power sources* **2006,** *162* (1), 658.

(17) Moreno, M.; Simonetti, E.; Appetecchi, G.; Carewska, M.; Montanino, M.; Kim, G.-T.; Loeffler, N.; Passerini, S. Ionic liquid electrolytes for safer lithium batteries. *Journal of The Electrochemical Society* **2016,** *164* (1), A6026.

(18) Bayley, P. M.; Lane, G. H.; Rocher, N. M.; Clare, B. R.; Best, A. S.; MacFarlane, D. R.; Forsyth, M. Transport properties of ionic liquid electrolytes with organic diluents. *Physical Chemistry Chemical Physics* **2009,** *11* (33), 7202.

(19) Fan, Q.; Zhao, R.; Yi, M.; Qi, P.; Chai, C.; Ying, H.; Hao, J. Ti3C2-MXene composite films functionalized with polypyrrole and ionic liquid-based microemulsion particles for supercapacitor applications. *Chemical Engineering Journal* **2022,** *428*, 131107.

(20) Ganapatibhotla, L. V.; Zheng, J.; Roy, D.; Krishnan, S. PEGylated imidazolium ionic liquid electrolytes: thermophysical and electrochemical properties. *Chemistry of Materials* **2010,** *22* (23), 6347.

(21) Neale, A. R.; Murphy, S.; Goodrich, P.; Hardacre, C.; Jacquemin, J. Thermophysical and Electrochemical Properties of Ethereal Functionalised Cyclic Alkylammonium-based Ionic Liquids as Potential Electrolytes for Electrochemical Applications. *ChemPhysChem* **2017,** *18* (15), 2040.

(22) Blümich, B.; Wiley Online Library, 1995.

(23) Tanner, J. E. Use of the stimulated echo in NMR diffusion studies. *The Journal of Chemical Physics* **1970,** *52* (5), 2523.

(24) Ogihara, W.; Washiro, S.; Nakajima, H.; Ohno, H. Effect of cation structure on the electrochemical and thermal properties of ion conductive polymers obtained from polymerizable ionic liquids. *Electrochimica Acta* **2006,** *51* (13), 2614.

(25) Aizamddin, M. F.; Mahat, M. M.; Ariffin, Z. Z.; Samsudin, I.; Razali, M. S. M.; Amir, M. A. Synthesis, Characterisation and Antibacterial Properties of Silicone–Silver Thin Film for the Potential of Medical Device Applications. *Polymers* **2021,** *13* (21), 3822.

(26) Song, Y.; Liu, L.; Zhu, X.; Wang, X.; Jia, H.; Xiao, X.; Yu, H.; Yang, X. Physicochemical properties of ionic liquids based on imidazolium/pyrrolidinium cations and maleate/phthalate anions. *Solid State Ionics* **2008,** *179* (13-14), 516.

(27) Fang, S.; Zhang, Z.; Jin, Y.; Yang, L.; Hirano, S.-i.; Tachibana, K.; Katayama, S. New functionalized ionic liquids based on pyrrolidinium and piperidinium cations with two ether groups as electrolytes for lithium battery. *Journal of Power Sources* **2011,** *196* (13), 5637.

(28) Schreiner, C.; Zugmann, S.; Hartl, R.; Gores, H. J. Fractional Walden rule for ionic liquids: examples from recent measurements and a critique of the so-called ideal KCl line for the Walden plot. *Journal of Chemical & Engineering Data* **2010,** *55* (5), 1784.

(29) Stickel, F.; Fischer, E. W.; Richert, R. Dynamics of glass-forming liquids. II. Detailed comparison of dielectric relaxation, dc-conductivity, and viscosity data. *The Journal of chemical physics* **1996,** *104* (5), 2043.

(30) Galiński, M.; Lewandowski, A.; Stępniak, I. Ionic liquids as electrolytes. *Electrochimica acta* **2006,** *51* (26), 5567.

(31) Shah, F. U.; Khan, I. A.; Johansson, P. Comparing the thermal and electrochemical stabilities of two structurally similar ionic liquids. *Molecules* **2020,** *25* (10), 2388.

Fluorine Free Ionic Liquids and Concentrated Electrolytes

Mukhtiar Ahmed[1], Andrei Filippov[1], Patrik Johansson[2*]and Faiz Ullah Shah[1*]

1Chemistry of Interfaces, Luleå University of Technology, SE-971 87 Luleå, Sweden

2Materials Physics, Department of Physics, Chalmers University of Technology, SE-412 96 Gothenburg, Sweden

[*]Corresponding authors:

patrik.johansson@chalmers.se

faiz.ullah@ltu.se

Synthesis

Synthesis of the targeted ILs were carried out by using a multistep synthesis protocol (Scheme 1). The synthetic procedure of (MBPyrr)(MEA) is regarded is discussed below and the other ILs were synthesised using the same procedure.

N-methyl-*N*-butylpyrrolidinium bromide[1] (22 g, 0.1mol) dissolved in 250 mL water, and 25.5 g (0.11 mol) silver oxide was added into the solution; The resulting biphasic solution was left to stir for 5 h; the reaction mixture was filtered to remove silver iodide and residual silver oxide from the liquid. The filtrate was collected and 13.4 g (0.1 mol) of 2-(2-methoxyethoxy)acetic acid (MEA) was added dropwise over the time of 45 minutes. The mixture was stirred at room temperature for 6 hours, water was evaporated under reduce pressure to obtain the product. The final product was dried in vacuum oven at 80 °C for more than 4 days.

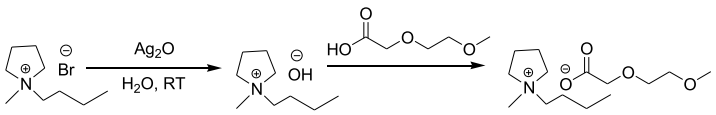

Scheme S1. Synthetic protocol for (MBPyrr)(MEA) IL.

(MMBIm)(MEA): Colourless oil; ^{1}H NMR (400 MHz, $CDCl_3$): δ 0.93-0.89 (t, 3H), 1.32-1.28 (m, 2H), 1.73-1.69 (m, 2H), 2.62 (s, 3H), 3.31 (s, 3H), 3.53-3.50 (m, 2H), 3.62-3.59 (m, 2H), 3.84 (s, 4H), 4.10 (s, 2H), 4.43 (s, 6H), 7.32 (s, 1H), 7.54 (s, 1H). ^{13}C NMR ($CDCl_3$, 100 MHz): δ 175.16, 144.06, 123.31, 121.04, 72.10, 70.87, 69.75, 58.83, 48.44, 35.53, 31.80, 19.67, 13.59, 9.78.

(MMBIm)(MEEA): Colourless oil; ^{1}H NMR (400 MHz, $CDCl_3$): δ 0.95-0.91 (t, 3H), 1.35-1.31 (m, 2H), 1.781.70 (m, 2H), 2.68 (s, 3H), 3.33 (s, 3H), 3.54-3.50 (m, 2H), 3.62-3.59 (m, 2H), 3.64 (s, 4H), 3.84 (s, 2H), 3.91 (s, 2H), 4.14-4.10 (m, 2H), 4.25 (s, 2H), 7.37 (s, 1H), 7.66 (s, 1H). ^{13}C NMR ($CDCl_3$, 100 MHz): δ 174.32, 143.91, 123.60, 120.89, 71.87, 71.19, 70.65, 70.19, 69.66, 58.72, 48.69, 35.30, 31.70, 19.63, 13.61, 9.93.

(MBPyrr)(MEA): Colourless gel; ^{1}H NMR (400 MHz, $CDCl_3$): δ 0.95-0.92 (t, 3H), 1.40-1.36 (m, 2H), 1.73- 1.65 (m, 2H), 2.21 (s, 4H), 3.17 (s, 3H), 3.31 (s, 3H), 3.47-3.43 (m, 2H), 3.53-3.51 (m, 2H), 3.64-3.62 (m, 4H), 3.73-3.71 (m, 2H), 3.88 (s, 2H), 4.27 (m, 2H). ^{13}C NMR ($CDCl_3$, 100 MHz): δ 174.77, 72.19, 71.51, 69.67, 64.30, 63.91, 58.88, 48.51, 25.97, 21.79, 19.90, 13.78.

(MBPyrr)(MEA): Colourless oil; ^{1}H NMR (400 MHz, $CDCl_3$): δ 0.97-0.94 (t, 3H), 1.42-1.37 (m, 2H), 1.71 (s, 2H), 2.22 (s, 4H), 3.19 (s, 3H), 3.33 (s, 3H), 3.47-3.45 (m, 4H), 3.72-3.59 (m, 8H), 3.91 (s, 2H), 4.40 (s, 2H). ^{13}C NMR ($CDCl_3$, 100 MHz): δ 174.64, 71.93, 71.30, 70.69, 70.27, 69.80, 64.23, 63.89, 58.91, 48.43, 25.86, 21.72, 19.82, 14.05.

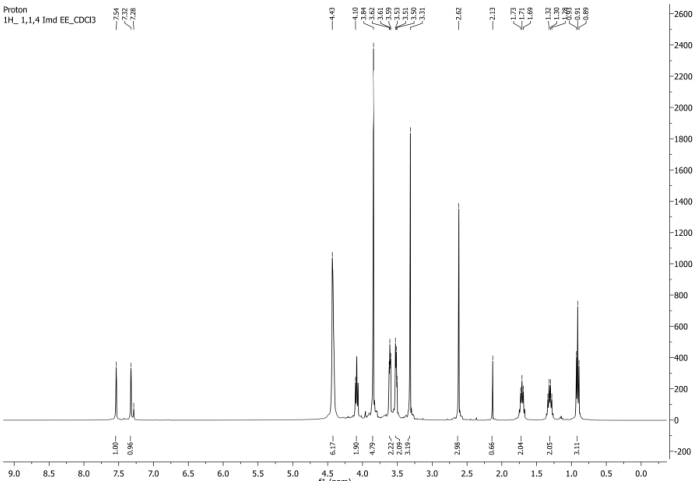

Figure S1. ^{1}H spectrum of (MMBIm)(MEA).

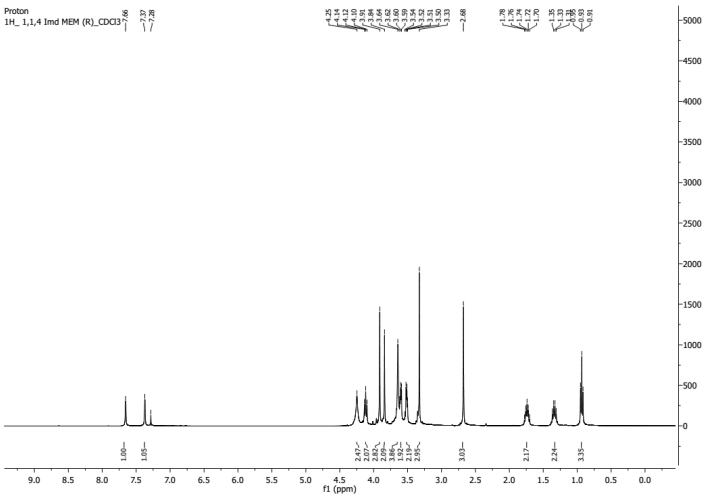

Figure S2. ^{1}H spectrum of (MMBIm)(MEEA).

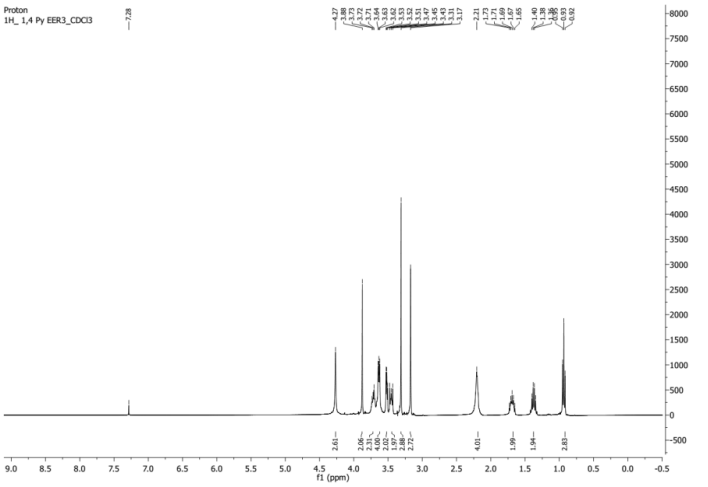

Figure S3. ^{1}H spectrum of (MBPyrr)(MEA).

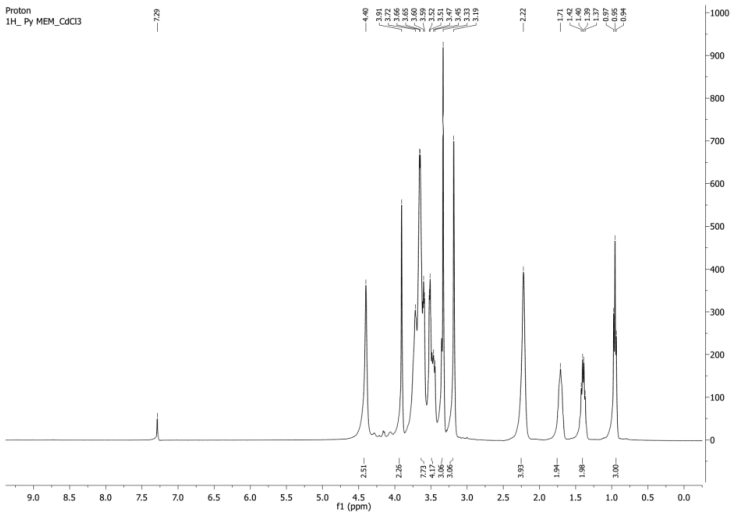

Figure S4. ^{1}H spectrum of (MBPyrr)(MEEA).

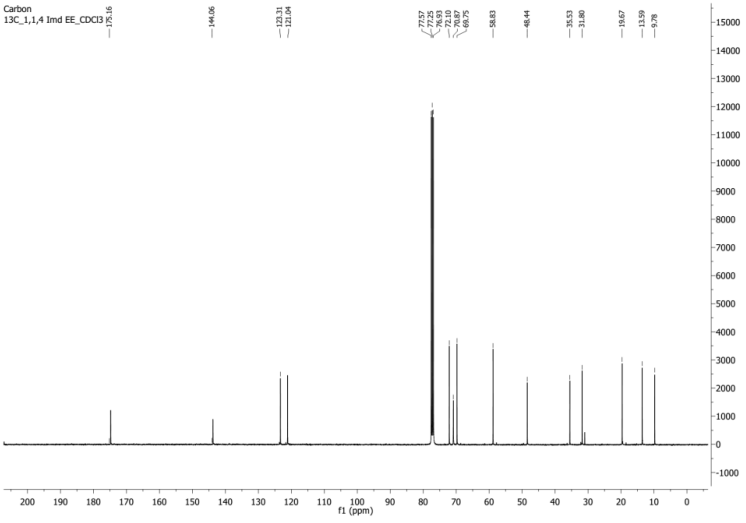

Figure S5. ^{13}C spectrum of (MMBIm)(MEA).

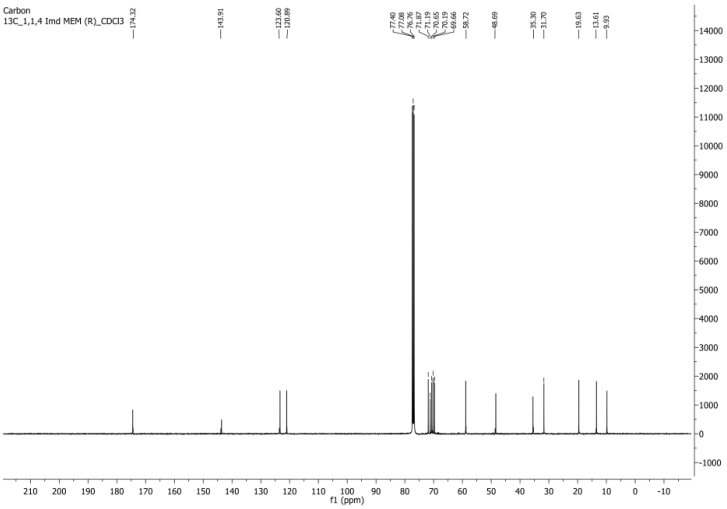

Figure S6. ^{13}C spectrum of (MMBIm)(MEEA).

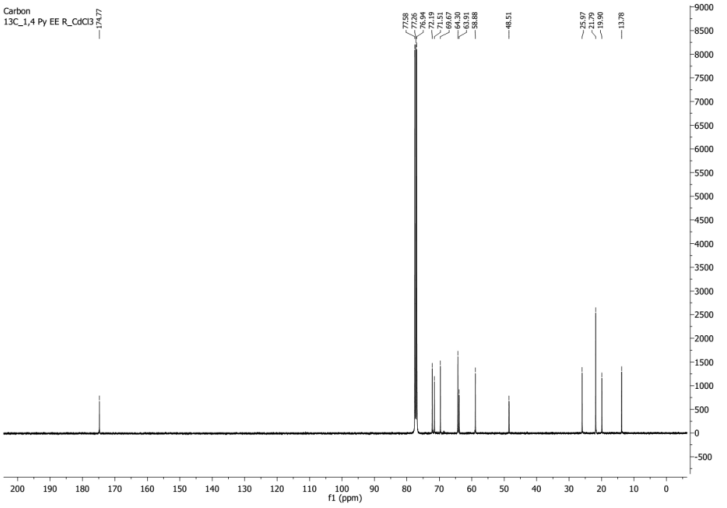

Figure S7. ^{13}C spectrum of (MBPyrr)(MEA).

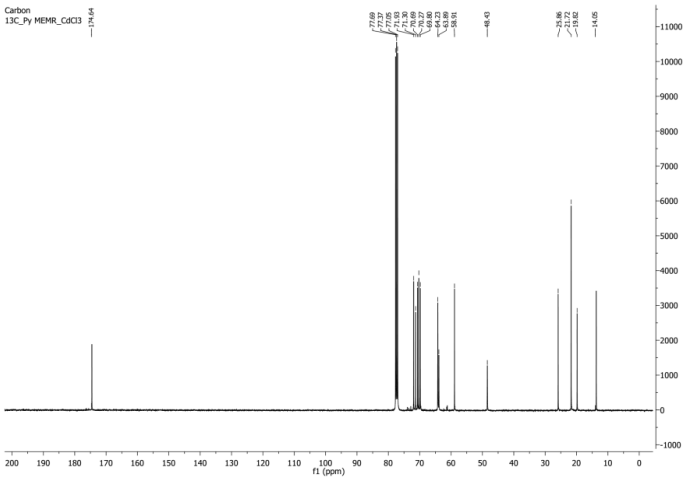

Figure S8. ^{13}C spectrum of (MBPyrr)(MEEA).

References

1. Qi, Z. H. A. N. G., Z. H. A. N. G. Miao-miao, and M. E. N. G. Lin. "Applications of N-methyl-N-butyl-pyrrolidinium bromide and N-methyl-N-ethyl-pyrrolidinium bromide in Zn-Br Flow Batteries." *Journal of Electrochemistry* 23.6 (2017): 694.

Department of Civil, Environmental and Natural Resources Engineering
Chemical Engineering

ISSN 1402-1757
ISBN 978-91-8048-121-2
ISBN 978-91-8048-122-9

Luleå University of Technology 2022

LULEÅ
UNIVERSITY
OF TECHNOLOGY